MINERALOGICAL CHARACTERIZATION OF URANIUM ORES, BLENDS AND RESULTING LEACH RESIDUES FROM KEY LAKE PILOT PLANT, SASKATCHEWAN, CANADA

A Thesis

Submitted to the College of Graduate Studies and Research

in Partial Fulfillment of the Requirements

for the Degree of Master of Science

in the

Department of Geological Sciences

University of Saskatchewan, Saskatoon, SK, Canada

By

MD. ALAUDDIN HOSSAIN

PERMISSION TO USE

In presenting this thesis in partial fulfilment of the requirements for a Postgraduate degree from the University of Saskatchewan, I agree that the Libraries of this University may make it freely available for inspection. I further agree that permission for copying of this thesis in any manner, in whole or in part, for scholarly purposes may be granted by the professor or professors who supervised my thesis work or, in their absence, by the Head of the Department or the Dean of the College in which my thesis work was done. It is understood that any copying or publication or use of this thesis or parts thereof for financial gain shall not be allowed without my written permission. It is also understood that due recognition shall be given to me and to the University of Saskatchewan in any scholarly use which may be made of any material in my thesis.

Requests for permission to copy or to make other use of material in this thesis in whole or part should be addressed to:

Head of the Department of Geological Sciences
University of Saskatchewan
114 Science Place
Saskatoon, Saskatchewan
Canada
S7N 5E2

ABSTRACT

The production and storage of uranium mine mill tailings have the potential to contaminate local groundwater and surface waters with metals and metalloids. As such, an understanding of the solids reservoirs for potential contaminants in uranium ore blends and leach residues (solid wastes generated by the milling of ore) is required to predict long-term controls on these contaminants in tailings porewaters. This study characterized the distribution of the elements of concern (EOCs; As, Mo, Ni, and Se) in uranium ores and waste rock used to blend the mill feeds in the milling process and leach residues from the Key Lake mining operation, Saskatchewan. This study also evaluated the alteration of the clay minerals in these uranium ores, waste rocks and leach residues. X-ray diffraction, electron micro-probe, and mineral liberation analyses showed that the reservoirs for As, Mo, Ni, and Se (in ores and ore blends) were dominated by sulphides including cobaltite, gersdorffite, molybdenite, pyrite, galena and chalcopyrite, secondary Ni-arsenates (annabergite?), Fe-arsenate (scorodite?) and Ni-Co/Ni-sulfates. The secondary arsenates and sulfates present in special waste were identified as major As, Mo, Ni, and Se bearing minerals and most likely the product of oxidation of arsenide-bearing sulphide minerals within the special waste rock. Analyses also showed that sulphides and arsenates occurred in trace amounts in the ores and special waste rock (0.5 to 1.0 wt %). Data showed that 55 to 90% pyrite, 36 to 51% chalcopyrite, 23 to 37% molybdenite, and 52 to 70% galena remained unleached in the leach residues after milling of the ore blends. The percentages of unleached minerals varied between mill feeds and were dependent on the grain-size distribution and the degree of mineral liberation. Cation exchange capacity (CEC) analysis indicated an increase of the CEC values in the leach residues suggesting possible evolution of 2:1 layers into high-charge layers during the milling.

ACKNOWLEDGEMENTS

I would like to express my special appreciation and gratefulness to my supervisors Prof. Dr. Jim Hendry and Prof. Dr. Yuanming Pan, for their guidance, advices and valuable suggestions throughout my M.Sc. study and research. I would like to thank them for encouraging me and for allowing me to grow as a graduate student. Sincere thanks to my committee member Dr. Tom Kotzer for his insightful comments and research questions about my research that improved my thesis. I also want to thank my defense external Dr. Derek Peak for an enjoyable defense, and for your brilliant comments and suggestions.

Sincere thanks to Dr. Joseph Essilfie-Dughan. His valuable suggestions, ideas and recommendations have encouraged me along the way. I am indebted to Dr. Mario Gomez for teaching me XRD and Raman spectroscopy.

Special thanks to Dr. Ali Hooshiar, for his cordial inspiration and guidance with clay minerals analysis. I would also like to thank Mr. Tom Bonli for helping me with the EPMA and SEM, and Dr. Jianzhong Fan for collecting ICP-MS data for me. Thanks to Mr. Michael Shaffer for teaching me Mineral Liberation Analysis (MLA) and helping me to collect MLA data.

Finally, I would also like to acknowledge Cameco Corp., NSERC, Department of Geological Sciences and the University of Saskatchewan for financial support.

TABLE OF CONTENTS

CHAPTER 1

INTRODUCTION

1.1 Overview

Increase in global energy demand coupled with global warming associated with fossil fuel has made nuclear energy a viable alternative option for both developed and developing economies. This has resulted in a demand for uranium (U) globally. U ore deposits spread out all over the world and are found in large quantities in Australia, Kazakhstan, and Canada. The Athabasca Basin, located in northern Saskatchewan, Canada, hosts the largest and richest reserves of U ore in the world (Jamieson and Frost, 1997). Presently 19% of the world's U is produced from this Basin (IAEA, 2012).

The mining and milling of U ores result in the generation of large masses of tailings, estimated to be about one billion tons from 4000 U mines world-wide (IAEA, 2004; Abdelouas, 2006). Globally, U ore with low carbonate content is extracted by acid leaching. In case of U ore with high carbonate contents, alkaline leaching is employed. After ore extraction, the residues are dominated by solid residues that contain unleached primary minerals and secondary minerals formed during raffinate neutralization. Raffinate is the remaining solution after U extraction. Both the solids and liquid raffinate are neutralized by the addition of $CaCO_3$ and/or $Ca(OH)_2$ (Abdelouas, 2006). Then these materials are discharged into the tailings management facility (TMF) which can be a large waste retention pit or lake. The highest amount of tailings has been generated so far in Kazakhstan (IAEA, 2004). Canada has produced 3% of the global U tailings which is equal to around 30 million tonnes of tailings (Scissons, 1997; IAEA, 2004). In 1953, Beverlodge mill first started U production and associated tailings (Donahue, 2000). Before 1996, the U mill tailings were discharged in above ground TMFs at Rabbit Lake, Cluff Lake and Key lake sites (Scissons, 1997; Donahue, 2000).

The tailings consist of the processed waste materials from the mill. These materials usually contain naturally occurring radionuclides (e.g. U^{238}, Ra^{226}, Rn^{222}, Th^{230}), and toxic metals (e.g. As, Se, Pb, Hg) found in U ores (Nilsson and Forssberg, 1988; Landa et al., 1991; Lottermoser and Ashley 2005; Abdelouas, 2006). These elements are frequently referred to as elements of concern (EOCs). Tailings located in this region are generally characterized by

elevated concentrations of Ra^{226}, As, Ni, Mo and Se (Essilfie-Dughan et al., 2013, 2012, 2011; Gomez et al., 2013; Liu and Hendry, 2011; Moldovan and Hendry, 2005; Moldovan et al., 2008, 2003; Shaw et al., 2011). Some of these elements can have adverse effects on human health and aquatic life/biota (Lener and Bibr, 1984, USEPA, 1998 and Goldhaber, 2003). Their concentrations in tailings porewaters often exceed the maximum acceptable concentrations (MAC) of drinking water quality and for aquatic life set by Health Canada, WHO and USEPA (Table 1.1) (Morrison and Cahn, 1991, Somot et al., 1997).

Tailings impact ecosystems by negatively affecting the growth of the microbial community, plants, and animals. The Canadian U mines are leading in tailings management to minimize the deleterious effects that the U tailings might cause to the surrounding environment. The key target in waste management by the miners is to minimize the release of toxic materials into the environment. Extensive multidisciplinary studies have been executed on proper disposal of tailings to ensure 200 to 1000 years of stability (Abdelouas, 2006). Both primary and secondary minerals control the solubility of these elements, and are important factors in the prediction of the long-term stability of the tailings. Most of these elements are associated with primary As- and Ni-bearing sulphides, and Fe- and Ca-oxyhydroxides formed during the bulk neutralization of the raffinate. Sulphide oxidation may cause acidification of the tailings, which might mobilize the EOCs. One of the major catalysts of the sulphide oxidation is microbial activity. The rate of oxidation is controlled by the composition of the sulphide minerals (Claassen, 1993; Jiang et al., 2007). For example, chalcopyrite has a higher oxidation rate than pyrite in the presence of A. ferrooxidans (Jiang et al., 2007).

The Key Lake mill is the largest U processing facility in the world and currently processing the McArthur River (McA) U ore deposit. It will provide the bulk of the U ore for the Key Lake mill and associated tailings for at least the next 25 years. Future U ore deposits, including the Millennium, Tamarack and Phoenix ore bodies and others, are in feasibility stages. Concentrations of EOCs vary in these deposits depending on the primary mineralogy of the ores and may yield different source terms for the tailings.

High grade U ore (average grades of 15.24% U_3O_8 monometallic U deposit) is currently being mined at McArthur River operations of Cameco, located 80 km northeast of Key Lake, in the Athabasca Basin of northern Saskatchewan, Canada (Fig. 1.1) (Jamieson and Frost 1997;

Cloutier et al. 2009). In general, this deposit has significantly lower concentrations of EOCs than previously mined polymetallic ores at Key Lake (Jamieson and Frost, 1997). The Key Lake ores consisted of sulphide and arsenide minerals containing significant amounts of Ni, Co, Cu, Pb, Zn, and Mo, whereas the McArthur River ore contain just traces of metals other than U. Prior to milling at Key Lake, the ore is diluted to target grades of 4% U_3O_8 by blending it with low-grade Key Lake Special Waste which includes Deilmann and Gaertner Special Wastes (Shaw et al., 2011). After extraction of U from the leach feed, leach residues are produced as processing waste, and added into final tailings after several washes. Tailings from the mill have been discharged to the Deilmann tailings management facility (DTMF) since 1996. DTMF is a mined-out pit used for the disposal of tailings generated in the Key Lake milling process.

Extensive studies of hydrometallurgical solutions associated with U processing showed that leaching of EOC's largely depends on the primary minerals (which determine the initial oxidation states), initial concentrations, the Fe/As, Fe/Mo and Ni/Mo molar ratios, and the stability of the secondary minerals formed in the neutralized acidic solution (Harris, 2000; Essilfie-Dughan et al., 2011; Riveros et al., 2001 and Essilfie-Dughan et al., 2012). Presently treating U mill wastes includes maintaining the molar Fe(III)/As total ratios at ≥3, neutralizing the mine tailings with lime to neutral or mildly alkaline pH, and finally discharging the tailings as oxic slurries (Essilfie-Dughan et al., 2012). Secondary minerals of Fe, As and Ni form during the stepwise neutralization process of raffinate. These minerals control the concentration of these elements in the tailings porewater at very low levels (Mahoney et al., 2007 and Essilfie-Dughan et al., 2012).

Hydrometallurgical and geochemical investigations of present and future U ore milling process at Key Lake along with geochemical stability of tailings are under experimental investigation in the pilot mini-mill. The design of the mill scale model at Key Lake replicates the hydrometallurgical mill process from grinding through to tailings generation. The mini-mill is constructed at a scale of 1:310,000 the size of the Key Lake mill. Prior to mini-mill experiments, high grades ores from McArthur River (McA) and Millennium (MLM), and low grade materials from Deilmann (DSW) and Gaertner (GSW) special wastes, and McArthur River mineralized waste (McW) were mixed in different ratios to prepare three different blends as mill feed. Subsequently, these blends were milled using the pilot mini-mill to extract U. Information on the

variability and distribution of EOCs within the source minerals, and the evolution of the clay minerals during the ore processing are important for optimizing the mill design so that the tailings meet regulatory requirements regardless of the type of ores milled. A full mineralogical characteristic (such as concentrations of metals and metalloids, and ratio of acid-producing to acid-neutralizing minerals) of the solid residues is significant in the tailings management, and minimizing the long-term environmental liabilities. These characteristics are expected to regulate the potential release of contaminants (metals and metalloids) from the tailings to the soil and groundwater (Hiller et al., 2013).

Clay minerals can play important role in controlling sedimentation/consolidation behavior of the tailings. They are very active due to their high surface area and charge density. As a result of these properties, U extraction efficiency can decrease as much as 10% with high clay minerals contents in the ores due to the adsorption by the clay mineral surfaces (Abdallah, 2009). Ring and Levins (1982) showed that ores containing higher contents of clay minerals caused lower concentration of Ra^{226} in solution as it tend to adsorb on the clay surfaces. Moreover, mineralogical controls on Al and Mg in U mill tailings could be linked to the clay minerals content of the ore. Partial to complete dissolution of clay minerals, e.g. chlorite, could be major source of Al and Mg to the raffinate. These two elements precipitate as secondary Mg-Al-hydrotalcite during bulk neutralization of the raffinate (Gomez et al., 2013). The association among the Mg-Al hydrotalcite and both As and Ni revealed that this phase can potentially contribute to control the EOCs concentrations in tailings porewaters (Douglas et al., 2014; Gomez et al., 2013).

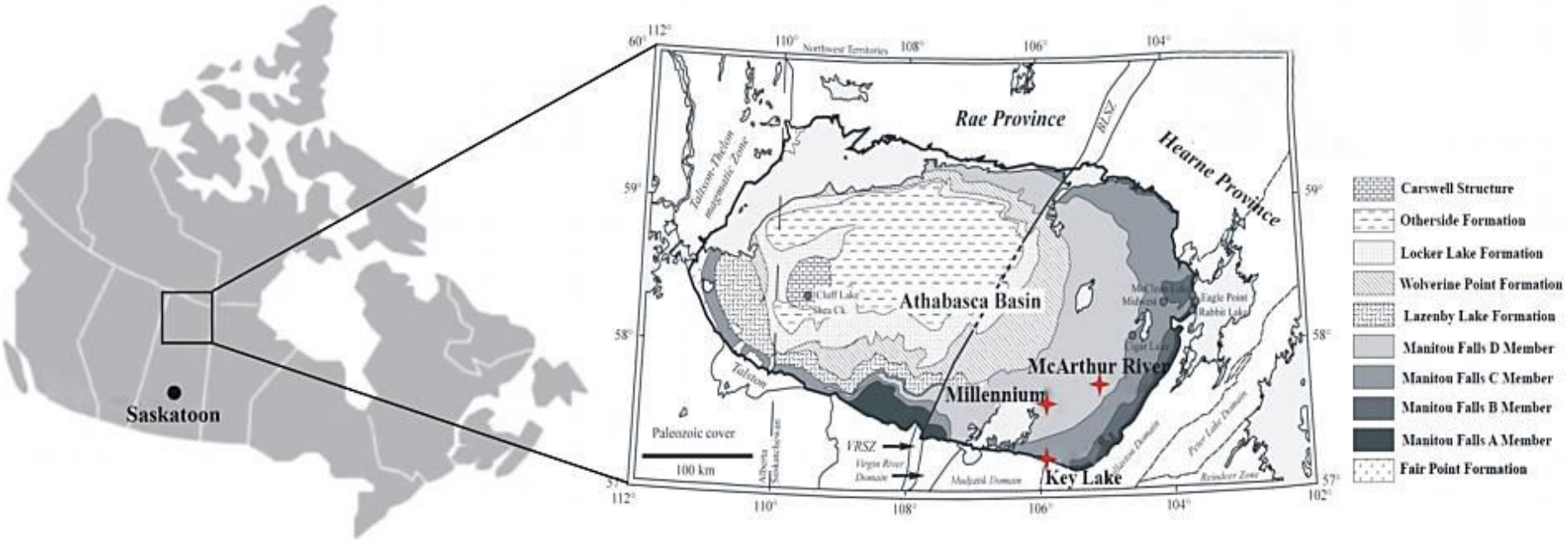

Figure 1.1 Location map for Key Lake and McArthur River mine sites (modified after Sibbald and Quirt, 1987; Cloutier et al., 2009; Shaw et al., 2011).

Table 1.1 Maximum acceptable concentrations (MAC) in drinking water.

Inorganic Elements (Mg/L)	Health Canada	WHO	USEPA
As	0.01	0.01	0.01
Se	0.01	0.04	0.05
Pb	0.01	0.01	0.015
U	0.02	0.03	0.03
Ba	1	0.7	2
Cd	0.005	0.003	0.005
Cr	0.05	0.05	0.1
Radionuclides(Bq/L)			
Pb-210	0.2	0.1	
U-238		10	
U-234		1	
Ra-226	0.5	1	0.185

Source: Health Canada (2012); WHO (2011); USEPA (2009)

1.2 Tailings Management

The main purpose of tailings management is to contain mill wastes generated after the extraction of the ore. Disposal of these wastes has to be economically, environmentally and technically viable. Tailings management is a vital activity of any mining project to protect both the surface water and groundwater from contamination. Accordingly, the tailings management facilities are needed to be designed and functioned to minimize long term effects on the environment. The management of the tailings varies from mine to mine depending on the ore grade and the geography. High grade ore bodies (e.g. in northern Saskatchewan) have higher U to ore ratios and thus produce much lower volume of tailings.

During 1980's, dumping tailings in a semi-dry state was initiated around the world because of reduced seepage, dust and rapid rehabilitation (Robinsky, 1981; Levins and Davy, 1983; Forssberg and Nilsson, 1987). Tailings with higher liquid to solid ratio dissolve more Ra^{226} in comparison to semi-dry disposal methods (Nilsson and Forssberg, 1988). Another technique of tailings disposal is underground backfilling (Nilsson and Forssberg, 1988). However, this practice is more common in mining of non-radioactive ores. Due to the greater exposure of the miners to radioactivity, this method is used less frequently than the surface disposal.

In the beginning of U mining in Canada, tailings were discharged into natural water body and topographic depression (Donahue, 2000). This type of tailings management offered no protections from the harmful impacts of the U tailings. Between 1983 and 1996, tailings from the Key Lake mill was deposited into the Above Ground Tailings Management Facility (AGTMF) built 5 meters above the groundwater table (Cameco, 2010). Its dimensions were 600 metres by 600 metres and 15 metres deep. Bentonite liner was used to make the bottom impervious.

Currently, the Deilmann tailings management facility (DTMF), build in the basement rock, is used to manage the tailings generated at the Key Lake mill (Fig. 1.2). The containment design of DTMF is a little different from RTMF (Rabbit Lake Tailings Management Facility). A pervious liner was implemented, for the disposal of the Key Lake mill tailings. A highly permeable envelope of coarse rock and filter sand was placed into the bottom and part way up the sidewalls to collect the under-drain and the side-drain respectively (Cameco, 2010). This drainage system increases consolidation rate of the tailings. A raise well dewatering system

connects the under-drain through a tunnel and removes the water squeezed out during the consolidation process. This water along with residual water on the surface are collected for treatment. The consolidated tailings are expected to become a low-permeability mass enclosed in a permeable envelope. As a result, the groundwater should flow around the tailings instead of through them.

1.3 Objectives of the Study

The goals of this study are to understand the mineralogical characteristics of present and future ores. These data are important for predicting geochemical stability of the tailings (e.g. acid mine drainage), and optimizing the mill design for processing future ores. The specific objectives of the present study were to:

i) Identify and quantify EOC-bearing minerals in mill feeds and associated leach residues from McArthur and Millennium ore blends used in the mini-mill experiments.

ii) Characterize the distribution of EOCs in minerals found in the ores and leach residues from the mini-mill experiments.

iii) Characterize the clay minerals in the mill feeds and leach residues from the mini-mill experiments.

Analytical techniques used to attain these objectives included inductively coupled plasma mass spectrometry (ICP-MS), electron micro-probe analysis (EPMA), X-ray diffraction (XRD) and mineral liberation analyzer (MLA).

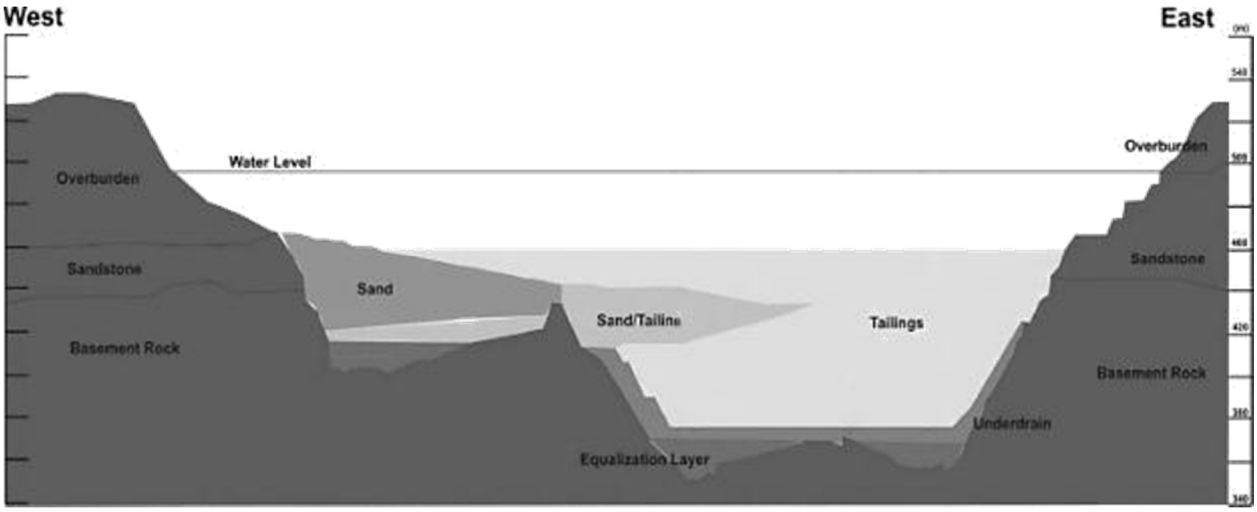

Figure 1.2 Schematic cross section of the Deilmann tailings management facility (modified after shaw et al., 2011)

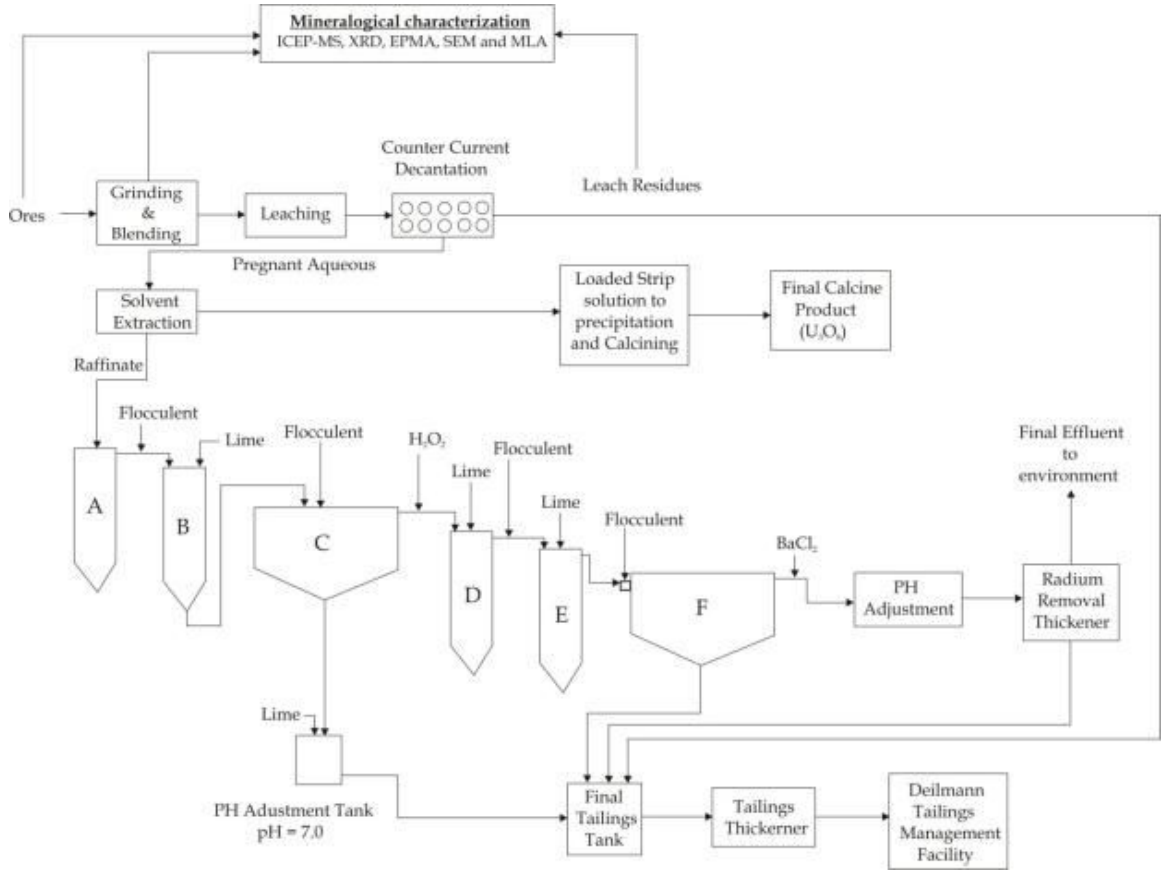

Figure 2.1 Simplified process flowsheet of the Key Lake pilot milling operation (modified after Koshinsky et al., 2012).

CHAPTER 2

LITERATURE REVIEW

2.1 Location of the Mill and Milling Process

The Key Lake U mill (57°13′N, 105°38′W) is located at the southern edge of the Athabasca Basin in north-central Saskatchewan, approximately 570 km north of Saskatoon, Canada (Bharadwaj et al., 2010) (Fig. 1.1). Several lakes, for example Lake Athabasca and Wollaston Lake are situated with the area. This part of Saskatchewan is covered with spruce, balsam fir and Jack pine forest (Cameco, 2010). The climate of mill area is sub-arctic and experiences cold artic air (Ecometrix, 2005). The annual mean temperature and precipitation are -2°C and 473.5 mm (Cameco 2009). The Key Lake area experiences the highest amount of precipitation during months of May to September (Cameco 2009).

It is currently the world's largest producer of U producing 8.5 million Kg U_3O_8/y. Ore feed has changed at Key Lake mill with time (Shaw el al., 2011). From 1996 to 1999, the mill feed was derived entirely from the polymetallic U–Ni Deilmann ore body containing varying amounts of Ni–Co–As–S minerals (von Pechmann, 1985). Ore from the McArthur River mine, located 80 km northeast of Key Lake (Fig. 1.1), has been the primary source of mill feeds for the mill since March 2000 (Shaw el al., 2011). In general, the McArthur River ore has lower concentrations of EOCs than previously mined polymetallic ores at Key Lake (Jamieson and Frost, 1997).

The Key Lake Mill processes U-containing ore to U_3O_8 for shipping to an enrichment facility. The mill process is shown in Figure 2.1. Currently the mill is processing ore with an average grade of 15.24% U_3O_8 mined from the McArthur River site. The first step in the mill process is crushing, which pulverizes materials too large to be fed directly through the semi-autogenous grinding (SAG) mill. After Crushing, the ore is sent to Ore Receiving where it is blended with low-grade slurry composed of special waste rock from the Grinding circuit. The two slurries from the Grinding and Ore Receiving circuits are combined in Blending to produce a ~4% U_3O_8 leach feed. This leach feed is sent to Leaching/Counter Current Decantation (CCD). At Leaching, the ore is treated with sulphuric acid in conjunction under strong oxidizing conditions to separate the U bearing solution from the waste solids and residue. These conditions

also oxidize the metal sulphides and arsenides and liberate metals such as As, Ni, Mo and Se from the ore, as follows (Essilfie-Dughan et al., 2012):

$$4NiAsS + 6H_2O + 13O_2 \longrightarrow 4SO_4^{2-} + 4AsO_4^{3-} + 4Ni^{2+} + 12H^+$$

Subsequently, the U bearing acidic solution reports to Counter Current Decantation (CCD) where the acidic U-bearing leach solution is separated from the leach residue to produce a aqueous solution containing approximately 12-14g U_3O_8/L along with dissolved metal and metalloid contaminants. The leach residues are sent to the tailings area for treatment using $Ca(OH)_2$ and then to the DTMF. The soluble U is extracted from the acidic leachate using a solvent extraction process. The resulting acidic waste solution (raffinate) is devoid of U and contains elevated concentrations of As, Ni, Mo and Se. The acidic raffinate is sent to bulk neutralization, where it is incrementally neutralized in a series of 4 neutralization tanks (pachucas) with hydrated lime. In the pachucas, the pH is sequentially raised to 1.0, 3.5, 6.5, and finally 9.2. The slurry from the final pachuca (pH = 9.2) and leach residues enter a tailings thickener where flocculent is added. Finally, lime is added to increase the final tailings discharge to approximately pH 10.5.

In the milling process, most of the soluble EOCs in the raffinate are precipitated as secondary minerals as lime neutralization proceeds (Shaw et al., 2011). Discharged tailings contain approximately 35% solids which are largely comprised of original clay and silicate gangue minerals, minor sulphides and oxides and gypsum precipitates from neutralization.

2.2 Geology of the McArthur River Deposit

The McArthur River unconformity-related U deposit is located in the southeastern part of the Athabasca Basin, near Cable Bay shear zone (Derome et al., 2005). The unconformity is located in between 500 and 600 m depth (McGill et al., 1993). Graphitic metapelites are present in the basement and are associated with both shears and ore deposits (Farquharson and Craven, 2009).

The McArthur River deposit is comprised of six ore zones, of which five are sediment-hosted and one basement-hosted ore bodies (Cameco 2008). The basement-hosted P2 ore body is currently being mined. The crystalline (gneissic) basement is an assemblage of Aphebian pelitic, semipelitic and arkosic gneisses, with minor interlayered calc-silicates (amphibolites) and quartzites (McGill et al., 1993). U mineralization is mostly basement-hosted and close to the unconformity which separates the flat-lying unmetamorphosed, middle Proterozoic sandstones of the Athabasca Group from folded and metamorphosed lower Proterozoic and Archaean rocks beneath (Fig. 2.2; Alexandre et al., 2005). Ore mineralization occurs mostly in the cordierite-rich metapelites (Derome et al., 2005).

The Athabasca Group rocks are sandstones and conglomerates of late Paleo- to Meso-Proterozoic age (Rainbird et al., 2007) with an approximate thickness of 500m. Sandstones near U mineralization are highly altered with hematite and bleached (Quirt, 1991). These sandstones are comprised of four members of the Manitou Falls Formation (Ramaekers, 1981). The members are, from bottom to top, MFa, MFb, MFc and MFd. The McArthur River ore deposit is structurally controlled by a major reverse P2 fault. The deposit is located where the P2 fault intersects the basement. It is a southeast dipping (40º to 45 º) reverse fault and it offsets the basement by 60 – 80 metres (McGill et al., 1993).

The alteration characteristics of the McArthur ore deposit are unique compared to many other U deposits in Saskatchewan. This deposit lacks an extensive clay alteration halo or cobalt-nickel-arsenide mineral assemblage, has extensive silicification and weak bleaching (McGill et al., 1993). Weakly altered basement host rock abruptly changes into extensive chlorite alteration and monometallic high-grade U mineralization over a very short distance (McGill et al., 1993). In the sandstone above the unconformity, the deposit is characterized by early silica alteration

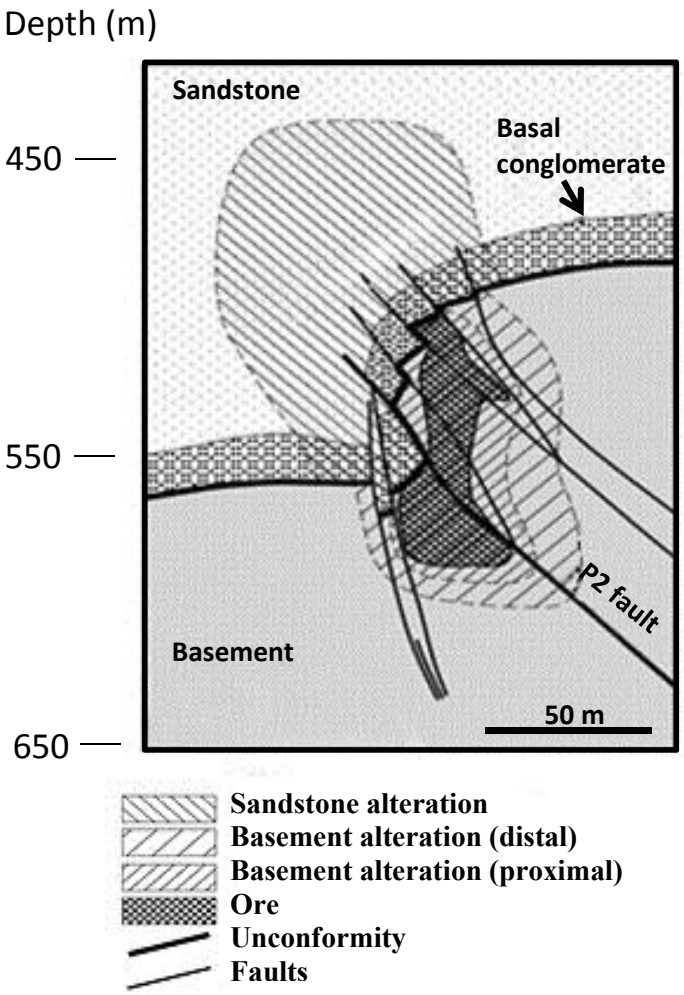

Figure 2.2 Simplified schematic cross-section of the basement-hosted McArthur River deposit (modified from Alexandre et al. 2005).

(McGill et al. 1993). Silicification is mainly intense below 375m to the basal fanglomerate unit (McGill et al. 1993). Hematite is commonly preserved between the detrital quartz and quartz overgrowths (Qz1) (Derome et al., 2005). A postdiagenetic and extensive silica alteration (Qz2) is observed in the sandstone developed up to 150m above the mineralization (Derome et al., 2005).

Coarse-grained illite, Mg-chlorite and Mg-tourmaline (magnesiofoitite) are the major components associated with minor amounts of pyrite, chalcopyrite and quartz of the main

alteration assemblage (Table 2.1) (McGill et al., 1993; Kotzer and Kyser, 1995; Zhang et al., 2001; Derome et al., 2005).

Table 2.1. Alteration characteristics, mineralogy and paragenesis of silicate and clay minerals in altered sandstones and metasedimentary rocks from McArthur River uranium deposit (after Kotzer and Kyser, 1995).

Site	Alteration	Paragenesis
P2 North	High-grade unconformity-type uranium; well-developed early quartz overgrowths and euhedral quartz breccias; significant sudoite in basement rocks; illite-chlorite-dravite in sandstones; abundant kaolinite formed in late, reactivated faults.	Q1, U1, C1, C2, Q2, I1, K1, T1, T2, U2, K3
P2 Main/BJ	Altered unconformity-type uranium; moderate development of quartz overgrowths and strongly developed euhedral quartz; euhedral quartz-dravite breccias; sporadic sudoite formed in basement; variable mixtures of ilite-kaolinite proximal to hydrothermal alteration haloes; reactivated faults contain large amounts of late kaolinite.	Q1, U1 (minor), I1, K1, C1, C2, Q2-T1, T2, U2, K3

2.3 Geology of the Millennium Deposit

The Millennium U deposit, discovered in 2000, is a basement-hosted unconformity related deposit. It is located in the Cree Extension project, which is situated approximately 45 kilometers from the southeastern edge of the Athabasca Basin, and 35 kilometers to the north of the Key Lake mine (Fig. 1.1; Beshears 2010). This deposit is estimated to have 46.8 million pounds (18000 m.t. U) with an average grade of 4.53% U_3O_8 (Cloutier et al., 2009).

Paleoproterozoic metasedimentary rocks of the Wollaston Domain and the Mudjatik Domain host almost the whole deposit at a depth ranging from 600 to 750 m (Roy et al., 2005). The basement rocks comprise predominantly paleo-Proterozoic gneisses with intercalation of highly conductive graphitic metasedimentary rocks (Smith et al., 2010). Athabasca sandstone is separated from the basement by an unconformity. The mineralization occurs near to a graphitic horizon at a depth of 650 m from the surface and 100 m below the unconformity (Tran et al., 2003; Roy et al., 2005; Cloutier et al., 2009). The mineralization in this deposit is mostly strata-bound and the main orebody is located in the footwall of a major reverse fault, known as the Mother fault (Cloutier et al., 2009). The deposit is located along the northwest-trending limb of a fold structure associated with the east limb of a larger, regional, north-plunging synformal fold (Thomas, 2002).

The U minerals are primarily uraninite with minor amounts of coffinite (Roy et al., 2005). The mineralization styles include massive replacement, matrix in breccias, disseminated filling of fractures, thin vein-type uraninite, colliform aggregates etc. (Thomas, 2002). Among all these mineralization styles, massive foliation-controlled replacement is predominant.

Basement alteration ranges from distal saussuritization and sericitization through proximal chloritization to central argillic alteration (Roy et. al, 2005). Bleaching and dravitization occur in close proximity to the major reverse fault (Roy et. al, 2005). The main ore body roughly overlaps the zone of chloritization and argillic alteration (Beshears 2010).

2.4 Key Lake Special Wastes

The Key Lake mill site accommodates several waste rock stockpiles resulting from mining of the Gaertner and Deilmann ore bodies including the Deilmann North Waste Rock, Deilmann South Waste Rock, Gaertner Waste Rock, Deilmann Special Waste and Gaertner Special Waste piles (Fig. 2.3; Cameco, 2010). The excavation of the Deilmann and Gaertner pits allowed for the construction of these wastes piles. Mineralized wastes from the McArthur River site are also transported to the Key Lake mill site and stored on a lined facility. These wastes were used to make blends for mill feeds. Figure 2.2 illustrate the layout of the wastes in the Key Lake area.

Waste rocks are separated into two categories; clean waste rock and special waste rock (Cameco, 2010). Clean waste rock is non-mineralized country rocks that have been quarried to access the U ore. It includes sand and till, sandstone and basement rock. Special waste is material with some U and elevated sulphide and arsenide mineral contents (Cameco, 2010).

The Gaertner Waste Rock Pile is sited south of the Gaertner pit. It was constructed between 1981 and 1987 during mining of the Gaertner pit (Cameco, 2010). Generally, the pile is comprised of outwash sand, which was mined first, followed by sandstone, and finally, by a small quantity (about 1%) of basement rock (Cameco, 2010; Cameco, 1998). The stockpile has an average grade of about 0.0056% U_3O_8 (Cameco, 2010; Cameco, 1994).

The Deilmann South Waste Rock Pile is located adjacent to the south of the Deilmann pit. This pile is comprised predominantly of sand/till (about 67% by volume) and sandstone (about 33% by volume) with an average grade of about 0.005% U_3O_8 and low metal content (Cameco, 2010, 1994). The Deilmann North Waste Pile is located north of the Deilmann pit and consists of sand/till, sandstone and basement rock. This pile contained about 27% outwash sand/till, 43% sandstones and 29% basement material (Cameco, 2010, 1996).

Materials excavated from the margin of the Gaertner and Deilmann ore-bodies were stock piled as the Gaertner and Deilmann special waste piles (Cameco, 2010). These materials contain U grades greater than 0.03% U_3O_8 but less than 4% U_3O_8, as well as sulphide and arsenide minerals (Cameco, 2010). These wastes have higher possibility to generate acidic seepage containing elevated concentrations of heavy metals, metalloids and radionuclides due to natural

weathering. Consequently, Gaertner and Deilmann special wastes are stored on lined pads so that runoff and seepage water can be collected for treatment.

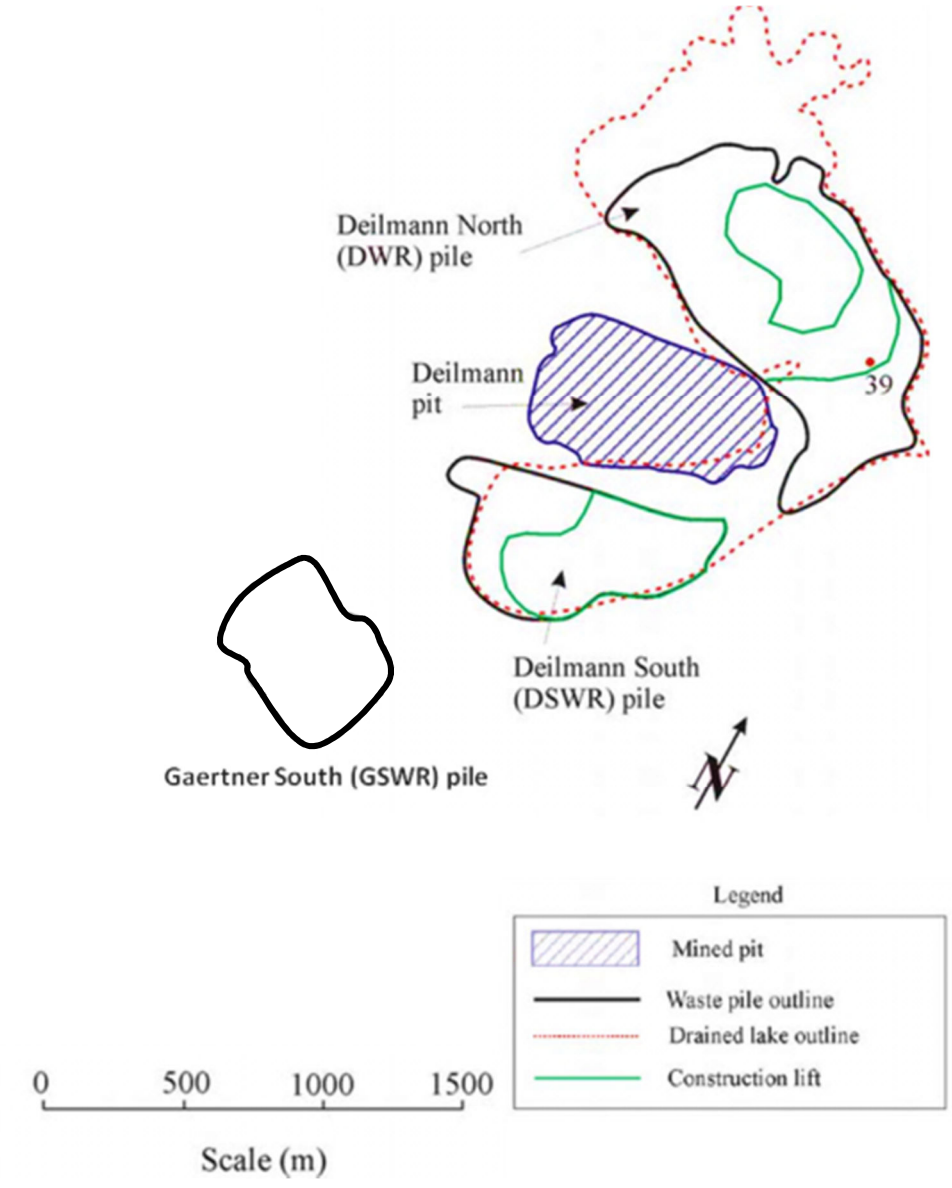

Figure 2.3 Location of waste piles in Key Lake (modified after Lieu, 2004).

2.5 Mineralogy of Uranium Deposits

In general, U ore bodies consist of U ore minerals, sulphides, arsenidse, oxides, carbonates and silicates. The major ore minerals include both primary and secondary U minerals. The primary minerals of U are uraninite (UO_2) or amorphous uraninite (i.e., pitchblende,U_3O_8), coffinite ($U(SiO_4)_{1-x}(OH)_{4x}$), brannerite (UTi_2O_6) and davidite ($(REE)(Y,U)(Ti,Fe^{3+})_{20}O_{38}$). Primary U minerals occur in veins or pegmatites, and in exceptional case in sedimentary rocks (Gabelman, 1988; Klemic, 1962; Ruzicka, 1993).These minerals are generally dark colored with shiny lustre. Secondary U minerals are formed when these primary minerals undergo weathering and are brilliantly coloured. Some of the well-known secondary minerals are uranophane ($CaH_2(SiO_4)_2(UO_2).5(H_2O)$), autunite ($Ca(UO_2)_2(PO_4)_2.12(H_2O)$) and sklodowskite ($(H_3O)_2Mg(UO_2)_2(SiO_4)_2.4(H_2O)$).

In the Athabasca basin, U ore minerals are uraninite, pitchblende, coffinite and uranophane with variable Ni, Co, As, Pb and traces of Au, Pt, Cu, REEs, and Fe (Jefferson, 2007). The U deposits are classified as monometallic and polymetallic based on their metal associations (Thomas et al., 2000; Jefferson, 2007). Monometallic deposits contain U minerals and some metals in trace amounts. On the other hand, polymetallic deposits are high in sulphide and sulpharsenide minerals (Jefferson, 2007). Sulphide and arsenide minerals contain significant amounts of Ni, Co, Cu, Pb, Zn, Se and Mo. The sandstone and conglomerate hosted Cigar Lake deposit is an example of polymetallic deposits. The Key Lake deposit consisted of polymetallic Deilmann and Gaertner orebodies.

Monometallic McArthur River deposit is high-grade U ore bodies containing significantly fewer Ni–Co–As sulphide minerals (Jamieson and Frost, 1997; Table 2.2). The ore consists of uraninite/pitchblende (U_3O_8) with trace metals associated with pyrite (FeS_2), chalcopyrite ($CuFeS_2$) and arsenopyrite (FeAsS) (Delaney et al., 1998). The mineralogy of few U deposits in the Athabasca Basin is summarized in table 2.2.

Table 2.2 Summarized mineralogy of uranium ores in the Athabasca Basin.

Key Lake Ore	McArthur River Ore	Millennium Ore
Ore: Uraninite, coffinite, Uranophae, galena, pyrite, arsenopyrite, pentlandite and chalcopyrite, gerdorffite, millerite, bravoite, linnaeite, covellite, niccolite, ettringite, sphalerite, pararammelskergite, rammelsbergite, hematite, gypsum, bassinite Alteration minerals: chlorite, illite (Von Pechmann, 1985).	Ore: Uraninite; Galena, Pyrite, Chalcopyrite, minor, nickel-cobalt sulfarsenides, covellite, chalcocite, carbonate, gold Alteration minerals: In sandstone- quartz, kaolinite, chlorite, tourmaline In basement- illite, chlorite, tourmaline with local apatite and carbonate (Gandhi, 2007) (McGill et al., 1993)	Ore: Uraninite, coffinite; galena, hematite Alteration minerals: Sericite, chlorite, tourmaline, hematite, illite, kaolinite; muscovite, rutile (Gandhi, 2007) (Cloutier et al., 2009)

Table 2.3 Classification of Planar Hydrous phyllosilicates

Interlayer material[a]	Group	Octahedral character[b]	Species
1:1 Clay minerals			
None or H2O only, z ~ 0	Serpentine–kaolin	Tri	Amesite, berthierine, brindleyite, cronstedtite, fraipontite, kellyite, lizardite, nepouite
		Di	Dickite, halloysite (planar), kaolinite, nacrite
		Di–tri	Odinite
2:1 Clay minerals			
None, z ~ 0	Talc–pyrophyllite	Tri	Kerolite, pimelite, talc, willemsite
		Di	Ferripyrophyllite, pyrophyllite
Hydrated exchangeable cations, z ~ 0.2–0.6	Smectite	Tri	Hectorite, saponite, sauconite, stevensite, swinefordite
		Di	Beidellite, montmorillonite, nontronite, volkonskoite
Hydrated exchangeable cations, z ~ 0.6–0.9	Vermiculite	Tri	Trioctahedral vermiculite
		Di	Dioctahedral vermiculite
Hydrated exchangeable cations, 0.6> z <0.9	Illite	Tri	Trioctahedral illite
		Di	Illite, glauconite
Non-hydrated monovalent cations, z ~ 0.6–1.0	True (flexible) mica	Tri	Biotite, lepidolite, phlogopite, etc.
		Di	Celadonite, illite, glauconite, muscovite, paragonite, etc.
Non-hydrated divalent cations, z ~ 1.8–2.0	Brittle mica	Tri	Anandite, bityite, clintonite, kinoshitalite
		Di	Margarite
Hydroxide sheet, z variable	Chlorite	Tri	Baileychlore, chamosite, clinochlore, nimite, pennantite
		Di	Donbassite
		Di–tri	Cookeite, sudoite
Regularly interstratified 2:1 clay minerals			
z Variable		Tri	Aliettite, corrensite, hydrobiotite, kulkeite
		Di	Rectorite, tosudite

[a]z, net layer charge per formula unit; [b]tri, trioctahedral; di, dioctahedral.
Source: Adapted from Bailey (1980a, b), Martin et al. (1991) and Bergaya and Lagaly (2013).

2.6 Clay Minerals: Structures and Properties

Most clay minerals are hydrous aluminium phyllosilicates constructed from tetrahedral and octahedral sheets. A classification of planar hydrous phyllosilicates is presented in table 2.3. These minerals may contain variable amounts of iron, magnesium, alkali metals, alkaline earths, and other cations. These minerals have variable compositions but possess platy morphology and 1–directional cleavage (Moore and Reynolds, 1997).

The basic structure of the phyllosilicates is composed of sheets of interconnected SiO_4 tetrahedra with the basic structural unit is $Si_2O_5^{2-}$. A tetrahedral sheet (T) is made of SiO_4 tetrahedra sharing the basal oxygen at all three corners with three other tetrahedra (Fig. 2.4) (Bennett & Hulbert, 1986; Moore and Reynolds, 1997). Normally this is a hexagonal sheet in which the O-O and Si-O bonds have bond distances of about 2.64 Å (0.264 nm) and 1.62 Å (0.162 nm), respectively. Al^{3+} and Fe^{3+} may replace the Si^{4+}. An octahedron is a pack of six oxygen and/or hydroxyl ions around a cation site (Moore and Reynolds, 1997). The common octahedral cations are Al^{3+}, Mg^{2+}, Fe^{2+} and Fe^{3+} etc. The cation-to-anion ratios in the octahedral sheets give rise to two groups of phyllosilicates, brucite-like dioctahedral and gibbsite-like trioctahedral. In dioctahedral sheet silicates each O or OH ion is surrounded by 2 trivalent cations, usually Al^{+3}, whereas each O or OH ion is surrounded by 3 divalent cations, like Mg^{+2} or Fe^{+2} in the trioctahedral sheet silicates. The cation-to-anion ratios are 1:2 and 1:3 in the dioctahedral and trioctahedral sheets, respectively.

The tetrahedral and octahedral sheets can be linked to give rise 1:1 and 2:1 layer silicates (Fig. 2.5). The free corners of all apical oxygen atoms in the tetrahedral sheet point to the same side of the sheet and connect tetrahedral and octahedral sheets to form a common plane with the octahedral anionic position (Brigatti et al., 2013).

The structures of the clay minerals and their interaction with other substances (water, organic compounds etc.) give them special properties (Moore and Reynolds, 2001). Some of the well observed properties are their surface charges, cation-exchange capacity, swelling and high surface area.

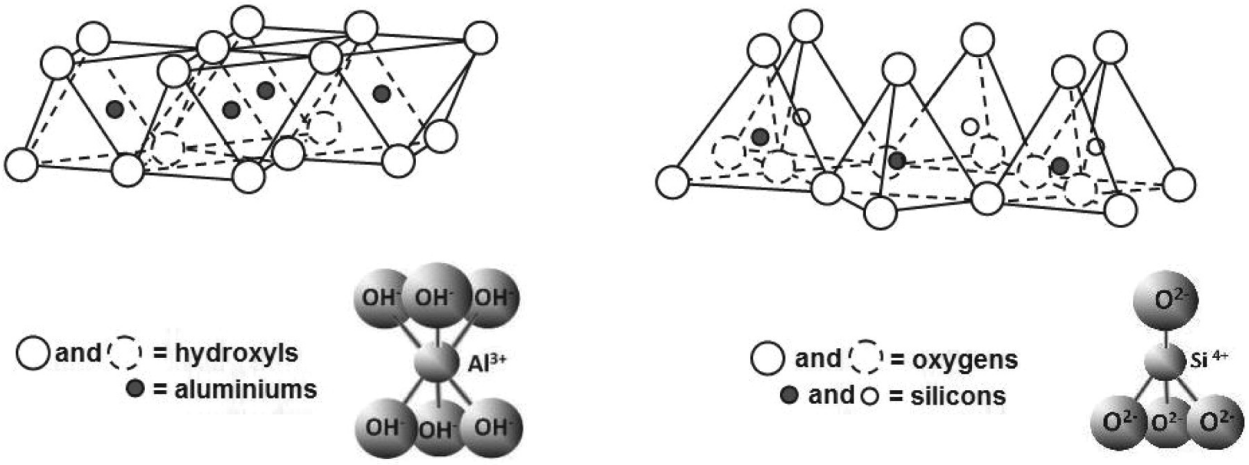

Figure 2.4 Structure of an alumina octahedral sheet (left) and a silica tetrahedral sheet (right) (modified after McLaren & Cameron, 2000; Floody et al., 2009).

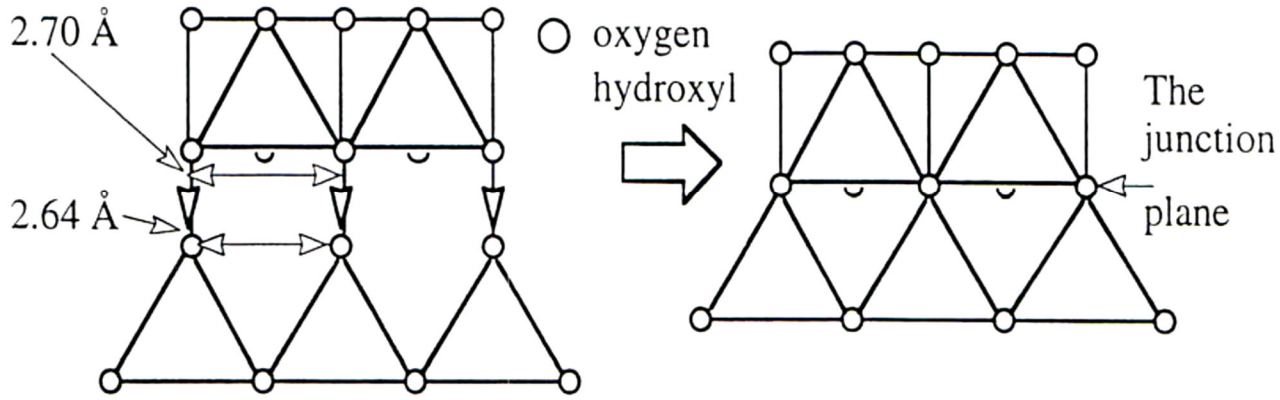

Fig. 2.5 Joining octahedral and tetrahedral sheets together to form a 1:1 layer silicate (Moore & Reynolds, 1997).

2.6.1 The 1:1 clay minerals

The assemblage of one tetrahedral sheet and one octahedral sheet is called a 1:1 layer silicate structure, or TO layer (Moore and Reynolds, 1997). The unit cell of TO layer consists of six octahedral sites and four tetrahedral sites. Each layer is approximately 0.7 nm thick. The apical oxygen atoms (Ox_b) of the tetrahedral sheet and the octahedral anions (Ox_o) of the octahedral sheet form the two surfaces of the TO layer respectively (Fig. 2.6). Typically, Si^{4+}

occupies the tetrahedral cation sites and all Al^{3+} or all Mg^{2+} occupies the octahedral cation sites. As a result, the 1:1 layer type (TO) have zero to a minute layer charge. In case of any substitution in one sheet, overall neutrality of the TO layer is maintained by substitutions in the other sheet. The kaolin group consists of dioctahedral 1:1 layer structures with the general composition of $Al_2Si_2O_5(OH)_4$ and Z=0.

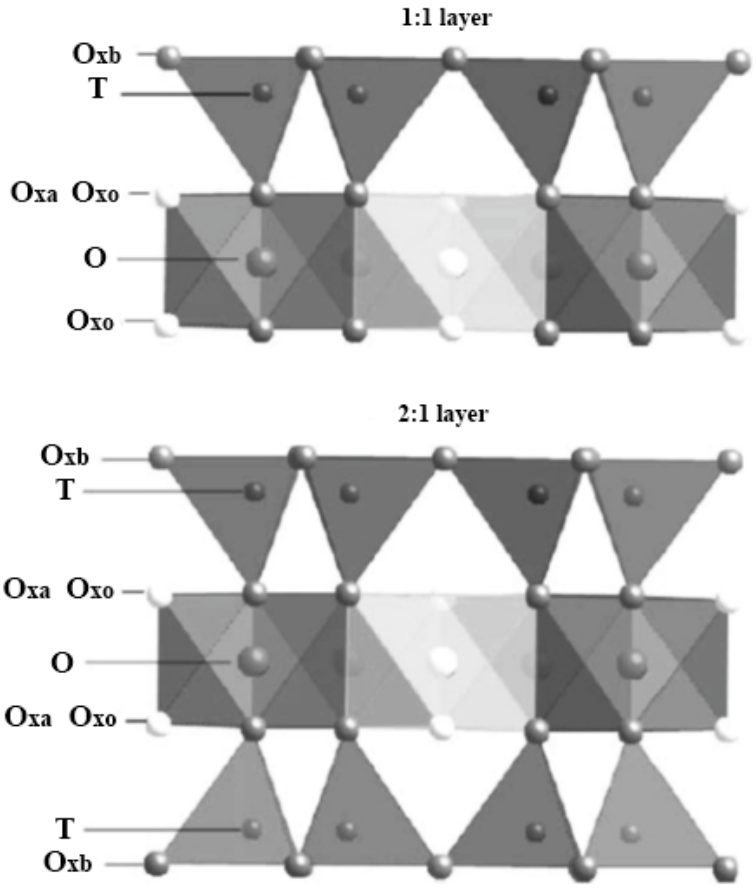

Figure 2.6 Models of 1:1 and in 2:1 layer structures. Oxb, basal oxygen atoms; T, tetrahedral cations; O, octahedral cations; Oxa, apical oxygen atoms; Oxo, octahedral anions (OH, F, Cl) (modified after Brigatti et al., 2013).

2.6.2 The 2:1 clay minerals

A 2:1 clay layer (TOT layer) consists of an octahedral sheet packed in between two tetrahedral sheets (Fig. 2.6). In this type of structure, the unit cell contains six octahedral and

eight tetrahedral sites. The tetrahedral sheets point towards reverse directions. Tetrahedral apical oxygen atoms substitute two-thirds of the hydroxyl group (Brigatti et al., 2013). Examples of 2:1 clay layer clay minerals are talc, micas, vermiculite and montmorillonite.

There are usually three octahedral sites with non-equivalent symmetry (Drits et al., 2006). They are referred to as trans-site (M1), and cis-sites (M2 and M2'). These sites are not always occupied by cations. For instance, one of the cation sites remains vacant in dioctahedral phyllosilicates. Depending on the position of the OH groups with respect to the vacant site, it can be either cis-vacant or trans-vacant. It is cis-vacant or trans-vacant if OH groups are in the same side or in the opposite side with respect to the vacant site respectively (Sainz-Diaz et al., 2001).

2.6.3 The 2:1:1 clay minerals

These clay minerals are phyllosilicates with a talc like 2:1 (T-O-T) layer alternates with a brucite-like octahedral interlayer sheet. Brucite interlayer is composed of $(Mg^{2+}, Fe^{3+})(OH)_6$. Trioctahedral chlorites are the most important representatives of this structure (Bailey, 1975).The crystal unit contains two silica tetrahedral sheets and two magnesium-dominated trioctahedral sheets building the 2:1:1 or 2:2 type structure. The negative charge in the talc layer is the result of substitution of Al^{3+} for Si^{4+} in the tetrahedral sites. The octahedral sheet is positive charge in charge as trivalent cations (Al^{3+}, Fe^{3+}) replace bivalent cations (Mg^{2+}, Fe^{2+}).

2.6.4 Mixed-layer clay minerals

Mixed-layer clay minerals are composed of alternation of two or more layer types (Hendricks and Teller, 1942; MacEwan, 1958; Reynolds, 1967, 1980; Plancon, 1981; Bethke and Reynolds, 1986; Drits et al., 1997; Brigatti et al., 2013). The possible ways the layers can vertically stake are ordered, random or partly ordered (Reynolds, 1980; Wilson, 1987) (Fig. 2.7). Ordered staking structure shows unique properties than the original layers and recognized by its 001 refection in XRD spectrum (Sawhney, 1989). The 001 basal reflection in this case is a result of a supercell along the C direction (Brigatti et al., 2013). It equals to the sum of the spacings of each individual layer (Sawhney, 1989). In randomly staked mixed-layer clay minerals, the original layers are interstratified without any sort of order (Brigatti et al., 2013). Corrensite and illite-smectite are the examples of orderly and randomly staked clay minerals respectively.

A parameter known as Reichweite (R) is commonly used to characterize the degree of order in the interstratified clay layers (Reynolds, 1985; Drits, 2003). The R is equal to zero for random staking of layers. Conversely, R is >1 in ordered mixed-layer clay minerals.

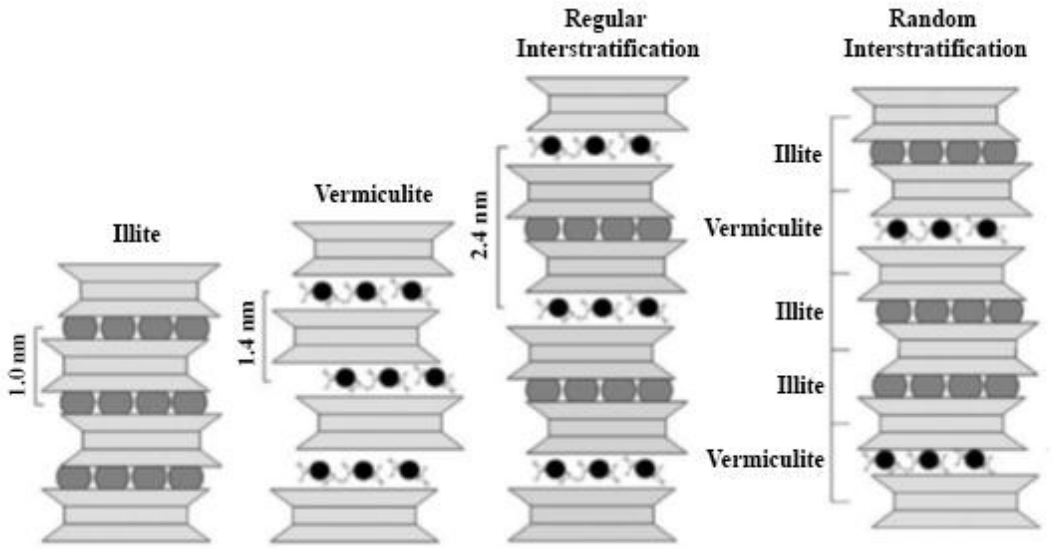

Figure 2.7 Regular and random interstratified clay minerals.

2.6.5 Layer Charge and Variable Charge

Clay minerals carry charges on their large surface area. The distribution of charges is the basis for cation exchange, swelling and adsorption of water and other molecules (Eslinger and Pevear, 1988; Moore and Reynolds, 2001). There are two kinds of charges on the clay surfaces. Layer charges are permanent and result of isomorphic substitutions, whereas surface charges are pH dependent (Eslinger and Pevear, 1988).

Layer charge occurs as one element substituting for another one of a different valence state without altering the structure. For example, Al^{3+} substitutes for $Si^{4+}$and Mg^{2+}/Fe^{2+} substitute for Al^{3+} in the tetrahedral sheets and octahedral sheets, respectively. As a result, the structural layer achieves a net negative charge.

Variable charges occur at the broken edges dominated by charge-unsatisfied dangling bonds and exposed OH-terminated planes of clay layers (Van Olphen, 1963; Johnston and Tombácz, 2002). H^+ or OH^- ions are attracted to the broken bonds to maintain the chemical

composition and structure. However, this charge is referred to as variable charge because it depends on the pH of the surrounding medium. At low pH, clay mineral surface adsorbs H^+ ions and as a result surface becomes positively charge. At high pH, negative charge increases since H^+ ions dissociate from the mineral surfaces.

2.6.6 Cation exchange capacity

Clay minerals have charges on the surfaces and obtain electrical neutrality by adsorbing cations on them. The cation exchange capacity of soils (CEC) is the sum of positive (+) charges of the cations that a clay mineral can adsorb at a given pH and is available for exchange with solution. Ca^{2+}, Mg^{2+}, H^+, K^+, and Na^+ are some common exchangeable cations in clay minerals. These cations are adsorbed to the clay surfaces by electrostatic forces and are easily exchangeable with the cations in the solution. The permanent layer charges and the negative variable charges along broken bond edges of the clay minerals are responsible for the CEC. The variable charges are main causes of the CEC in kaolinite and smectite, respectively. Both types of charges play significant roles in illite and chlorite. As the CEC is pH dependent, it increases at near-neutral pH than under acidic conditions. In pH range of 5 to 7, the CEC gets close to zero. The ranges of the CEC in some important clay minerals are presented in Table 2.4. The CEC values in montmorillonite and vermiculite are many times higher than that in illite or kaolinite (Moore and Reynolds, 1997; Sparks, 2003).

Table 2.4 Cation Exchange Capacities of Clay Minerals (Grim, 1962; Sparks, 2003).

Clay Minerals	CEC (cmol/kg)
Kaolinite	2-15
Chlorite	10-40
Illite	10-40
Montmorillonite	80-150
Vermiculite(Trioctahedral)	100-200
Vermiculite (Dioctahedral)	10-150

CHAPTER 3

GEOCHEMICAL AND MINERALOGICAL ANALYSIS

3.1 Inductively Coupled Plasma Spectrometry (ICP-MS)

Inductively coupled plasma mass spectrometry (ICP-MS) detects metals and several non-metals at concentrations down to parts per trillion (ppt) levels. The main advantages of ICP-MS relative to atomic absorption spectroscopy (AAS) and ICP atomic emission spectroscopy (ICP-AES) are greater speed, detection limits to parts per trillion (ppt) levels and isotopic analysis. ICP-MS can measure more than 70 elements quantitatively and semi-quantitatively (Olesik, 2014). However, there are some disadvantages of this techniques, i.e. dissolved solids/matrix effects (need to dilute samples).

Some of the main components of ICP-MS are sample introduction system, argon plasma generator, vacuum system, collision/reaction cell, mass spectrometer and detector (Beauchemin, 2008). A nebulizer and spray chamber system convert the samples into aerosol droplets (Hall, 1992). The argon plasma dehydrates the aerosol, separates the molecules and removes an electron from them to form singly-charged ions. The ions pass through a series of quadrupoles and are detected by a mass spectrometry on the basis of their mass-to-charge ratio (Hall, 1992; Beauchemin, 2008). A detector measures signals generated from the collision between the ions and the detector. A computer program compares measured signals to those from the standards.

3.2 X-Ray Diffraction

X-ray diffraction (XRD) collects information on an atomic scale from crystalline and amorphous materials. The impact between the X-rays and the phases generates diffraction patterns. Every phase has a definite diffraction pattern. X-rays are high-energy electromagnetic radiation. Their energy ranges from about 100eV to 10MeV and places in between gamma-rays and ultraviolet radiation in the electromagnetic spectrum (Waseda et al., 2011). These rays are produced by the interactions between an external beam of electrons and the electrons in the shells of an atom. The wavelength of the X-rays can be written as

$$\lambda = hc/E$$

where λ is wavelength of the X-ray, c is 2.998 x 10^8 ms^{-1}, h is Planck's constant (4.136 x 10^{-15} eV.S) and E is the energy. The useful range of wavelengths for XRD studies is between 0.05 and 0.25 nm (Suryanarayana and Norton, 1998).

X-rays are generated in a tube consisting of two electrodes enclosed in a vacuum chamber. When a tungsten filament cathode is heated, it produces electrons. The electrons are accelerated towards the metal anode using high voltage energy (Waseda et al., 2011). The high-speed electrons collide with the anode and loss kinetic energy. The loss of energy of the electrons is manifested as X-rays (Suryanarayana and Norton, 1998; Waseda et al., 2011)

When a crystal is bombarded with X-rays of a fixed wavelength and at certain incident angles, intense reflected X-rays are generated when constructive interference occurs. As a result, a diffracted beam of X-rays will leave the crystal at an angle equal to that of the incident beam (Fig. 3.1). A detector collects the diffracted X-rays and rotates at an angle of 2θ.The general relationship among the wavelength of the incident X-rays, angle of incidence and spacing between the crystal lattice planes of atoms is known as Bragg's Law. Bragg's equation is expressed as:

$$n\lambda = 2d\sin\theta$$

where n is the order of reflection, λ is the wavelength of the incident X-rays, d is the interplanar spacing of reflecting planes and θ is the angle of incidence. The interplanar spacing (d-spacing) of a crystal is used for identification and characterization purposes. One of the widespread uses of XRD is identification and quantification of multiple phases in powdered rocks. The detection limit of this techniques ranges from 2 to 3 wt% (Beaufort et al., 2005), which is a disadvantage

for trace minerals analysis.

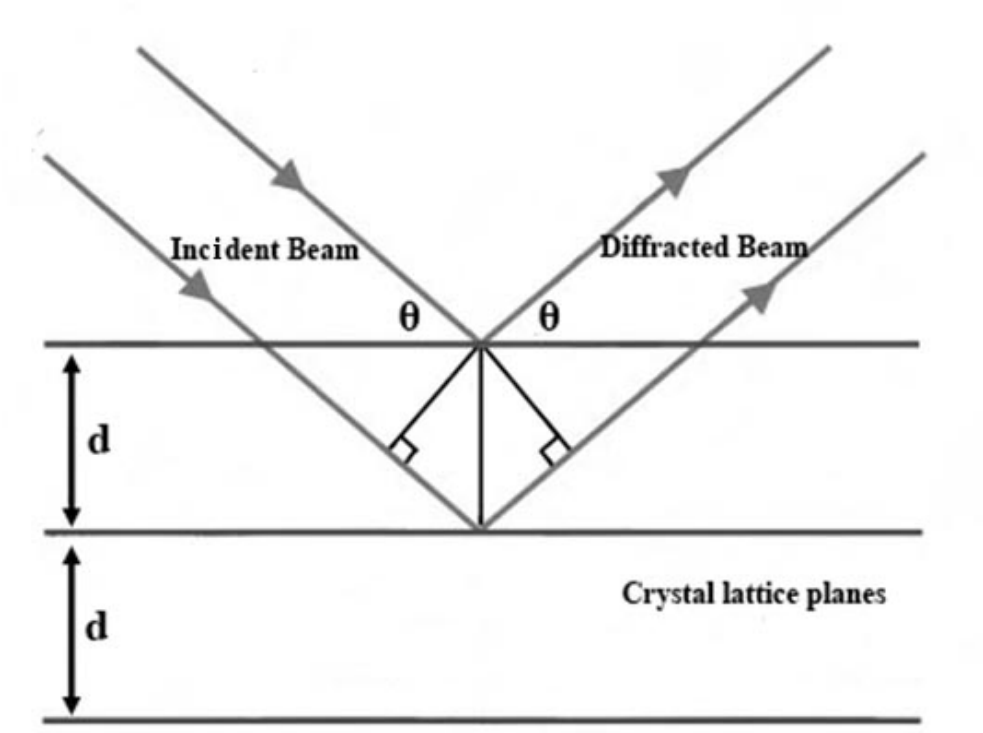

Figure 3.1 Bragg diffraction

3.3 Electron Probe Micro-analyzer (EPMA)

An EPMA is an analytical tool used to non-destructively determine the chemical composition of small volumes of solid materials. It works similarly to a scanning electron microscope: the sample is bombarded with an electron beam, emitting X-rays at wavelengths characteristic to the elements being analyzed (Jansen and Slaughter, 1982). This enables the determination of the abundances of the elements present within a sample (Wittry, 1958).Micro-textures that are invisible under light microscopy become resolvable in this technique. .

A typical configuration in a probe is a vertical electron-beam column, an array of detectors placed around the sample chamber block, a sample entry vacuum lock, a console to control operating conditions, screens to view control interfaces and sample output, and a computer for data acquisition. The conditions desirable for proper analysis of phases of interest

are dependent on the elements to be analyzed and the detection limits required. For routine analysis of rock forming silicates 15 kV voltage and 10 to 12 nA current are sufficient. On the other hand, analysis of sulphides requires 20 kV voltage and 15-20 nA current. A beam diameter of 1-20 microns is commonly used depending on the nature of the sample and requirements.

The characteristics of the X-rays are used for qualitative to quantitative chemical analysis. Wavelength dispersive X-ray spectroscopy (WDS) or energy dispersive X-ray spectroscopy (EDS) collects and counts X-ray wavelengths or energy spectrum. EDS distributes the energy spectrum into different ranges. Each range corresponds to specific element. WDS system separates X-rays of different wavelengths. The spectrometer consists of an analyzing crystal and a detector. Only X-rays of a given wavelength enters the detector at any given time. To measure another wavelength, the crystal and detector move to a new position. Therefore, a WDS system usually has an array of spectrometers to work efficiently. The detection limits of WDS generally ranges from 100 to 300 parts per million (ppm), depending on the mean atomic number of the matrix and x-ray counting times.

EPMA is also capable of different types of imaging, i.e. secondary electron (SEI) image, backscatter electron (BSE) image and elemental X-ray mapping. SEI image provide topographic information about a sample, e.g. grain morphology. BSE image is the result of the mean atomic mass a material. A definite BSE gray value is assigned to a sample depending on the mean atomic mass of the material. The BSE image of a material with higher atomic mass will be brighter than that of a lower atomic mass. Elemental X-ray maps show the two-dimensional distribution of elements on the surface of a material. Elemental X-ray maps are produced by rastering an electron beam over a rectangular area and recording the energy ranges for a specific element.

3.4 Automated Mineralogy

Automated mineralogy (both qualitative and quantitative) helps the process mineralogists to predict the ore behavior during the milling process, design the mill flowsheet and mass balance. Two major systems are available, Mineral Liberation Analyzer (MLA) and QEMSCAN. These systems are SEM-based mineralogical software programs. Metallurgists generally use

these systems for characterizing ores and mill feeds. A key use of this technique is quantitative phase analysis. Mineral abundance and an empirical balance between the mill feeds and the solid residues (as part of final tailing) can predict the behavior and contribution of different minerals in weathering conditions (Price 2009).

Mineral characterization begins with the collection of representative samples. The sample integrity must be preserved during collection, storage and sample preparation. Chemical analysis of the sample can be used to estimate the presence of minerals with acidic and neutralizing abilities, quantify the trace metals, and determine whole rock composition. The chemical analysis are usually destructive, such as using acid digestion or fusion followed by Atomic Absorption Spectroscopy (AAS) or Inductively Coupled (Argon) Plasma spectrometry (ICP), or non-destructive, such as using X-ray Fluorescence (XRF) Spectroscopy.

Optical microscopy (reflected or polarized light), x-ray diffraction (XRD), and scanning electron microscope (SEM) in conjunction with an energy or wavelength dispersive spectrometer (EDS and WDS, respectively) can be used to determine the mineralogy. XRD cannot be used to identify amorphous minerals, which often include the secondary phases generated during the ore processing and weathering processes within the tailings (e.g. iron oxyhydroxides and aluminosilicates). The application of the Rietveld method can establish the quantity of amorphous content (PANalytical, 2009). Analyses can be augmented by SEM which has a higher magnification capability than optical microscopy. WDS (and improved EDS) can be used to quantify the lower atomic number elements (i.e. ≤ 6). The mineralogical analysis determinations are improved if the samples are analyzed as polished thin sections, which are about 30 μm thick slices of whole rock. The combination of SEM and X-ray analysis vastly improves the ability to obtain compositional information for the smaller particle grains and fine features such as particle rim coatings (Sutherland et al., 1988).

Ore processing requires the detailed specification of mineral characteristics, both composition and texture, and quantification. These data are important because different types of metal-bearing ore mineral and gangue can have different effects on mill performance. The liberation of ore minerals depend on their textures (Lorenzen and van Deventer, 1994). The quantification of the relationship between texture and liberation was a major problem until the recent developments of automated mineralogy (MLA/QEMSCAN).

Quantitative mineralogical studies are traditionally performed manually using point-counting techniques which are time-consuming and prone to human error. Automated techniques offer the advantages of increased number of particles examined in terms of grain size distribution, liberation and modal mineralogy.

Automated mineralogy includes the modern tools which collect and analyse mineral data with some degree of automation. It relies on three key operations — the automatic identification of the minerals, the creation of an image representing the mineral sample and, finally, the analysis and measurement of the resulting image (Sutherland and Gottlieb, 1991). These technologies integrate Scanning Electron Microscopy (SEM), Energy Dispersive X-Ray Spectrometry (EDS) and imaging software to compile detailed analysis of mineral samples. One of the main advantages of these techniques is quantitative mineralogical data which used to be inferred from chemical analysis or XRD. It also provides valuable information on mineralogy and how they occur spatially (texture).

Most studies relate to the study of sulphides, especially of base metals and PGM. Initially, these techniques have been applied to study grinding, liberation and flotation problems. Examples vary from mill to experimental experiments with intention to expand the understanding of the fate of complex particles. Other aspects of ore beneficiation and processing such as grain size measurements, ore characterization of both sulphides and non-sulphides. In this current study, automated mineralogy was used for grain size measurements, liberation and modal mineralogy of U ores.

3.4.1 Mineral Liberation Analysis

Mineral liberation analysis is an important tool for characterizing applied mineralogy and metallurgical processing (Jones, 1987; Petruk, 1986, 1988, 2000; King, 1993). Mineral liberation data are fundamental parameters used in processing plant design and optimization (Gu, 2003; Fandrich et al., 2007).

It is a quantitative mineralogy system that integrates Scanning Electron Microscopy (SEM) and Energy Dispersive X-Ray Spectrometry (EDS) analysis technologies (Gu, 2003; Fandrich et al., 2007). It was developed by Ying Gu at University of Brisbane in association with JKC Tech, and first presented in 1997 (Gu and Napier-Munn, 1997). It was initially designed to

obtain detailed information on the ores and mill feeds in terms of grade recovery, liberation and mineral abundance (Gu 2003, Fandrich et al. 2007; Davis 2013). It reduces operator dependence, collects quantitative data that is reproducible and allows sophisticated imaging that allows for analysis of very fine-grained material (Pirrie et al., 2004). The definition of mineral liberation varies. The most useful definition for the present study is the dissociation of a mineral or phase of interest into a free particle consisting exclusively of that mineral (Austin & Luckie 1988).

It is an automated mineral analysis system that can identify and quantify a wide range of mineral characteristics, such as mineral abundance, grain size and liberation. The main image analysis functions used in the MLA include de-agglomeration and segmentation. Three key benefits of the MLA system are that: (1) Automated searches for trace or rare minerals are based on TV-rate image scanning (and are hence rapid), (2) X-Ray resolution is keyed directly to the integrated EDS X-ray system and (3) The use of a Field Emission Gun (FEG) electron source, rather than a traditional W-filament electron source by conventional SEM (Gu, 2003). The result is superior spatial and X-ray resolution with the capability of locating and positively identifying even sub-micron sized minerals, with improved confidence in data and more cost-effective instrument utilization and throughput. The minerals can be reported up to 0.01 wt%, which makes it very useful in studying trace minerals, where other traditional methods (e.g. XRD) are less useful. Disadvantages of the MLA are similar to EPMA, e.g. difficulty of distinguishing minerals with very similar compositions (*e.g.*, pyrite vs marcasite), inability to distinguish polymorphs (*e.g.*, rutile vs anatase) etc.

This automated mineral analysis technique (MLA/QEMSCAN) has already been used in several mineral industries to study Process diagnosis, flowsheet design and optimization. The relationship between mineralogy and metallurgical performance in a plant was recognised long ago (Petruk, 1976; Petruk and Hughson, 1977; Cabri, 1981; Petruk and Schnarr, 1981; Peyerl, 1983; Petruk, 1988, for example) to provide analytic sampling techniques of a plant (Restarick, 1976) and to improve the statistical reliability of mineralogical and process measurements (Henley, 1983; Lotter, 1995, 2005). The previous studies have found this technique useful in association with metallurgical test-works to improve metallurgical performance, for example Lesher, (1999), Langlois and Holmes, (2001), Lotter et al. (2002), Lotter et al. (2003), Fragomeni et al. (2005), Charland et al. (2006), Lotter and Laplante (2007), Dai et al. (2008),

McKay et al. (2007), Triffett et al. (2008), Xstrata Nickel (2008) and Goodall and Scales (2011). However all these works have been performed on Ni, Cu, Gold and PGE (Platinum Group Elements) minerals. Not much works have been done on mineralogical characterization and liberation of U and associated minerals (Lottering et al., 2008; Bowell et al., 2011).

In the current study, MLA was used to obtain an improved understanding of the ore feeds and the residues they produce after ore processing.

3.4.2 Instrumentation and Performance

MLA works by taking and analysing back-scatter electron (BSE) images. Generation of high quality and low noise images is essential for mineral identification and quantification (Gu, 2003). It is done by the latest hardware that is stable during an extended period of measurement time (Gu, 2003). Boundaries among mineral grains are distinguished based on brightness contrasts in the BSE image. The backscattering coefficient η is the number of electrons backscattered by a mineral (N_{BSE}) relative to the number of incident electrons from the SEM (N_{IE}) where,

$$\eta = N_{BSE} / N_{IE}$$

and is a function of the average atomic number (Z) of the mineral (Heinrich 1966) (Fig.3.1), $\eta = -0.0254 + 0.016\ Z - 0.000186\ Z_2 + 8.3\times10^{-7}\ Z_3$. As a result minerals with heavier elements (e.g., uraninite) appear brighter in the BSE image; whereas minerals composed of lighter elements (e.g., quartz) appear darker (Sylvester, 2012). The MLA attains BSE data as a 256 level grey scale image (0 = black, 255 = white). The η value for each mineral is then related to a range of greyscale values between 0 and 255 (Sylvester, 2012). The main image analysis functions used in the MLA are de-agglomeration and segmentation (Gu, 2003; Fandrich et al., 2007).

A 30mm diameter hardened mould is made by setting the particles into epoxy resin. It is then polished to a smooth representative cross-section of particles and subsequently coated with carbon before analysing using SEM. Some particles in this mould are expected to touch each other. If the system failed to distinguish free particles, the agglomeration of particles may lead to unreliable liberation results (Gu, 2003; Fandrich et al., 2007). The automated de-agglomeration

function installed within the MLA system identifies the agglomeration of particles and separates them accordingly (Gu, 2003; Fandrich et al., 2007). The figure 3.2 shows this process.

Particle shape parameters are used to recognize the agglomeration of particles (Gu, 2003; Fandrich et al., 2007). There are three methods to separate the particles, which are: a) shadow or boundary identification, b) linear feature recognition and c) an erosion/dilation procedure (Gu, 2003; Fandrich et al., 2007). The user can adjust the parameters to control the relative weighting to each of the separation method (Gu, 2003; Fandrich et al., 2007).

The next step of the liberation analysis is to recognize all individual mineral phases and define their boundaries. This process is known as phase or image segmentation (Gu, 2003; Fandrich et al., 2007). Figure 3.3 shows the enlarged image of a composite particle. The segmentation results show that it contains 5 mineral grains. The MLA image segmentation function outlines the regions of more or less homogeneous grey level in a particle image (Gu, 2003; Fandrich et al., 2007). The average BSE grey value of every region is directly related to a mineral of unique average atomic number (AAN; Jones 1987). For example, Fig. 3.4 shows a histogram of the grey level distribution of minerals in a lead-zinc ore (Gu, 2003; Fandrich et al., 2007). Phase segmentation also recognize and eliminate features of a BSE particle based on cracks, shading, tiny voids or the dark perimeter or halo that appears around many particles (Gu, 2003; Fandrich et al., 2007).

In the absence of system generated noise, a definite BSE gray value is assigned to each mineral in the sample under a particular set of measurement conditions (Gu, 2003; Fandrich et al., 2007). In practice, however, gray level of a mineral varies over the time period required to analyze a sample. When two minerals having the same average atomic number (AAN), MLA distinguish between them with x-ray analysis.

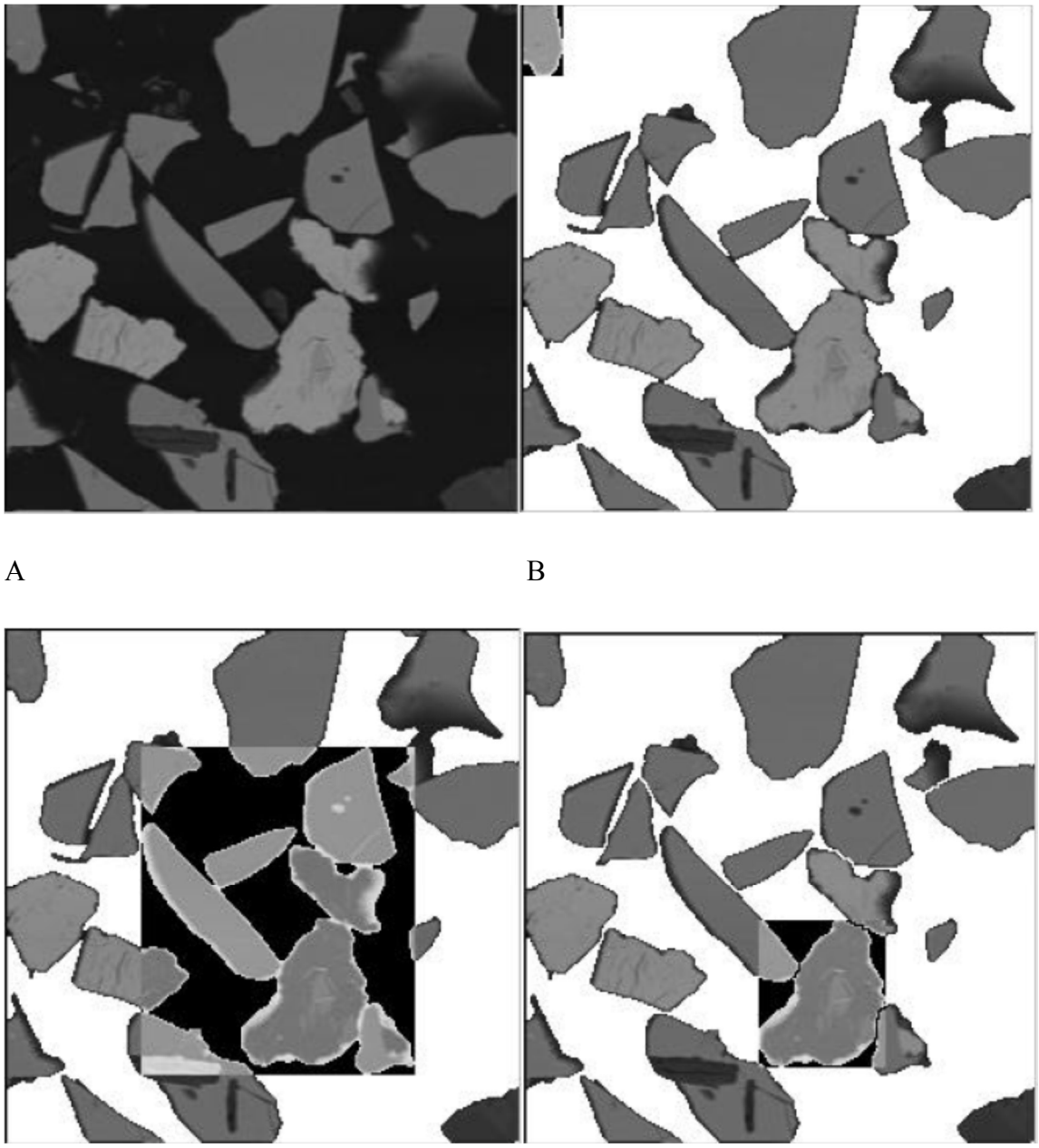

A B

C D

Figure 3.2 Example of de-agglomeration process: (A) Original BSE image. (B) After background removal, several particles show agglomerated. (C) One of the agglomerated particle is highlighted; (D) After de-agglomeration, the agglomerated particle is broken into 6 particles, one of them is highlighted (Fandrich et al., 2007). Reused with permission.

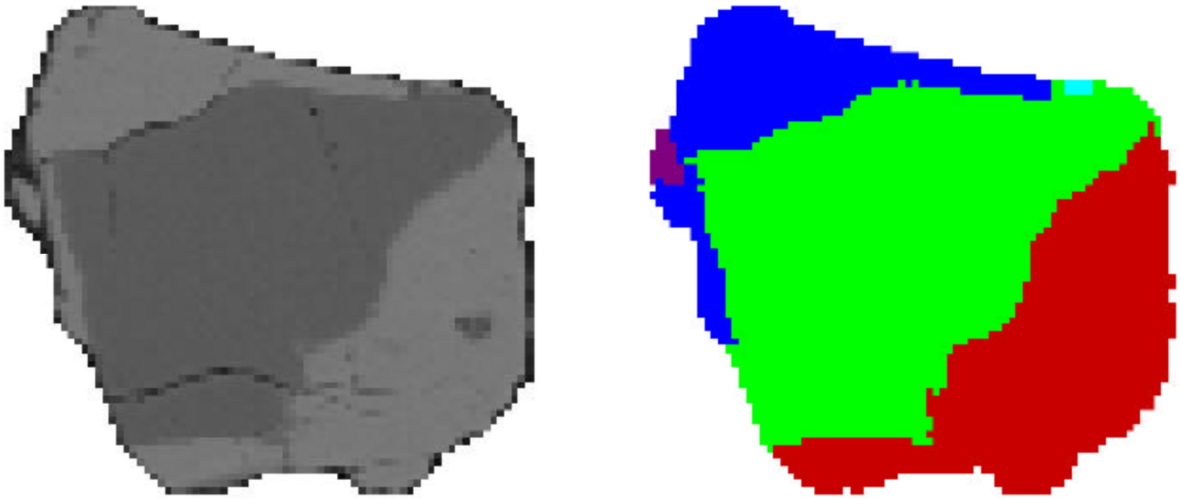

Figure 3.3 Grey level and segmented particle image (Fandrich et al., 2007). Reused with permission.

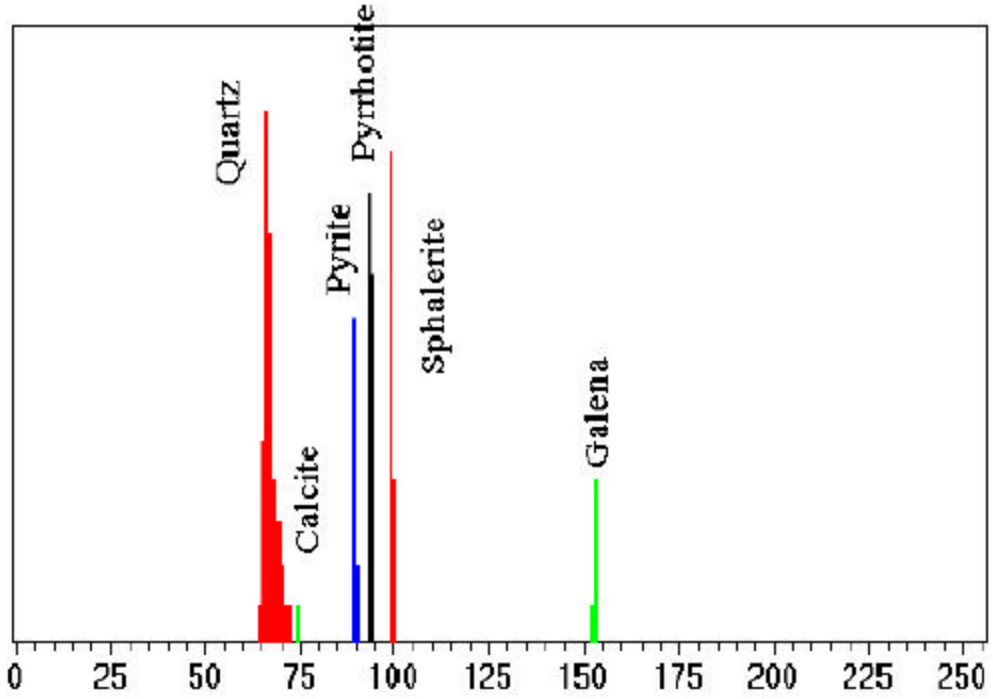

Figure 3.4 Grey level distribution of a typical lead-zinc ores. The x-axis is the BSE grey level and the y-axis is the frequency (Fandrich et al., 2007). Reused with permission.

The MLA uses three X-ray analysis techniques to identify mineral species: point X-ray, area X-ray and X-ray mapping (Fandrich et al., 2007).

i) Point X-ray analysis

MLA executes one x-ray analysis for each gray level area found in a particle (Fandrich et al., 2007). The EDS spectrum is collected at the centre of a phase to avoid overlapping with bordering phases. This spectrum is linked to its corresponding particle and grain in the segmented image to generate an X-ray image.

ii) X-ray mapping

MLA gathers spectra by rastering the beam over the phase area. To avoid overlapping with the surrounding phases/particles, the perimeter of the phase/particle is not scanned during this procedure. This method is very useful where two or more minerals have the same average atomic number (Hall, 1977; Gu and Sugden, 1995; King, 1993). Fig 3.5 illustrates how area X-ray mapping detects two phases where point X-ray analysis identifies the particle as one phase. A regular grid is imposed on a particle image and x - ray data is collected at each grid point to determine the mineral identity.

There are seven basic MLA measurement modes to handle different sample types and to meet different mineralogical information requirements (Gu, 2003). They are:

i) standard BSE liberation analysis (BSE),

ii) extended BSE liberation analysis (XBSE),

iii) sparse phase liberation (SPL) analysis,

iv) particle X- ray mapping (PXMAP) analysis,

v) selected particle X- ray mapping (SXMAP) analysis,

vi) X - ray modal (XMOD) analysis and

vii) rare phase search (RPS) methods.

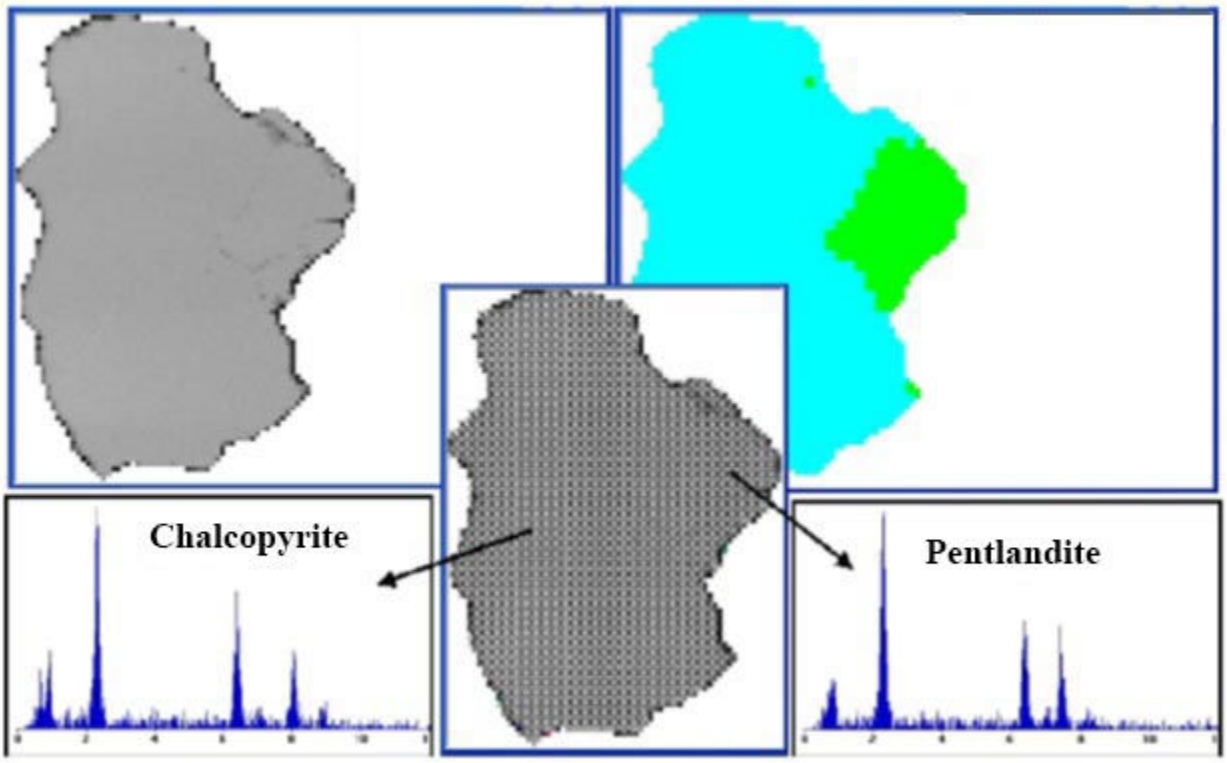

Figure 3.5 Illustration of X-ray mapping for a particle containing pentlandite and chalcopyrite (Fandrich et al., 2007). Reused with permission.

BSE is the most basic method. Several images are gathered and then refined by MLA software to produce liberation data based on BSE grey level distribution. XBSE is a more sophisticated method and widely used for characterizing ores. Mineral grain boundaries are outlined using image segmentation procedures. Image segmentation is followed by area X-ray analysis of individual mineral grain. The particle segmentation data are used to create minerals distribution maps. (Gu, 2003).

CHAPTER 4

MATERIAL AND METHODS

4.1 Mini-mill Design and Sample Collection

Samples of ground McArthur River (McA) and Millennium (MLM) ores, Deilmann (DSW) and Gaertner (GSW) special wastes, McArthur River mineralization waste (McW), three blended mill feeds (S1, S2 and S3) and associated leach residues (LR1, LR2 and LR3) were collected from the Key Lake pilot-mill for chemical and mineralogical characterization of the ore and gangue minerals (Fig. 2.1). Based on the plan for mining operation at the McA and MLM deposits, the ores were blended with three different U bearing (0.3%-0.4% U_3O_8) waste rocks: DSW, GSW, and McW. Their mixing ratios are presented in table 4.1. Current ore from the McA was blended (S1, 5% U_3O_8) to approximate the milling practice at Key Lake. Millennium ore was blended into two different ratios: S2 (5% U_3O_8) with the McArthur ore and special wastes to reflect concurrent mining and milling of these ores, and S3 (2% U_3O_8) with only the special wastes considering absence of the McArthur River ore.

The pilot milling process includes blending, leaching, separating pregnant solution and bulk neutralization of raffinate. The leach slurry was prepared by wet grinding at 50% solids in a 4L grinding mill with 24 rods to achieve 75µm (50% passing). A 25 L stainless steel leaching vessel was used for leaching experiment. The vessel was equipped with oxygen flow (300 KPa), a warming blanket to attain the 60°C temperature required for leaching. The slurry was leached using 96% H_2SO_4 in the presence of strong oxidizing conditions (Eh > 580mV) for 24 hours.

Steady state was fixed at free acid ~30 g/L H_2SO_4 and EMF > 600 mV. At these conditions, the slurries were filtered through a pressure filter and the filtrates were collected as the pregnant aqueous solutions (PAS). The remaining solids in the pressure filter were the leach residues. The leach residues were washed with 2% H_2SO_4 followed with reverse osmosis (RO) water to remove any remaining leached solution in them. The washing procedure repeated until the U_3O_8 concentration was less than 0.1 g/L in the washed solution.

Table 4.1 Ore blends ratios

High Grade (Ratio %)	Scenarios		
	S1, 5% grade	S2, 5% grade	S3, 2% grade
Tonnes -McArthur River (McA) ore	1	0.75	0
Tonnes -Millennium (Me) ore	0	0.25	1
Blended materials (Ratio %)			
Tonnes -KL Deilmann Special Waste (DSW)	0.45	0.3	0.3
Tonnes -KL Gaertner Special Waste (GSW)	0.45	0.5	0.5
Tonnes -McArthur Mineralized Waste (McW)	0.1	0.2	0.2

4.2 Whole-rock Geochemistry

Whole-rock elemental analyses were conducted on samples using a Perkin Elmer NexIon 300D ICP-MS with a relative standard deviation (RSD) of ±10%. EOCs (As, Mo, Ni and Se) along with Ba, Co, Cr, Cu, Fe, Mn, Zn, U, and Pb were analyzed. The samples were dried in oven at 60^0 C for 2 hours and lightly ground with the help of mortar and pestle. In all cases, 0.5 g of ground subsamples was digested in 5 mL of double distilled concentrated hydrofluoric (48-51%) and (16N) nitric acids and left overnight to dissolve (Jenner et al, 1990; Stefanova et al., 2003). Samples were diluted for analysis of the trace metals including EOCs.

4.3 X-ray Diffraction Analysis

A representative portion of each sample (2g) was taken for XRD analysis after additional gentle crushing. Each sample was lightly grinded in ethanol using a ceramic mortar and pestle to make uniformly sized powder. Powder XRD analysis was performed on 4 different size fractions separated from the bulk samples of ores, special wastes and blends and leach residues. The size fractions are < 5, <20, <50 and >50 μm fractions separated by the centrifuging technique.

An Empryrean Pro PANalytical diffractometer equipped with a cobalt target (Cu Kα1 radiation, 1.54 Å), a crystal graphite monochromator, and a scintillation detector was used to

collect the X-ray diffractograms. The operating conditions of the diffractometer were 40 kV and 45 mA. The air dried powder was loaded into an aluminium holder as smear mounts on glass plates and scanned from 2 to $80^0 2\theta$ with a 0.01^0 step and a scan step time of 85 s. Patterns were interpreted with the aid of X'Pert HighScore Plus software using the Powder Diffraction File 2002.

For clay mineral analysis, clay fraction (<2μ) from the powdered samples was separated by centrifugation without chemical pre-treatment (Moore and Reynolds, 1989; Bergaya et al., 2006). The clay fraction was mounted as an oriented aggregate mount for clay-mineral identification using XRD. Oriented aggregate mounts were prepared by the filter-peel technique (Moore and Reynolds, 1997). The samples were run after air-drying, after saturation with ethylene glycol for at least 16 h at room temperature, and after heating for 1 h at 400ºC (Poppe et al., 2001).

4.4 Electron Micro-probe Analysis

Air dried samples were put in cylindrical plugs (5 mm diameter) filled with epoxy, and allowed to harden at room temperature. Afterwards, the surfaces of plugs were polished to analyze them under EPMA. Electron micro-probe analyses were performed on a JOEL JXA-8600 Superprobe Micro-analyzer outfitted with three automated wavelength dispersive spectrometers (JOEL USA, Inc., Peabody, MA) and operated at 15 kV with beam current of 25 nA. Backscattered electron images (BSI) and X-ray elemental maps of As, Ni, Mo, Se, Cu and Fe (WDS) were collected from sulphides and arsenide/arsenate in the samples. Quantitative WDS and qualitative EDS analyses were conducted on the minerals of interest to determine elemental ratios of co-localized EOCs (As, Fe, and Ni) and for mineralogical evaluation. The following X-ray lines and standards were used: S Kα (marcasite), Fe Kα (marcasite), Ni Kα (pentlandite), As Kα (lollingite), Mo Kα (molybdenite), Se Kα (selenite).

4.5 Mineral Liberation Analysis

Mineral Liberation Analyzer (MLA) provides information that cannot be obtained by other analytical techniques, such as mineral abundance, grain size and liberation. It integrates Scanning Electron Microscopy (SEM) and Energy Dispersive X-Ray Spectrometry (EDS) analysis technologies (Gu, 2003; Fandrich et al., 2007). The mineral abundance and liberation

characteristics were studied using FEI Quanta 400 SEM with JKMRC mineral liberation analyzer (MLA) at Memorial University of Newfoundland.

A rotary micro riffler was used to divide larger samples (10g) into smaller representative samples (2g). Representative portions of two size fractions (+38 and -38 µm) of each sample were mixed with epoxy resin in 30mm mounts, polished, and then analyzed using XBSE (Extended BSE liberation analysis) analytical protocol (Fandrich et al., 2007). The samples were analyzed with the MLA software to determine the distribution of the mineral group or phases and their liberation characteristics. Mineral grains were analyzed for elemental content by spot assessment using SEM through the EDS spectrums generated. A number of spectrums were collected for each mineral and were added to the MLA reference database. MLA processes raw particle image and X-ray data into mineral maps, and measures parameters such as liberation, mineral grain sizes, mineral locking and mineral associations (Fandrich et al., 2007).

4.6 Cation Exchange Capacity

A simple direct $BaCl_2$ exchange procedure was used to determine the CEC of the samples under their pH conditions (Gillman, 1979, Gillman and Sumpter, 1986; Hendershot and Duquette, 1986). Hendershot and Duquette (1986) showed CEC calculated from the sum of the exchangeable cations (Al, Ca, Mg, Na, and K) in the extract by $BaCl_2$ exchange provides identical results for acidic solids as the other methods. 0.1M $BaCl_2.2H_2O$ extracting solution was prepared by dissolving 24.428 g of barium chloride ($BaCl_2.2H_2O$) in 1000 mL of distilled water. 2g of the dried solids and 20 mL of 0.1 M $BaCl_2.2H_2O$ were added in a 50mL centrifuge tube. Then the tube was shaken for 2 hours. After centrifuging, direct measure for CECe can be obtained at this point by measuring Ca, Mg, K, Na and Al in this extract by ICPMS (Hendershot and Duquette, 1986). The equation used for ICPMS results in mg/L was-

$$\text{CEC (cmol/kg)} = \frac{Ca}{20} + \frac{Mg}{12} + \frac{K}{39} + \frac{Na}{23} + \frac{Al}{9} \qquad (1)$$

CHAPTER 5

RESULTS AND DISCUSSION

5.1 Elemental analysis

The elemental concentrations of important metals and metalloids for all samples are summarized in Table 5.1 and illustrated in Fig. 5.1. The most abundant analytes in order of abundance were U, Fe and Pb with minor amounts of trace metals and metalloids. The total assay of the elemental concentrations was considerably higher in McA compared to MLM and wastes samples (DSW, GSW and McW). Significant decreases in concentrations of the total assay in leach residues after the milling of the blends were observed. The percentages of the leached solids in S1, S2 and S3 were 61 %, 88% and 67% respectively. Elemental analysis showed that significantly greater eaching was achieved for blends made by mixing the two ores. This result supports the general hypothesis that blends of ores with similar metallurgical properties (e.g. hardness) display synergistic metallurgical performances (Van Tonder et al., 2010).

The highest concentrations of As and Ni were found in the Gaertner special waste, whereas the Millennium ore was substantially Mo rich. These attributes are most probably due to the higher proportion of Ni- and As-bearing sulphides in the Gaertner special waste (Von Pechmann, 1985), and Mo-bearing sulphide in the Millennium ore. The differences in the distribution of As, Ni and Mo related to the quantities of As, Ni, As, Co, Mo and Fe-bearing sulphides in the different ores and special wastes (Shaw et al., 2011; Donahue and Hendry, 2003). Selenium occurred in trace amounts in all the ore and special waste samples with a relatively higher amount in Millennium ore. Three different ore blends were considered to run acid leaching for U processing. Both As and Ni have similar distribution within the ore blends and their corresponding leach residues and positively correlated (Fig. 5.3). These two elements show a general trend of abundance, S 1 > S2 < S3 and LR1 > LR2 < LR3 (Fig. 5.2). Se was most likely associated with the Mo as shown a positive correlation in the blends (Fig. 5.3). The highest and lowest amounts of U in leach residues are found in the leach residues 1 and 2 respectively (Fig. 5.2). It is apparent from the elemental analysis that the optimum level of EOCs removal except for Pb and Se was found in the S2 (Fig. 5.2).

Concentrations of U, Pb, Ba, Ni, As, Mo, Cu, Cr, Co and Se for all the leach residues are either higher or near the background ranges observed in crustal rocks (Table 2; Rudnick & Gao, 2003; Taylor, 1964). U, Pb, Ni, As, Mo are enriched in the leach residues over average crustal abundances by several orders of magnitude. Moreover, leach residues 1 and 3 contain As and Ni values in concentrations higher than those in the original ores. U in the leach residues was due to the residual U minerals, i.e. U-Ti oxide, uraninite and coffinite. However, the total elemental analysis of the residue samples does not infer anything about the distribution of EOCs in different phases or fractions. Quantitative phase analysis was carried out to account for the distribution of these elements in different mineral phases.

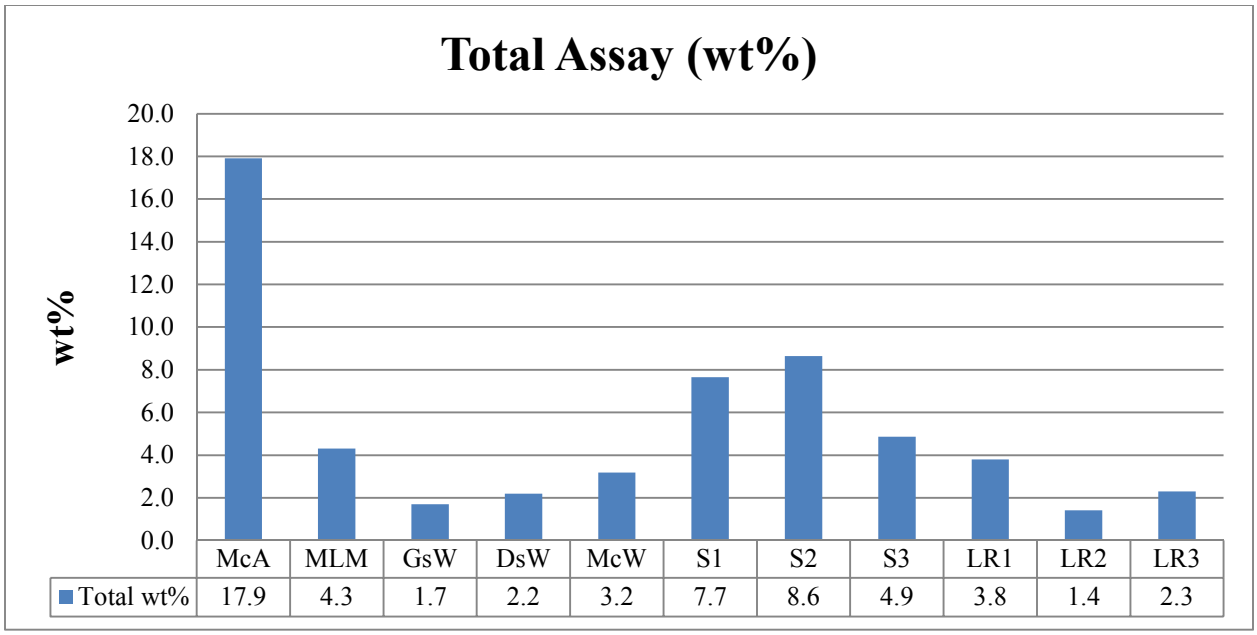

Figure 5.1 Total concentrations of EOCs, base metals, U and Pb in the ores, wastes, blends, and leach residues.

Table 5.1 Metal compositions of ores, blends and leach residues.

Elements	Units	MCA	MLM	GSW	DSW	MCW	S1	S2	S3	L.R1	L.R2	L.R3	Crustal Abundance*
As	µg/g	119.88	96.96	1826.70	221.24	45.05	628.61	549.46	549.71	283.50	82.43	261.52	2.5
Mo	µg/g	377.89	849.72	17.86	42.95	89.01	104.72	231.48	432.03	107.78	104.31	317.82	0.8
Ni	µg/g	92.24	143.72	1687.00	200.15	81.83	609.27	535.38	553.02	399.10	164.00	353.22	75
Se	µg/g	12.99	26.44	8.99	1.37	3.08	8.92	12.75	27.10	9.45	11.76	20.22	0.13
Cr	µg/g	101.02	159.87	38.62	49.53	51.89	67.13	82.16	78.36	162.61	102.94	206.79	135
Co	µg/g	210.80	69.13	87.48	46.04	55.52	130.37	123.68	63.68	86.25	67.14	33.80	26.6
Fe	µg/g	29549.07	17979.34	11443.38	19137.04	25789.14	23753.64	19789.44	19189.62	14422.44	7116.12	12877.41	5.63
Mn	µg/g	327.94	83.64	78.15	132.77	164.03	209.72	190.14	127.73	112.52	37.36	67.17	950
Ba	µg/g	291.93	148.35	171.50	162.25	2136.92	388.23	274.50	497.60	558.47	374.80	517.08	456
Cu	µg/g	524.88	300.16	60.78	117.57	215.71	297.50	327.88	230.22	212.99	193.67	146.66	55
Zn	µg/g	46.13	30.65	64.69	32.20	37.30	81.31	40.21	46.42	44.78	19.80	25.31	72
Pb	µg/g	13619.66	2041.00	218.19	170.16	226.06	4959.81	6437.20	2577.24	7030.49	6216.94	1889.27	12.5
U	µg/g	132600.05	21263.75	1864.94	1585.25	2577.64	44862.78	57556.51	24356.36	14611.35	100.57	6028.58	2.7

Taylor, 1964; Rudnick and Gao, 2003

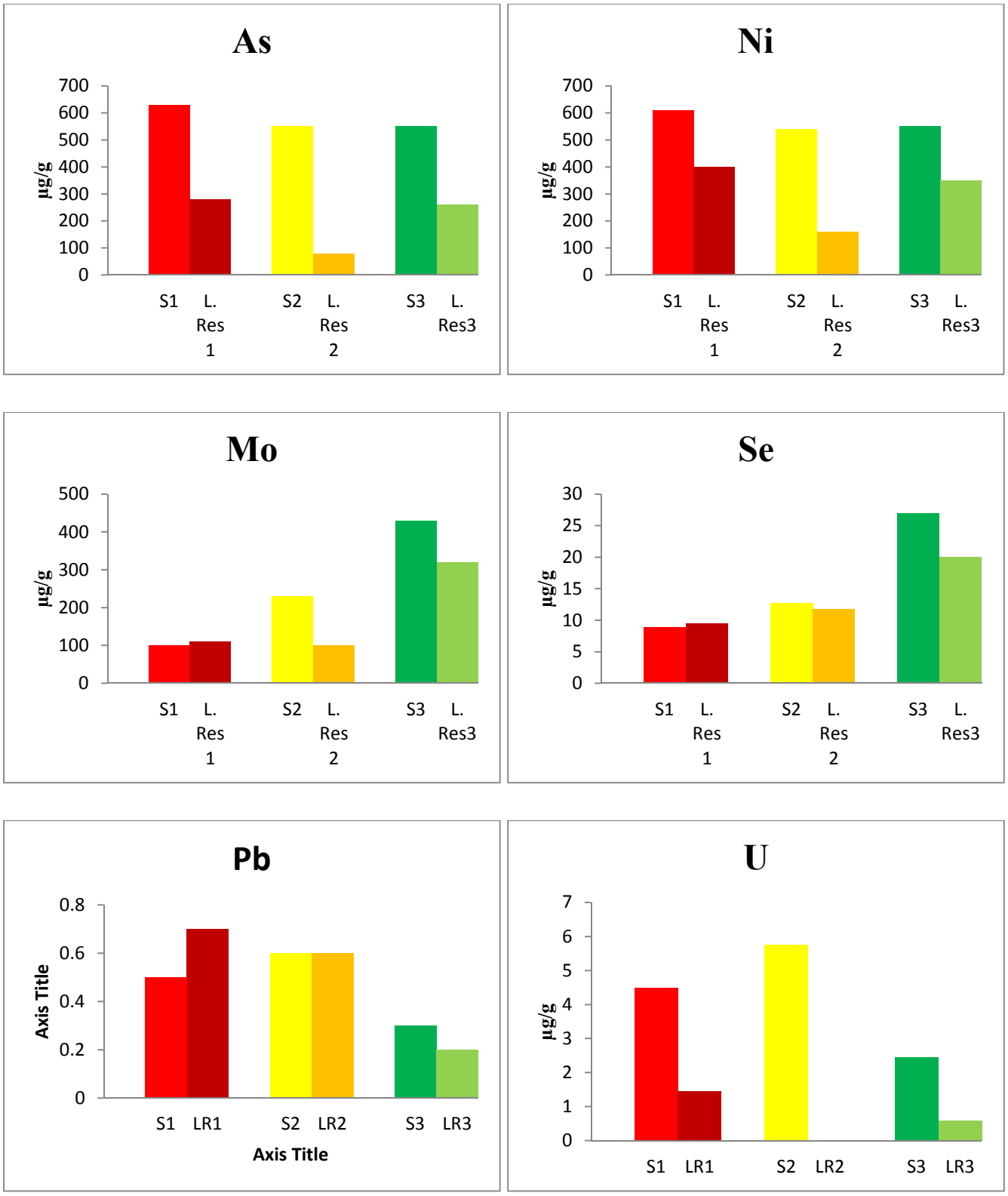

Figure 5.2 Comparisons of some EOCs in ore blends (S) and their corresponding leach residues (LR).

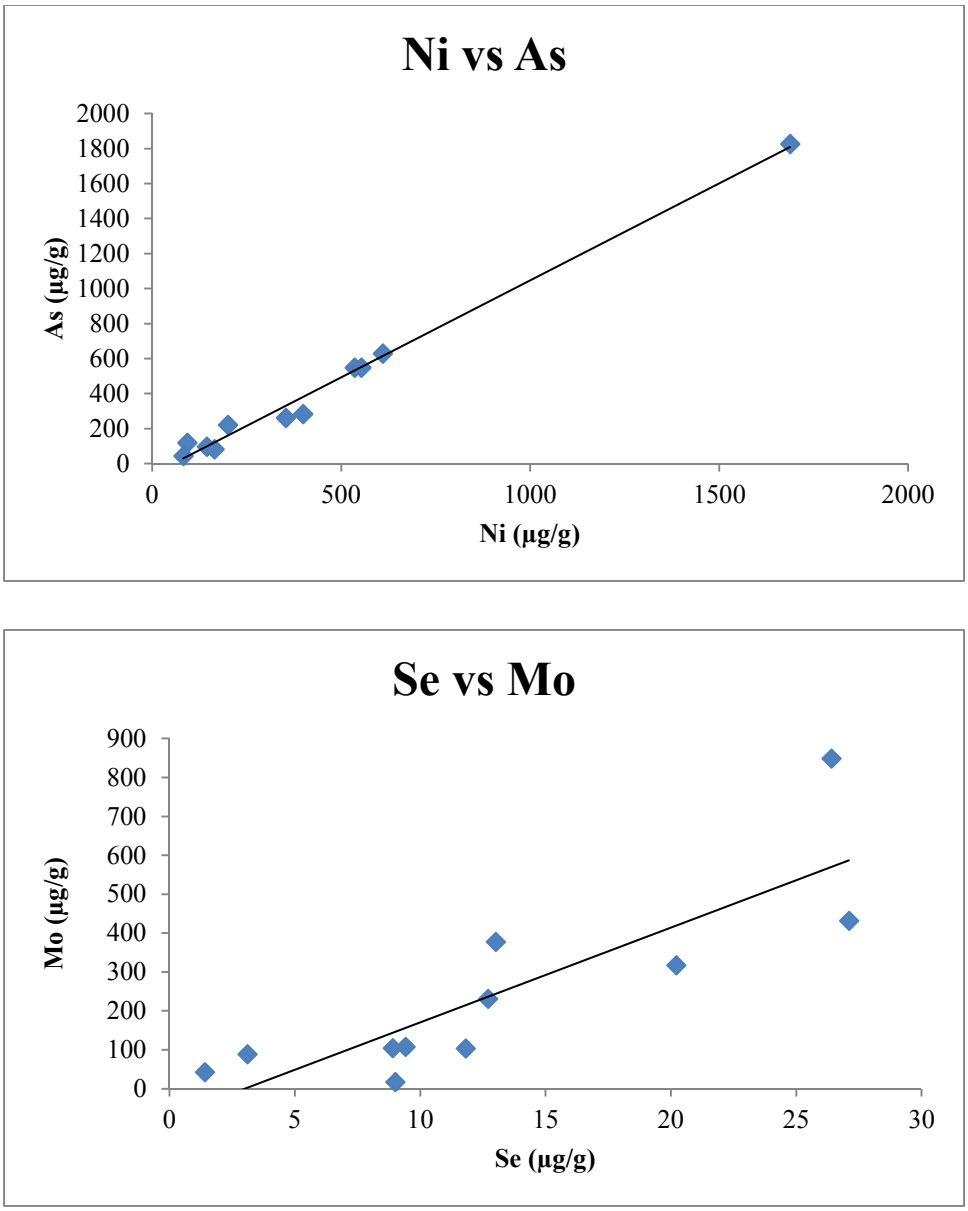

Figure 5.3 Correlation diagrams between Ni-As and Se-Mo in ores, blends and leach residues.

5.2 Primary Minerals

5.2.1 XRD Analysis

The primary minerals in the samples studied were analyzed using XRD, EPMA and MLA techniques. The powder XRD technique was used for reconnaissance analysis to identify the major phases constituting the source materials for the mill feed. A major limitation of this technique is that the detection limit is about 2-3 wt% for mixed materials (Beaufort et al., 2005). The EOC-bearing minerals occur in trace elements in the ores and other wastes and are not identifiable by XRD. The major phases identified are listed in the table 5.2.

Uraninite was identified only in the ores as U was present in small amount in the wastes as shown by the elemental analysis. Presence of Ca-rich uranophane was also identified in the McA. Uraninite was the main and primary U bearing minerals in the McArthur River ore and all stages of U ore are variably altered to Ca-rich, hydrous U minerals and coffinite (Fayek and Kyser, 1997). The major silicates presents were three different clays (chlorite, illite and kaolinite), muscovite, biotite, clinopyroxene and quartz. Only sulphide minerals detected was pyrite in the heavy the mineral portions of McA and DSW. Hematite was identified in McA, DSW and McW. Hematite occurs in alteration halos associated with U minerals (Fayek and Kyser, 1997).

An interesting characteristic of LR 1 was the presence of uraninite that agrees with the elemental data (Table 5.1 and 5.2). The presence of uraninite in the leach residue suggests incomplete dissolution of some uraninite grains during acid leaching. Gypsum precipitated as a result of milling in leach residues and was clearly evident in LR1 and LR3 samples. Gypsum possibly precipitated from the acidic U-bearing leach solution in Counter Current Decantation (CCD).

Table 5.2 Minerals identified in the studied sample using XRD.

McA	MLM	GsW	DsW	McW	S1	S2	S3	LR1	LR2	LR3
calcite										
chlorite	chlorite	chlorite	chlorite	chlorite	chlorite	chlorite	chlorite	chlorite	chlorite	chlorite
Clinopyroxene			Clinopyroxene	Clinopyroxene						
								Gypsum		Gypsum
hematite			hematite	hematite						
	Illite		illite	illite	illite	illite	illite	illite	illite	illite
kaolinite	Kaolinite	kaolinite								
muscovite /biotite	muscovite /biotite	muscovite/biotite	muscovite /biotite	muscovite /biotite	muscovite /biotite	muscovite /biotite	muscovite /biotite	muscovite /biotite	muscovite /biotite	muscovite /biotite
		Plagioclase		Plagioclase	Plagioclase	Plagioclase	Plagioclase	Plagioclase	Plagioclase	Plagioclase
pyrite			Pyrite							
quartz	Quartz	quartz	quartz	quartz	quartz	quartz	quartz	quartz	quartz	quartz
uraninite	uraninite				uraninite	uraninite	uraninite	uraninite		
Uranophane										

5.2.2 Electron Microscopy Analysis

EPMA/EDS examinations affirmed that the U ores and the special wastes were heterogeneous both in mineral contents and grain sizes. Mineral phases distinguished using EPMA/EDS analyses through (BSE) mages are demonstrated in Fig. 5.4, 5.5, 5.6 and 5.7. The major mineral phases identified were quartz, chlorite, illite, mica minerals (muscovite/biotite), pyroxene, feldspar and uraninite. The trace minerals included sulphides (e.g. pyrite and chalcopyrite), sulfarsenides (e.g. cobaltite and gersdorffite), Ni-arsenate, calcite, Fe-oxides and kaolinite. Pyroxenes were Ca-Fe-and Ca-Mg-Al-silicate type and feldspars were mainly plagioclase type with some K-feldspar in chemical composition. Secondary gypsum was identified in leach residues. In decreasing order of abundance the sulphide minerals included pyrite, chalcopyrite, galena and molybdenite.

The sample of McA ore comprised of liberated and, partially and completely locked U-bearing minerals such as uraninite (UO_2) or pitchblende (U_3O_8), coffinite [$U(SiO_4)_{1-x}(OH)_{4x}$) and uranophane [$CaH_2(SiO_4)_2(UO_2).5(H_2O)$. Electron probe analysis showed that uraninite grains varied in the sizes (clay fractions to ~100 μm) and shapes (Fig. 5.4). Anhedral uraninite grains showed highly irregular morphology and complex associations with other minerals. Locked grains preserved the original micro-textures of the ore minerals (Fig. 5.4 B-G). The unliberated ore minerals are associated with silicates and sulphides (Fig. 5.4B-G). Uraninite was found frequently in association with silicates like chlorite (Fig. 5.4C, E and I), and clinopyroxenes, i.e. Ca-Fe-Al silicate and Ca-Mg-Al silicate (Fig. 5.4G and H). Sulphide minerals mainly pyrite, chalcopyrite and galena also exhibit intergrowth texture in association with uraninite. Uraninite showed various micro-textures, e.g. uraninite veinlet in quartz and clinopyroxene, penetration intergrowths with chlorite, intergranular rim around pyrite and chalcopyrite within quartz host grains, and intergrowths of pyrite with uraninite (Fig. 5.4B-G). Coffinite exhibited emulsion like intergrowth texture with clinopyroxene. Sulphides were identified as pyrite, chalcopyrite, chalcocite, cobaltite and galena. Pyrite was the most frequent among the sulphide minerals and occurs as framboids within clinopyroxene, inclusion within pyrite, in association with chlorite, and complex intergrowth/exsolution texture with chalcopyrite. Cobaltite was found mainly as disseminated and liberated grains with diameters of ~5 μm (Fig. 5.4L).

Uraninite in the MLM ore sample was found as liberated and in association with sulphides and silicates. In some of the massive uraninite grains both in McA and MLM, a patchy dark BSE contrast was present, indicating some variation in chemical composition and/or alteration (Fig. 5.4A and 5.5A). Complex intergrowths with biotite and quartz are observed in Fig. 5.5B and C. It seems that uraninite was frequently associated with molybdenite (MoS_2) (Fig. 5.5B and E). Pyrite was not as frequent as in McA. Ni-As-sulphide mineral gersdorffite was also identified. It occurred mainly as liberated grains, and in association with pyrite.

In the Gaertner special wastes, uraninite was occurring in trace level and found as intergrowths within chlorite, Ni-arsenate and Mo rich iron oxide (Fig. 5.6B-F). In the Mo rich iron oxides uraninite were found as inclusions. A clear zoning was visible in the iron oxide with the core exhibiting a lighter grey level and more Mo rich than the periphery (Fig. 5.6D). Pyrite was identified and has grains size of <15 μm (Fig. 5.6B and D). This sulphide mineral was more common in the Deilmann special wastes. Unliberated pyrite was found as vein, framboids and emulsion in chlorite, kaolinite and illite (Fig. 5.6G-J). Gersdorffite was found in trace amounts in close association of pyrite (Fig. 5.6K). Fig. 5.6J and L show complex intergrowth of uraninite and kaolinite.

Liberation of valuable minerals from multiphase ores was one of the main goals of a size reduction process (Bonifazi & Massacci, 1995). Liberation of minerals has important implication in acid-leaching of the ore blends. Minerals of environmental concern, e.g. pyrite, chalcopyrite, gersdorffite and uraninite, occurring as unliberated state and locked within quartz and silicates do not get leached during leaching process. These minerals was eventually be found in the leach residues as unleached primary minerals (Fig 5.7A-F). Unleached sulphide and arsenides are susceptible to oxidation when exposed to air and water in the tailings facility as a result of the increased surface area (due to size reduction from milling and leaching). Fig. 5.7 shows the BSE images for leach residue samples. Pyrite occurs as spherical shaped partially liberated grain with clear evidence of leaching along the outer rim and locked state in leach residue samples (Fig. 5.7A). Uraninite was also present as liberated clay sized grains and unliberated in association with silicates (Fig. 5.7G and H). The edges of some silicates showed the indication of partial dissolution and alteration (Fig. 5.7G).

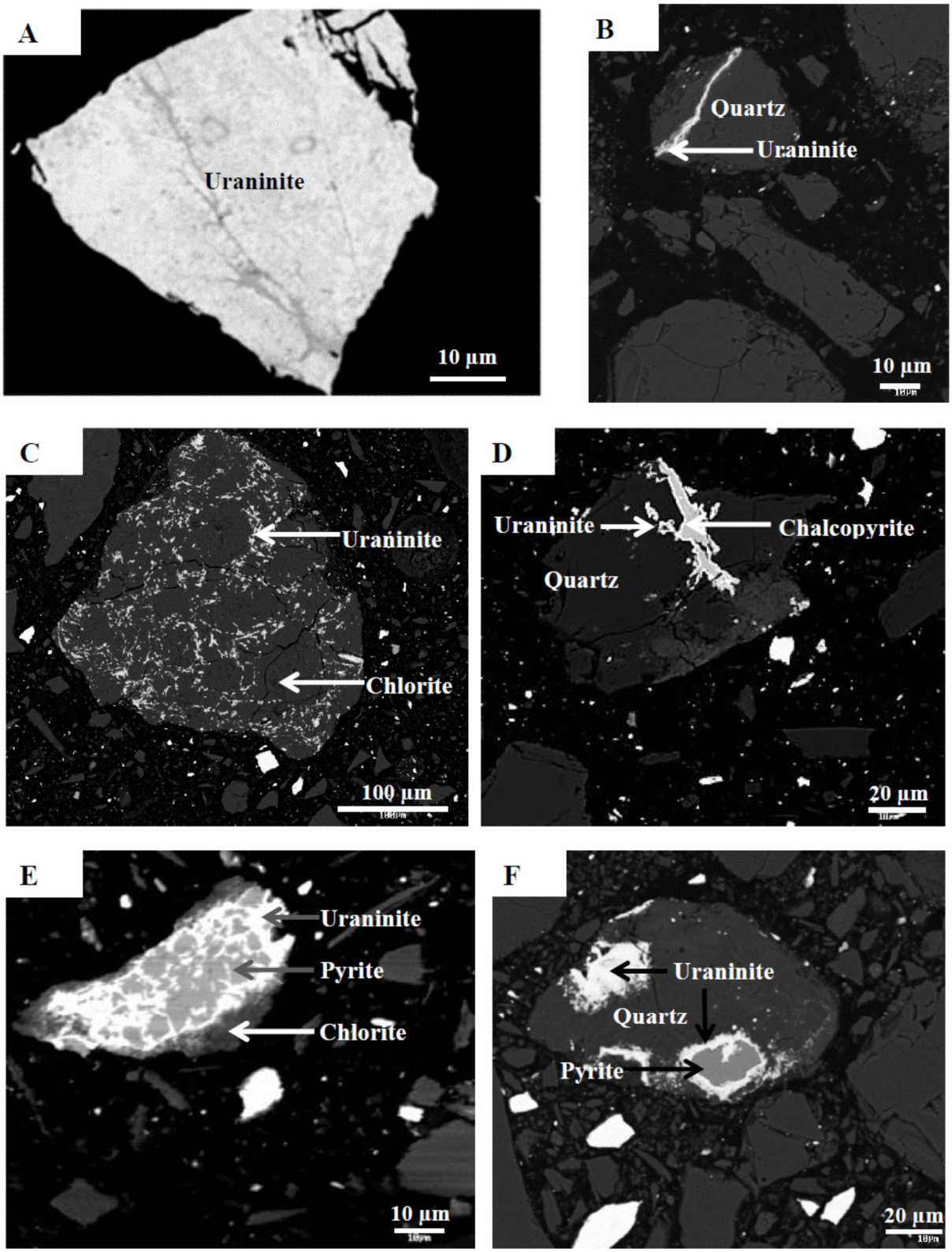
A
Uraninite
10 µm
B
Quartz
Uraninite
10 µm
C
Uraninite
Chlorite
100 µm
D
Uraninite
Chalcopyrite
Quartz
20 µm
E
Uraninite
Pyrite
Chlorite
10 µm
F
Uraninite
Quartz
Pyrite
20 µm

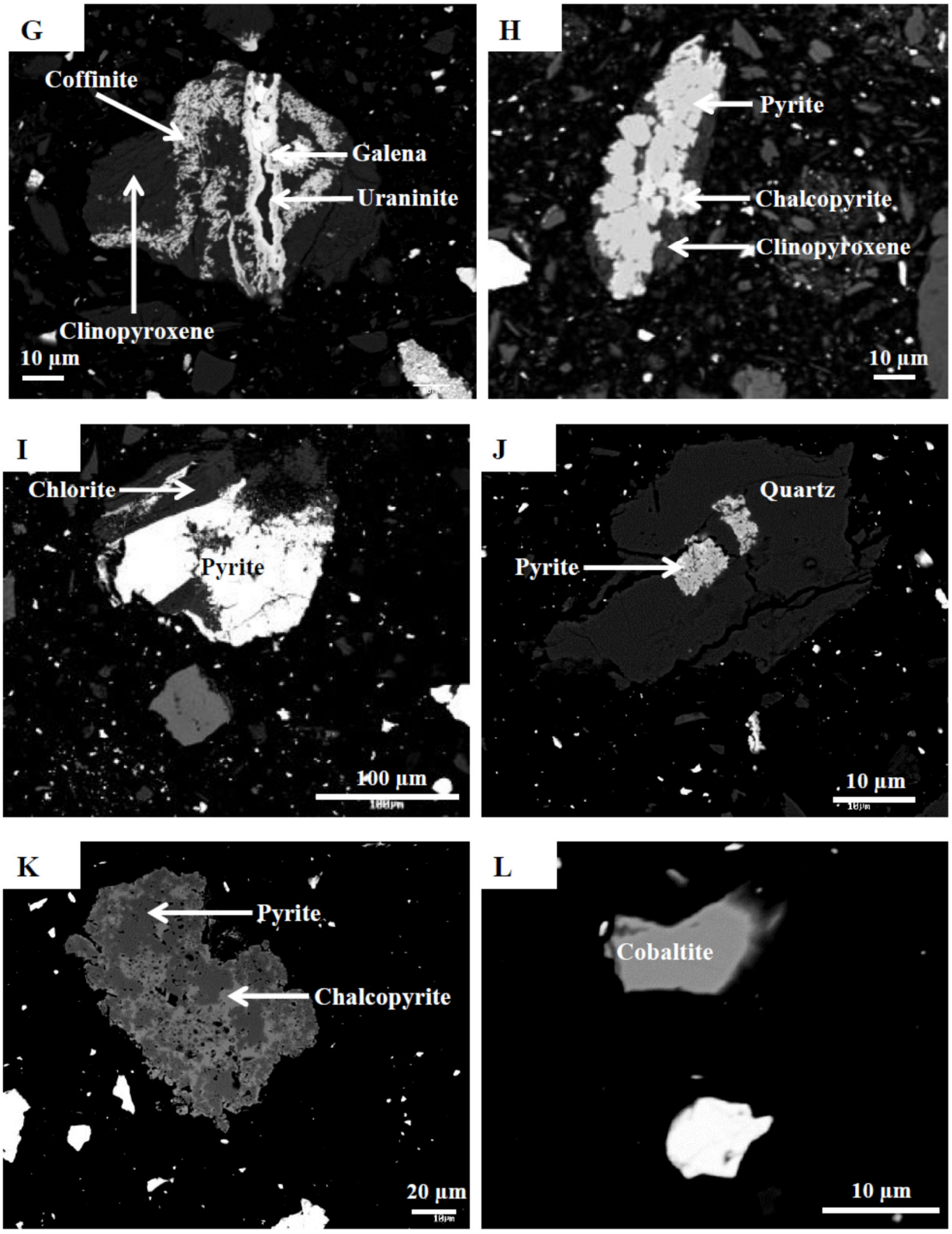

Figure 5.4 Backscattered electron images (BSE) of uraninite, sulphides and silicates in McA ore.

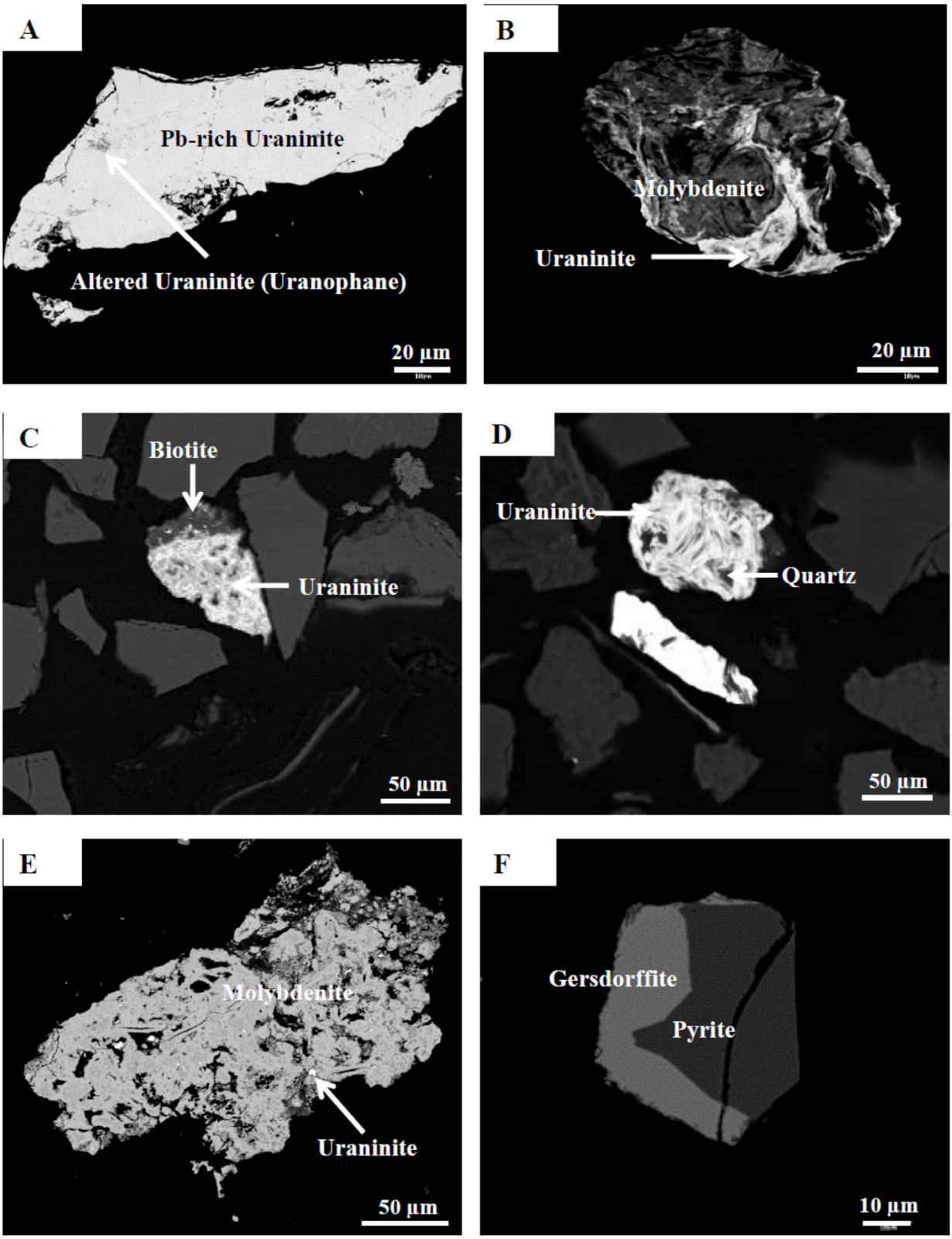

Figure 5.5 Backscattered electron images (BSE) of uraninite, sulfides and silicates in MLM ore.

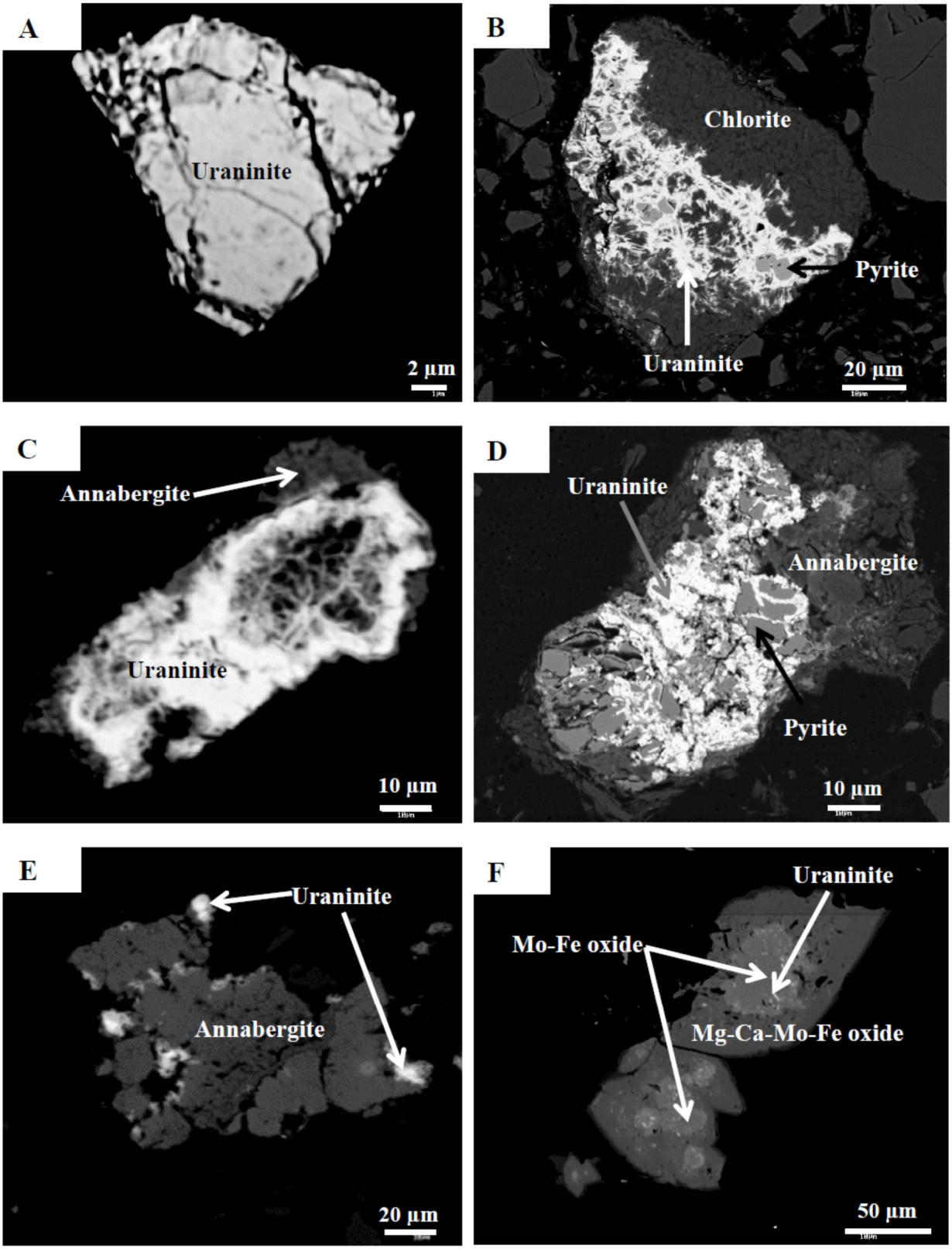
A
Uraninite
2 µm
B
Chlorite
Pyrite
Uraninite
20 µm
C
Annabergite
Uraninite
10 µm
D
Uraninite
Annabergite
Pyrite
10 µm
E
Uraninite
Annabergite
20 µm
F
Uraninite
Mo-Fe oxide
Mg-Ca-Mo-Fe oxide
50 µm

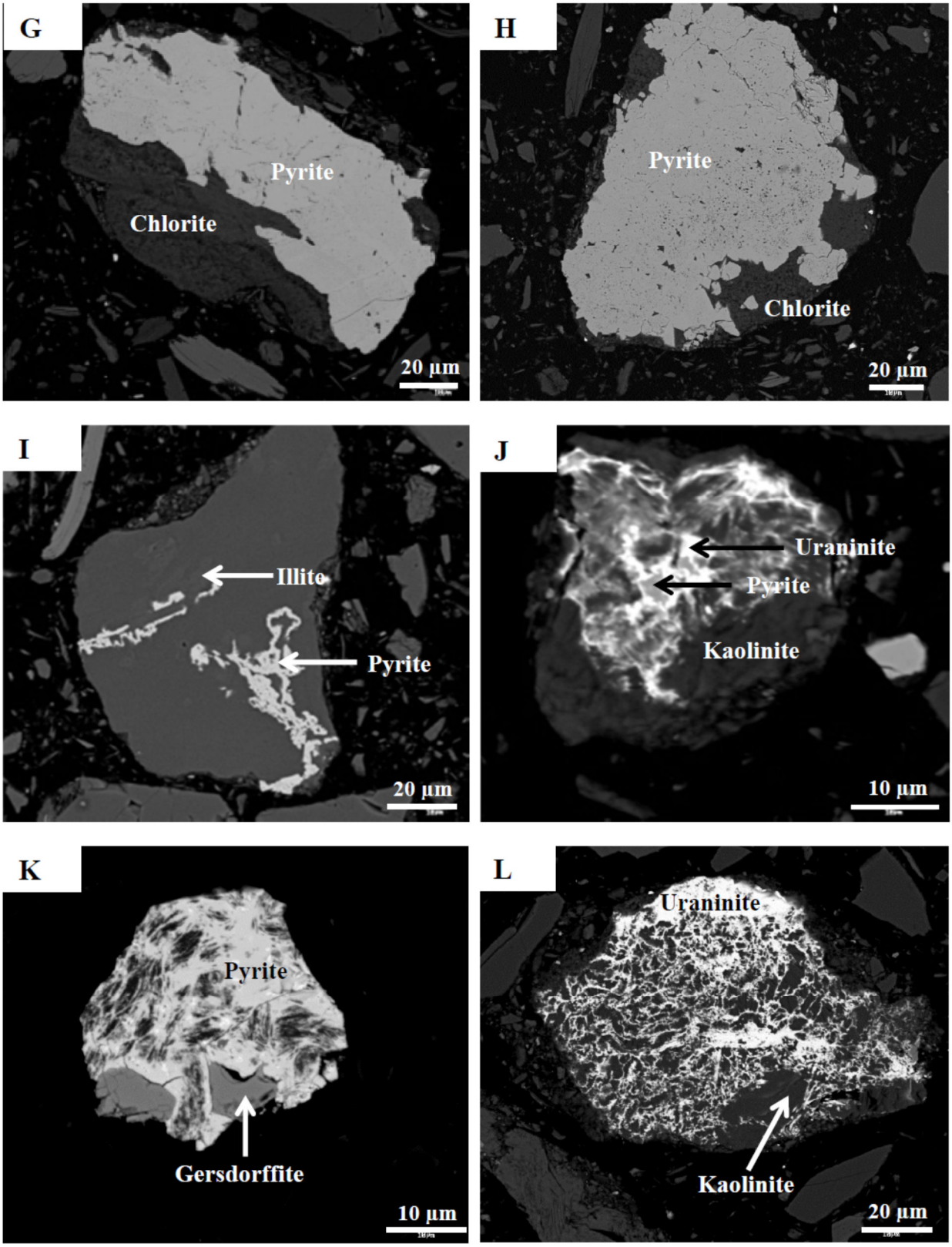

Figure 5.6 Backscattered electron images (BSE) of uraninite, sulfides, sulpharsenides and silicates in special wastes. GsW (5.6A-F) and DsW (5.6G-L).

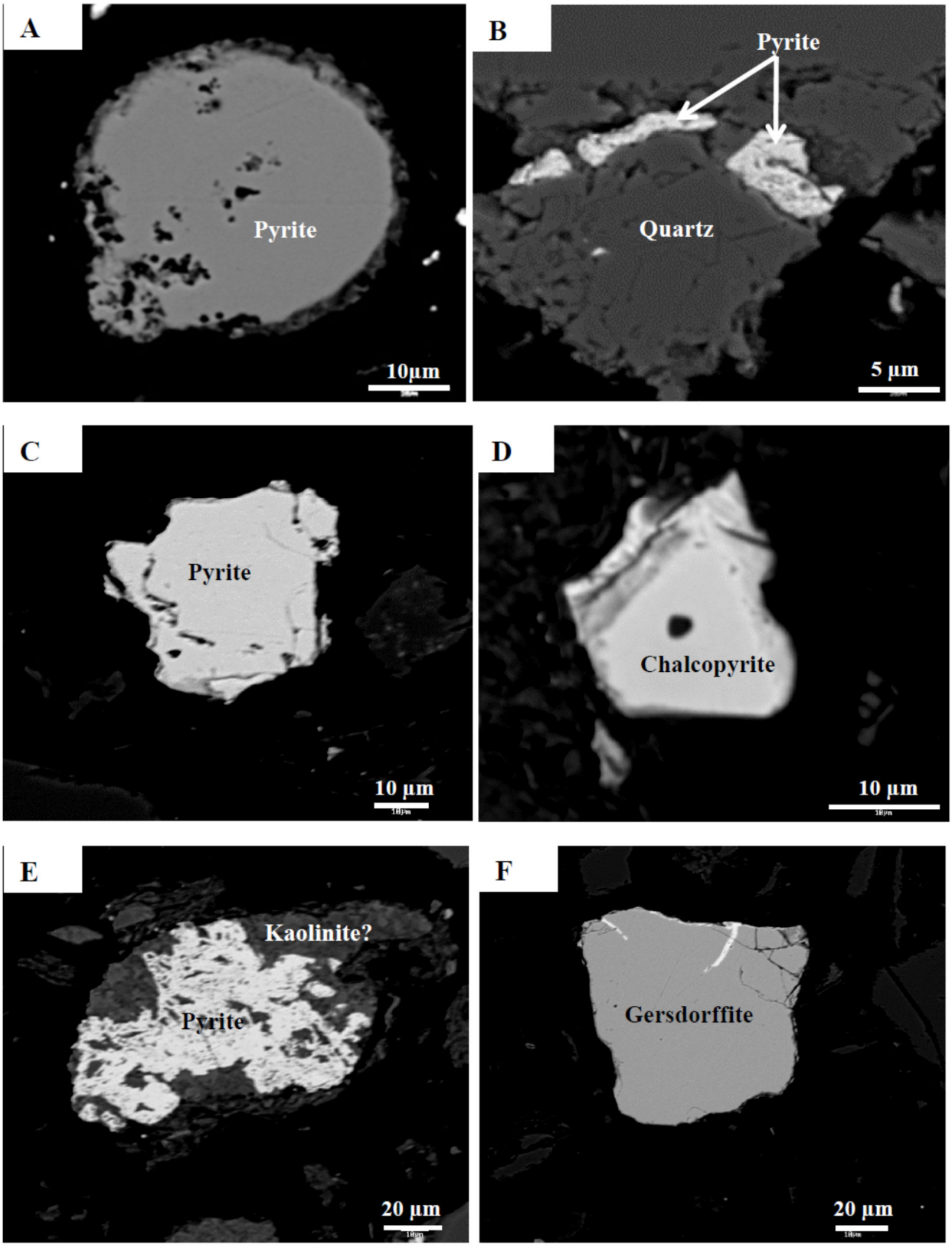
A
Pyrite
10µm
B
Pyrite
Quartz
5 µm
C
Pyrite
10 µm
D
Chalcopyrite
10 µm
E
Kaolinite?
Pyrite
20 µm
F
Gersdorffite
20 µm

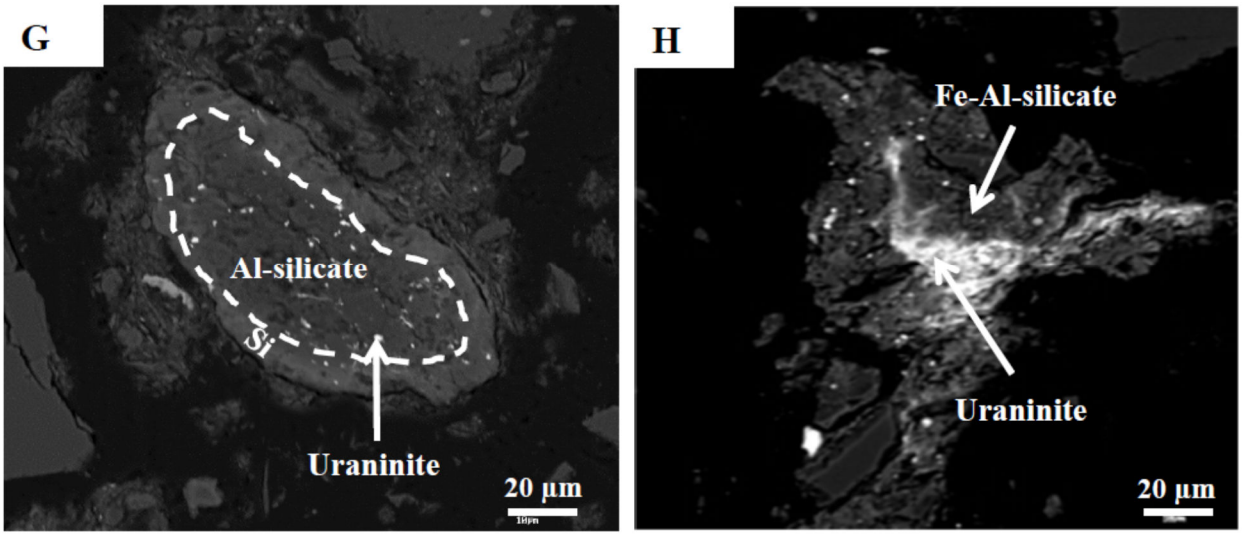

Figure 5.7 Backscattered electron images (BSE) of uraninite, sulphides, sulpharsenides and silicates in the leach residues.

5.2.3 Mineral Composition

The EPMA microanalysis of mineral grains in polished sections were focused on sulphides and sulfarsenides as these are the main reservoirs of EOCs, i.e. arsenic (As), nickel (Ni), molybdenum (Mo) and selenium (Se). Moreover, these minerals are the primary acid producers in the tailings. Tables 5.3, 5.4 and 5.5 show the compositions of the sulphides, sulfarsenides and arsenate minerals found in the source materials of the mill feed solids and the leached residues.

Pyrite

As, Ni, Mo and Se contents of pyrite grains were determined by electron micro-probe WDS analyses. Pyrite along with the other sulphides was present in trace amounts. The analyses showed totals of more than 98 wt%. Arsenic (As) contents ranged from nd (not detected) to the maximum values of 0.19 wt % (LR1). Ni was present in higher quantity than As with contents varying from nd to 1.55 wt % (MLM). Mo was not detected in pyrite. Se was detected frequently and ranged from nd to 0.18 wt % (LR1). Apart from these elements, other trace elements that were measured are Co (nd to 1.04 wt %), Cu (nd to 3.81 wt %) and Zn (nd to 0.07 wt %). The EPMA results showed negative correlations of Co and Ni with Fe in pyrite, and are consistent

with the substitution of metals for Fe in the pyrite structure (Fig. 5.8). These two elements occur as stoichiometric substitutions for Fe. No direct correlation was observed between Se and S.

Chalcopyrite

Chalcopyrite mostly occurred in the McA ore sample. Minor As, Ni and Se were present and ranged from nd to 0.06 wt % (DSW), nd to 0.03 wt % (McA), and nd to 0.04 wt % (DSW) respectively. Mo was only detected in MLM with a value of 0.52 wt % which might be the result of microscopic size molybdenite within the host chalcopyrite (Fleischer, 1955; Voudouris et al., 2013). The narrow and smaller (~10 μm) grains of chalcopyrite in McA and McW showed low Fe contents and low totals (<95 wt %), which might be a result of analytical error. Co was detected in some chalcopyrite grains and the content varied from nd to 0.19 wt % (McA).

Cobaltite

In the McA ore slurry, cobaltite was found as very small (5-10 μm) liberated grains. Electron-micro-probe analysis showed that the composition of cobaltite varies widely in terms of metal contents, from 30.28 to 33.98 wt % Co, 44.79 to 46.32 wt % As, and nd to 7.45 wt % Ni. Fe was detected in trace contents. Other metal contents did not get detected. The cobaltite containing a considerable amount of Ni can be termed as Ni-rich cobaltite. It is possible that Ni and Fe entered the cobaltite structure by the substitution for Co (Fanlo et al., 2004; Wagner and Lorenz, 2002).

Gersdorffite (NiAsS)

Gersdorffite occurred mainly in GSW and was also found in leach residues as unleached mineral. The metal content ranged from 28.86 to 32.66 wt % Ni, 40.71 to 43.45 wt % As, 0.95 to 1.75 wt % Co and 0.16 to 0.3 wt % Fe. Mo and Se were not detected.

Molybdenite (MoS_2)

Molybdenite was found to be the major phase of Mo in the ores. However, it was only encountered in MLM ore samples using EPMA analysis. The molybdenite grains were characterized by high metal and metalloid contents including Fe, Co, Ni, Se, and As. The metal contents ranged from 2.93 to3.48 wt % Fe, 1.83 to 2.85 wt % Co, 0.88 to 2.56 wt % Ni, 0.54 to

1.19 wt % Se, and 0.09 to 0.28 wt % As. Negative correlations were observed between Mo and Ni and Co and between S and As (Fig. 5.9). Ni and Co occur as stoichiometric substitutions for Mo and As enters the S lattice site. There was no clear relation found between Se and S. Se showed no correlation with S, but indicated negative correlation with As.

Ni-arsenate, Ni-Co-and Ni-sulfate

Secondary As and Ni bearing minerals were identified in GSW special waste. The majority of these minerals were appeared to be annabergite, a Ni-arsenate mineral which is generally a weathering product of gersdorffite (NiAsS), niccolite (NiAs) or rammelsbergite ($NiAs_2$). The metal content ranged from 26.35 to 35.2 wt % Ni, 20.24 to 30.69 wt % As, nd to 4.01 wt % Mo, 0.51 to 1.98 wt % Co, and nd to 0.16 wt % Fe. Negative correlations were observed between Ni and As and Mo, and Ni and Co (Fig. 5.10). Co entered as stoichiometric substitutions for Ni. Typical negative correlation between As and S was not found in this study. Metal contents (Fe+Co+Mo) showed weak negative correlation with Ni, meaning they substitute for Ni (Fig. 5.10).

Ni-Co-sulfate phase was identified with high Fe content (3.33 wt %). Ni-sulfate contained As (1.14 to 2.97 wt %), Mo (nd to 1.01 wt %), Se (nd to 0.4 wt %), Co (0.09 to 3.29 wt %), and Fe (0.17 to 1.05 wt %).

Galena

Galena was identified in ores and wastes and occurred as fine grains associated with both sulphides and silicates. Only few spots WDS analyses were run and were devoid of As, Mo and Se. Ni and Co were detected, and ranged from nd to 0.03 wt % (McA) and nd to 0.05 wt % (McA), respectively.

Table 5.3 Elemental composition of EOCs-bearing minerals in ores (wt %).

Sample ID	Minerals	Fe	Co	Ni	Cu	Zn	Se	Pb	Mo	As	S
McA	Pyrite	44.48	0.18	0.28	0.00	0.00	0.04	N/A	0.00	0.08	53.12
		45.30	0.15	0.23	0.00	0.00	0.03	N/A	0.00	0.03	53.70
		46.12	0.13	0.18	0.00	0.00	0.03	N/A	0.00	0.05	52.80
		46.82	0.10	0.00	0.00	0.00	0.00	N/A	0.00	nd	51.71
		45.99	0.10	0.00	0.00	0.00	0.00	N/A	0.00	nd	52.27
		44.42	0.32	0.05	0.56	0.01	0.01	N/A	0.00	nd	52.59
		42.44	0.94	0.00	3.81	0.00	0.02	N/A	0.00	0.04	52.60
		45.51	0.02	0.04	0.00	0.00	0.00	N/A	0.00	nd	53.46
		45.21	0.04	0.00	0.01	0.00	0.01	N/A	0.00	0.03	52.23
		45.90	0.10	0.03	0.00	0.00	0.00	N/A	0.00	0.00	53.37
		44.82	0.07	0.03	0.00	0.00	0.01	N/A	0.00	0.00	54.06
		45.84	0.09	0.01	0.01	0.01	0.00	N/A	0.00	0.00	52.98
	Chalcopyrite	29.04	0.00	0.02	35.15	0.00	0.00	N/A	0.00	0.00	32.44
		27.01	0.19	0.03	35.47	0.00	0.01	N/A	0.00	0.03	31.62
	Chalcocite	0.13	0.02	0.00	77.53	0.00	0.00	N/A	0.00	0.00	22.51
	Galena	0.67	0.05	0.03	0.00	0.04	0.00	83.02	0.00	N/A	12.95
		0.07	0.00	0.00	0.00	0.00	0.00	82.88	0.00	N/A	13.62
		0.07	0.00	0.00	0.00	0.00	0.00	84.58	0.00	N/A	13.61
		0.27	0.02	0.01	0.00	0.01	0.00	83.49	0.00	N/A	13.39
	Cobaltite	0.24	33.98	0.00	0.00	0.00	0.00	N/A	0.00	45.02	18.89
		0.00	30.28	7.45	0.00	0.00	0.00	N/A	0.00	44.79	18.11
		0.00	32.79	4.50	0.00	0.00	0.00	N/A	0.00	46.32	18.31
		0.08	32.35	3.98	0.00	0.00	0.00	N/A	0.00	45.38	18.44
Sample ID	Minerals	Fe	Co	Ni	Cu	Zn	Se	Pb	Mo	As	S
MLM	Pyrite	46.54	0.10	0.01	0.04	0.03	0.04	N/A	0.00	0.00	53.78
		46.05	0.17	0.00	0.38	0.07	0.08	N/A	0.00	0.00	53.76
		46.63	0.02	0.00	0.42	0.00	0.00	N/A	0.00	0.00	54.41
		47.02	0.08	0.00	0.00	0.00	0.03	N/A	0.00	0.00	55.77
		47.01	0.07	0.00	0.00	0.06	0.00	N/A	0.00	0.00	55.37
		44.38	0.90	1.55	0.01	0.00	0.19	N/A	0.00	0.00	55.02
		47.08	0.01	0.00	0.05	0.00	0.00	N/A	0.00	0.07	54.39
		46.78	0.11	0.01	0.00	0.04	0.00	N/A	0.00	0.00	54.74
		45.72	0.21	0.08	0.90	0.00	0.00	N/A	0.00	0.00	56.23
	Chalcopyrite	29.38	0.00	0.00	34.09	0.00	0.00	N/A	0.00	0.03	35.50
		30.50	0.02	0.00	33.15	0.00	0.00	N/A	0.52	0.00	35.40
	Molybdenite	2.95	1.99	0.89	0.23	0.00	0.56	N/A	59.27	0.24	34.86
		3.48	2.85	2.56	0.60	0.00	1.19	N/A	52.04	0.09	36.24
		2.93	2.26	2.30	0.87	0.00	1.13	N/A	55.58	0.10	33.90
		2.96	2.14	0.90	0.18	0.00	0.59	N/A	57.68	0.20	35.76
		2.94	1.83	0.88	0.28	0.00	0.54	N/A	58.86	0.28	33.95
	Gersdorffite	0.28	1.35	29.10	0.00	0.00	0.00	N/A	0.00	41.50	25.32

Table 5.4 Elemental composition of EOCs-bearing minerals in special wastes (wt %).

Sample ID	Minerals	Fe	Co	Ni	Cu	Zn	Se	Pb	Mo	As	S
GsW	Gersdorffite	0.30	0.95	31.44	0.00	N/A	0.00	N/A	0.00	43.12	23.50
	Ni-arsenate	0.11	0.51	26.35	0.00	0.00	0.00	N/A	0.06	30.69	0.23
		0.11	1.32	35.20	0.00	0.00	0.00	N/A	0.00	28.59	0.10
		0.07	1.46	30.66	0.00	0.00	0.00	N/A	0.16	25.31	0.07
		0.00	0.96	30.61	0.00	0.00	0.00	N/A	0.00	22.00	0.09
		0.13	1.01	31.76	0.00	0.00	0.00	N/A	0.09	20.69	0.08
		0.09	1.20	27.91	0.00	0.00	0.00	N/A	0.03	23.67	0.11
		0.16	0.55	31.10	0.00	0.00	0.00	N/A	1.39	22.04	0.23
		0.09	1.72	32.47	0.00	0.00	0.00	N/A	4.01	24.88	0.34
		0.07	1.98	29.74	0.00	0.00	0.00	N/A	0.61	20.24	0.80
	Ni-Co-sulfate	3.33	17.21	15.52	0.00	0.00	0.00	N/A	0.00	0.00	29.48
	Ni-sulfate	1.05	0.09	35.63	0.31	0.00	0.00	N/A	0.00	2.97	21.99
		0.17	3.29	28.14	0.00	0.00	0.40	N/A	1.01	1.14	18.08
DsW	Pyrite	41.94	0.26	1.46	0.00	0.02	0.02	N/A	0.00	0.02	49.75
		45.39	0.09	0.29	0.00	0.00	0.00	N/A	0.00	0.00	52.43
		41.45	0.04	0.01	0.50	0.00	0.00	N/A	0.00	0.00	45.42
		45.98	0.04	0.02	0.02	0.00	0.00	N/A	0.00	0.00	53.34
		46.83	0.07	0.00	0.00	0.02	0.00	N/A	0.00	0.00	51.97
		45.64	0.06	0.03	0.02	0.03	0.00	N/A	0.00	0.00	53.14
		45.73	0.06	0.01	0.05	0.00	0.06	N/A	0.00	0.02	52.25
		45.95	0.04	0.00	0.04	0.00	0.04	N/A	0.00	0.01	52.69
		45.95	0.03	0.04	0.00	0.00	0.03	N/A	0.00	0.00	52.99
		46.43	0.03	0.02	0.00	0.00	0.01	N/A	0.00	0.00	53.38
		42.60	0.89	1.14	0.19	0.00	0.02	N/A	0.00	0.02	51.89
		42.00	1.04	0.53	1.05	0.00	0.07	N/A	0.00	0.00	50.40
		44.67	0.10	0.11	0.00	0.00	0.01	N/A	0.00	0.00	52.39
		44.90	0.10	0.07	0.00	0.06	0.00	N/A	0.00	0.01	51.96
		45.06	0.03	0.00	0.04	0.01	0.00	N/A	0.00	0.00	51.99
		44.49	0.06	0.00	0.00	0.02	0.08	N/A	0.00	0.00	52.33
		45.34	0.04	0.06	0.00	0.00	0.00	N/A	0.00	0.00	50.12
		45.27	0.05	0.02	0.02	0.04	0.01	N/A	0.00	0.00	52.70
	Chalcopyrite	27.30	0.02	0.00	34.56	0.00	0.04	N/A	0.00	0.06	32.51
		28.96	0.07	0.00	34.27	0.00	0.04	N/A	0.00	0.01	32.53
McW	Pyrite	43.36	0.07	0.01	0.03	0.00	0.00	N/A	0.00	0.00	51.97
		46.99	0.13	0.00	0.36	0.00	0.02	N/A	0.00	0.00	53.58
		47.09	0.16	0.18	0.00	0.03	0.00	N/A	0.00	0.00	55.43
	Chalcopyrite	27.18	0.00	0.01	33.68	0.00	0.00	N/A	0.00	0.00	32.79
	Galena	0.01	0.04	0.01	0.04	0.00	0.00	82.30	0.00	N/A	12.52

Table 5.5 Elemental composition of EOCs-bearing minerals in blends and leach residues (wt %).

Sample ID	Minerals	Fe	Co	Ni	Cu	Zn	Se	Pb	Mo	As	S
S1	Pyrite	46.96	0.06	0.03	0.02	0.00	0.00	N/A	0.00	0.00	49.44
		47.41	0.08	0.03	0.00	0.00	0.00	N/A	0.00	0.00	50.93
S2	Pyrite	47.89	0.05	0.00	0.02	0.00	0.00	N/A	0.00	0.00	51.09
		46.90	0.04	0.10	0.07	0.00	0.01	N/A	0.00	0.08	49.55
S3	Pyrite	46.81	0.00	0.04	0.00	0.02	0.01	N/A	0.00	0.00	53.76
		44.48	0.14	0.28	0.00	0.00	0.03	N/A	0.00	0.00	53.12
LR1	Pyrite	46.25	0.05	0.00	0.00	0.00	0.00	N/A	0.00	0.00	41.38
		47.09	0.09	0.00	0.00	0.00	0.00	N/A	0.00	0.00	47.34
		47.10	0.08	0.00	0.00	0.00	0.18	N/A	0.00	0.19	46.19
LR2	Pyrite	47.88	0.03	0.00	0.00	0.00	0.00	N/A	0.00	0.00	44.03
LR3	Pyrite	46.42	0.00	0.06	0.39	0.00	0.00	N/A	0.00	0.00	44.49
		47.27	0.06	0.00	0.00	0.00	0.00	N/A	0.00	0.00	45.81
		47.19	0.04	0.04	0.01	0.00	0.00	N/A	0.00	0.00	46.77
		48.03	0.07	0.00	0.00	0.00	0.00	N/A	0.00	0.00	48.50
		44.93	0.21	0.05	0.06	0.00	0.02	N/A	0.00	0.00	48.45
	Chalcopyrite	31.12	0.06	0.00	36.92	0.04	0.00	N/A	0.00	0.00	30.27
	Gersdorffite	0.26	1.01	32.66	0.00	0.00	0.00	N/A	0.00	43.45	23.46
		0.24	1.75	28.86	0.00	0.00	0.00	N/A	0.00	40.71	14.53

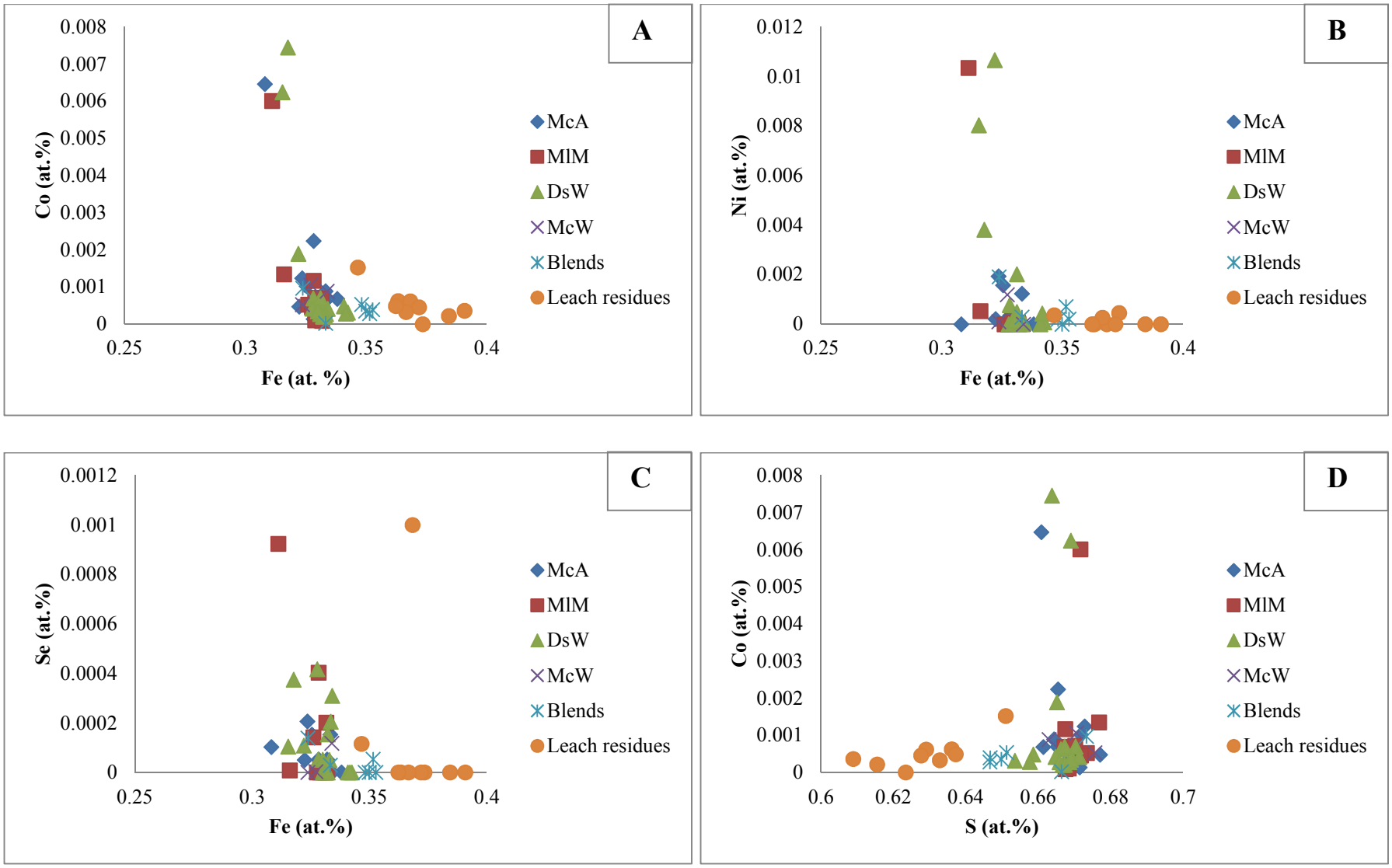

Figure 5.8 Correlation between trace elements in pyrite.

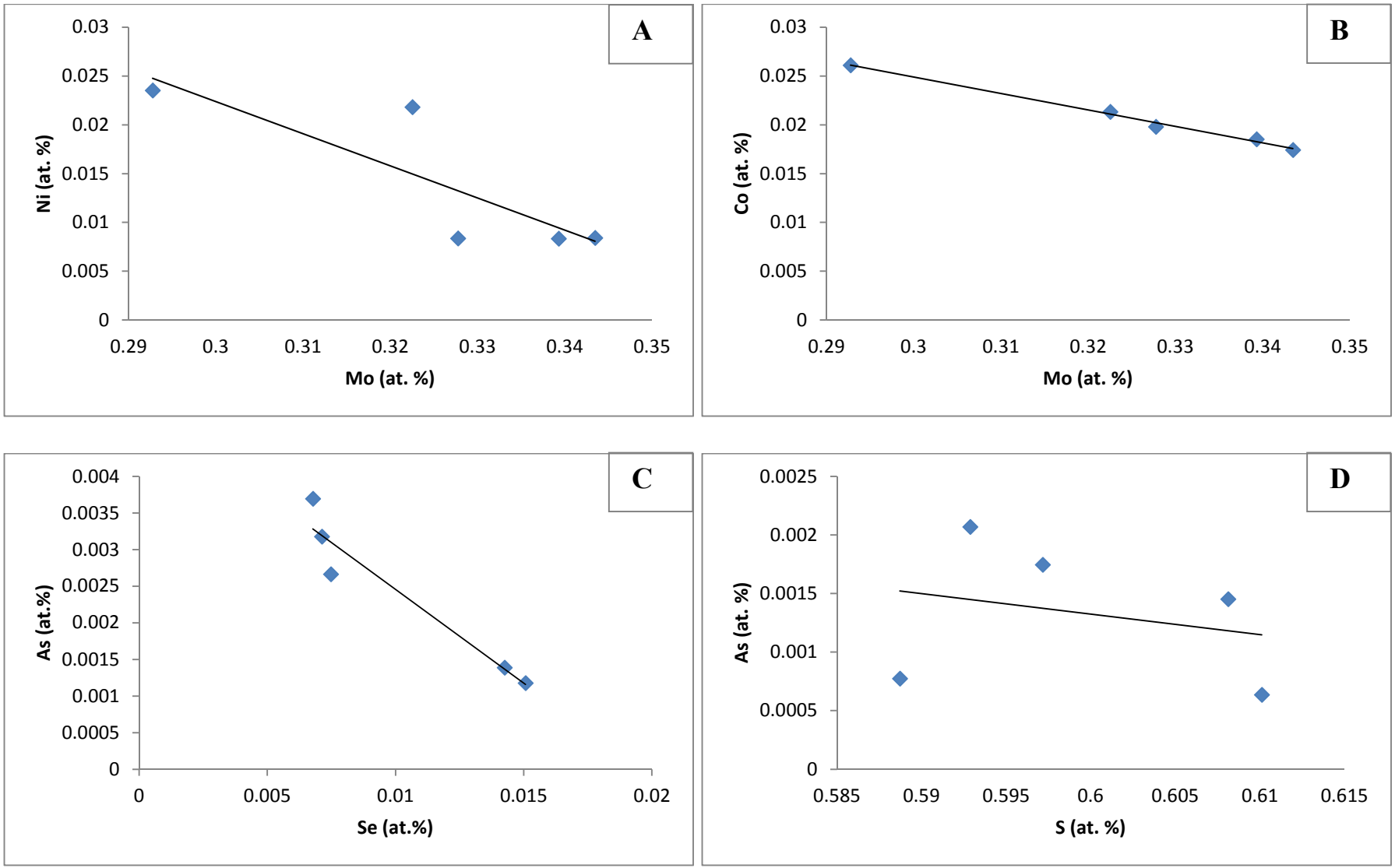

Figure 5.9 Correlation between trace elements in molybdenite.

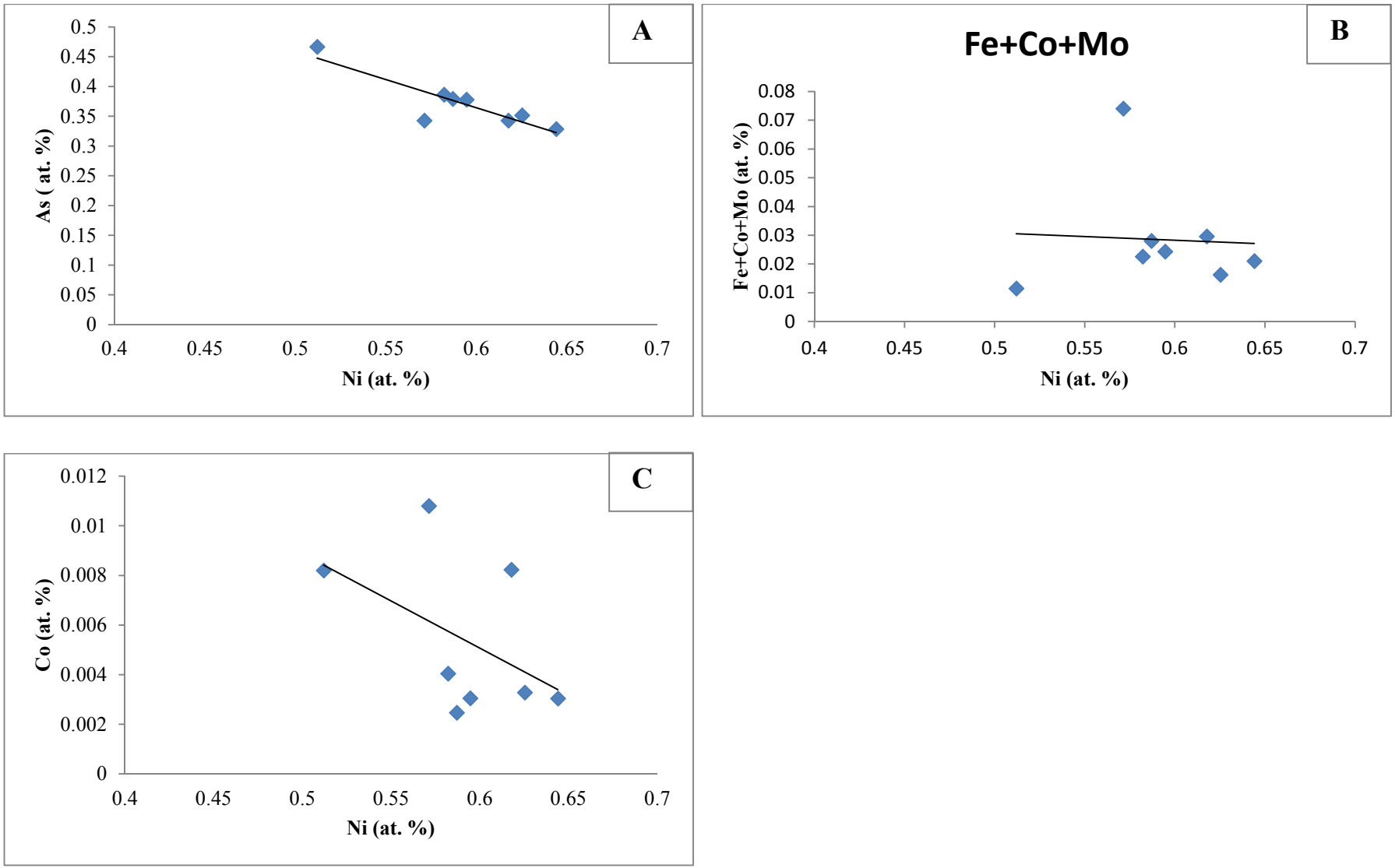

Figure 5.10 Correlation between trace elements in Ni-arsenate.

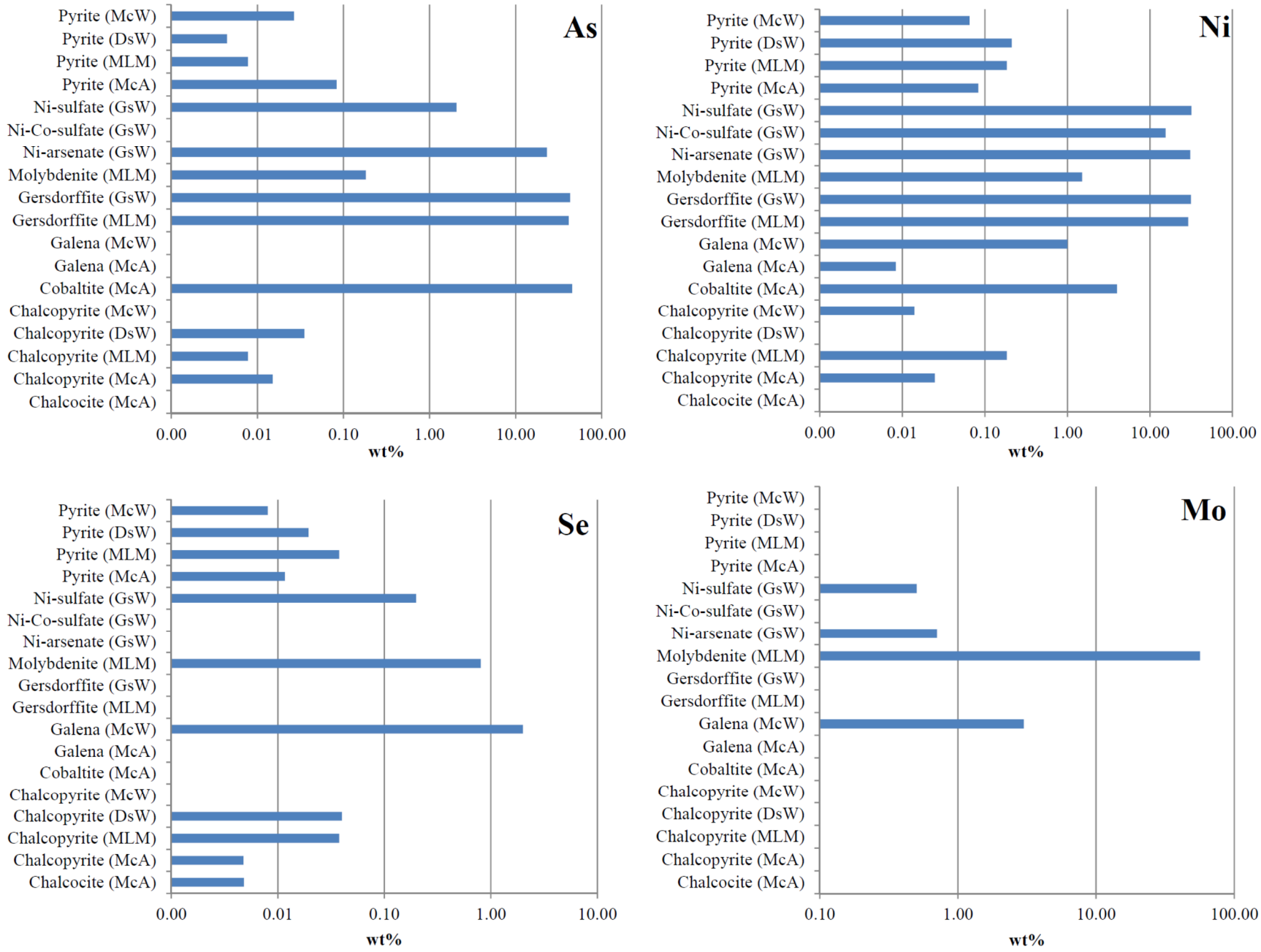

Figure 5.11 Distributions of As, Mo, Ni and Se in sulphides, arsenides, arsenates and sulfates.

5.2.4 Distribution of Elements of Concern (EOCs)

To understand the ECO distribution in the reservoir minerals, the X-ray mappings for these elements were undertaken. Figure 5.11 shows the comparative distribution of the EOCs within several sulphide, sulfarsenide, arsenate and sulfate minerals. As and Ni was relatively widespread compared to Mo and Se within these minerals. These two elements were found in association in most of the analyzed minerals, except Ni-Co-sulfate, galena and chalcocite as As was not detected in them (Fig. 5.11). However, there only few points were analyzed for these three minerals because of insufficient grains and/or very small grain size (<10μm). Ni occurred in higher concentrations than As. Therefore the source materials of the mill feed solids were somewhat richer in Ni. Cobaltite, gersdorffite, Ni-arsenate, molybdenite and Ni-sulfate were the As-bearing minerals whereas Ni was present mainly within Ni-sulfate, cobaltite, gersdorffite, Ni-arsenate, Ni-Co-sulfate, cobaltite, molybdenite, galena, chalcopyrite and pyrite (Fig. 5.11). The highest contents of As and Ni occurred in arsenate and Ni-sulfate phases, which were most probably the result of weathering in special wastes stockpiles under atmospheric exposure. Exposure of sulphide and sulfarsenide minerals to the atmosphere typically causes oxidation of S, Ni and As to sulfates and arsenates, for example annabergite [$Ni_3(AsO_4)_2.8(H_2O)$] is an oxidation product of nickeline (Nesbitt et al., 2003; references) or gersdorffite.

Molybdenum (Mo) was absent in sulphides (except chalcopyrite), whereas selenium was found in these minerals. Absence of molybdenum was probably because of its low concentrations in the minerals or due to analytical inaccuracy. The highest contents of these elements were observed in molybdenite (MoS_2) in the Millennium ore samples (Fig. 5.11). There was a close association of Mo and Se in molybdenite, galena and Ni-arsenate. Trace amount of Se was found to be occurring in association with U in MLM ore. It was reported that molybdenum and selenium in the unconformity ores were not only associated with sulphides, but also found in phyllosilicates and uraninite in very small quantity (Heinrich et al., 2010). Se was detected in high quantity in galena (McW) followed by molybdenite, Ni-sulfate, chalcopyrite and pyrite.

Elemental maps were collected for EOC-bearing minerals to observe their association with each other and other elements like U, Pb, Fe and S. Arsenic was detected in uraninite in GSW (Fig. 5.15 and 5.16). Uraninite was also found to host Se and Ni in MLM ore (Fig. 5.14).

Figure 5.17 showed the association of Pb, S and Se in galena intergrown with Ni-arsenate and uraninite. The most noticeable evidence of weathering of primary sulfarsenide into secondary arsenate in the wastes was depicted in the Fig. 5.18. The maps of As, Ni, S and Fe exhibited a gersdorffite grain partially weathered into a Fe-arsenate mineral (Fig. 5.18).

Mo and S were associated with As, Ni, Se and Fe in molybdenite (Fig. 5.12 and 5.14). Gersdorffite was devoid of any EOC other than As and Ni (Fig. 5.13). In a complex Fe-S-U-Ti-Si grain in leach residue 1 (LR1) sample, U was associated with arsenic, which is most likely to be a remnant of a composite grain of quartz (SiO_2), pyrite (FeS_2) and brannerite ($UTiO_6$) (Fig. 5.19).

Distribution of these elements was also controlled by particle size of the blends and residues. Ni and As were found to be occurring in the clay size fraction (<2μm), whereas Se and Mo were more evenly distributed in the bulk and clay size fraction (Fig. 5.20). These data suggested the occurrence of As and Ni in trace amounts associated with the clay minerals more likely as surface sorption(dos Anjos et al., 2014; Lin and Puls, 2000). As clay minerals have high adsorption and cation exchange capacity, major cations along with trace metals were exchanged between the clay structures and the surrounding solution (Gaudin et al., 2004; Maksimovic and Brindley, 1974). Moreover, Ni and As-bearing sulphides and sulfarsenides may depend on the metamorphic grade of host rocks in the ores. For example, as the low-grade metamorphic rocks generally contain fine grained pyrite (Tempelman-Kluit, 1970).

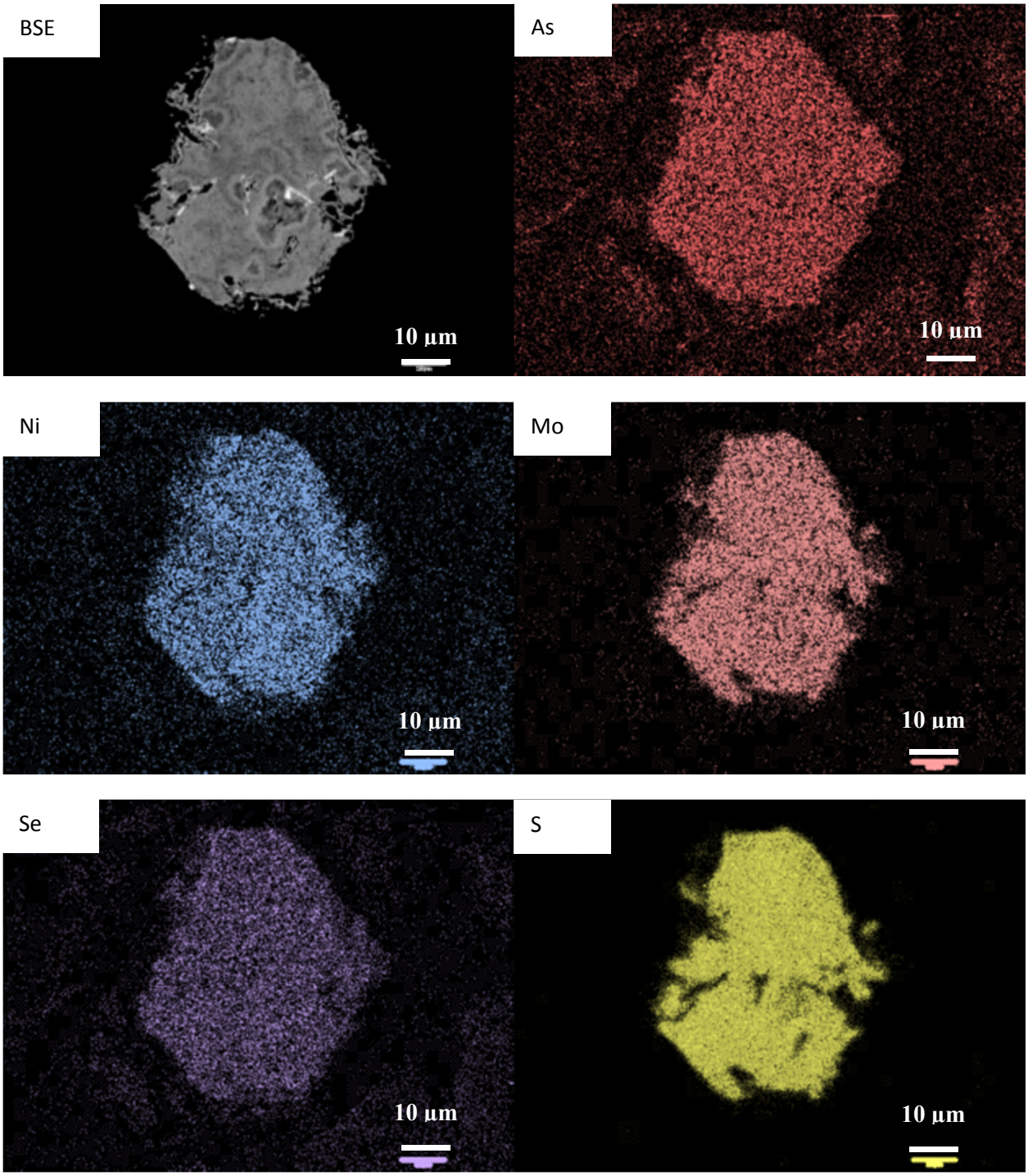

Figure 5.12 Association of As, Mo, Ni and Se in molybdenite in MLM ore.

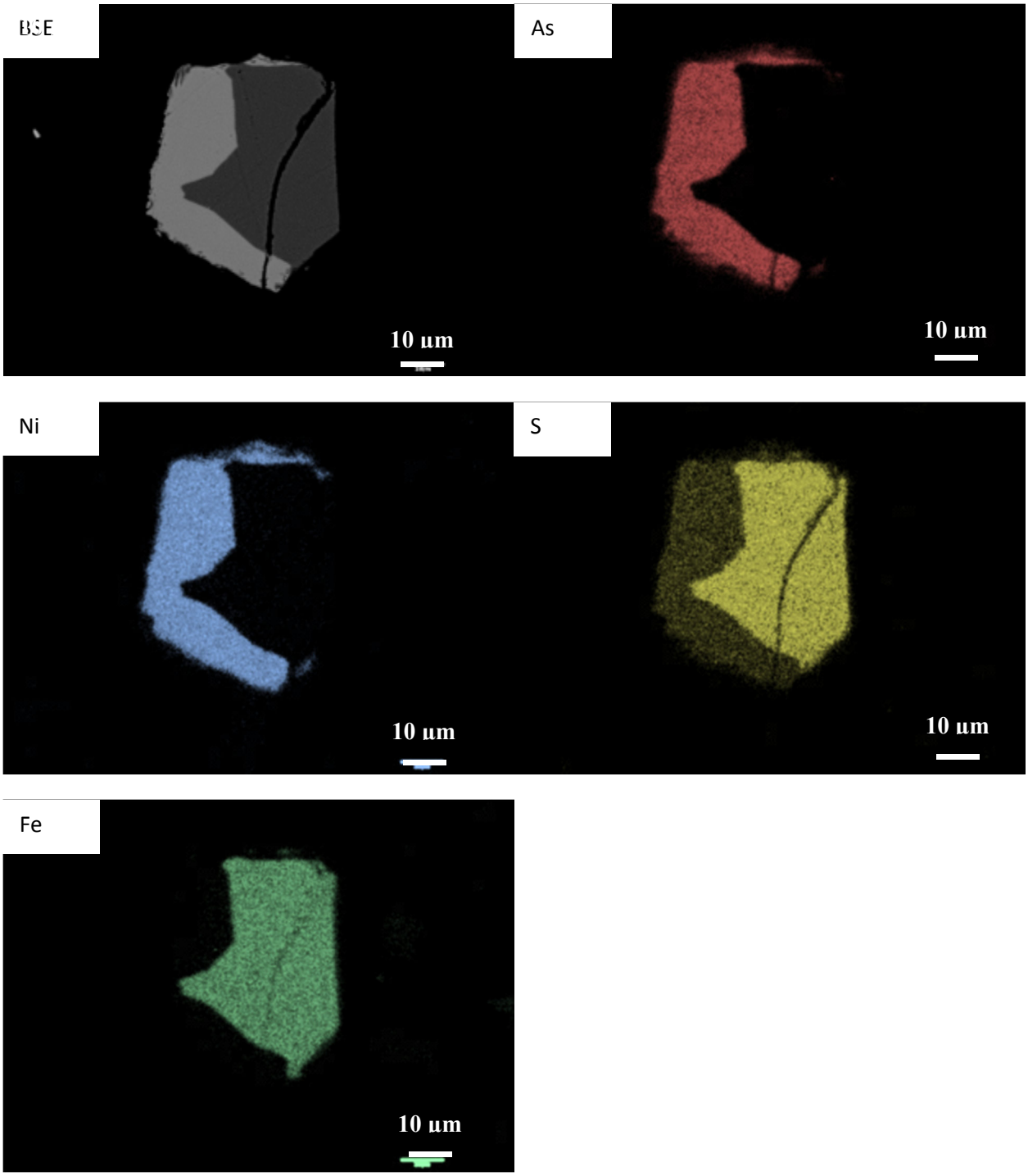

Figure 5.13 Association of As and Ni in gersdorffite and pyrite in MLM ore.

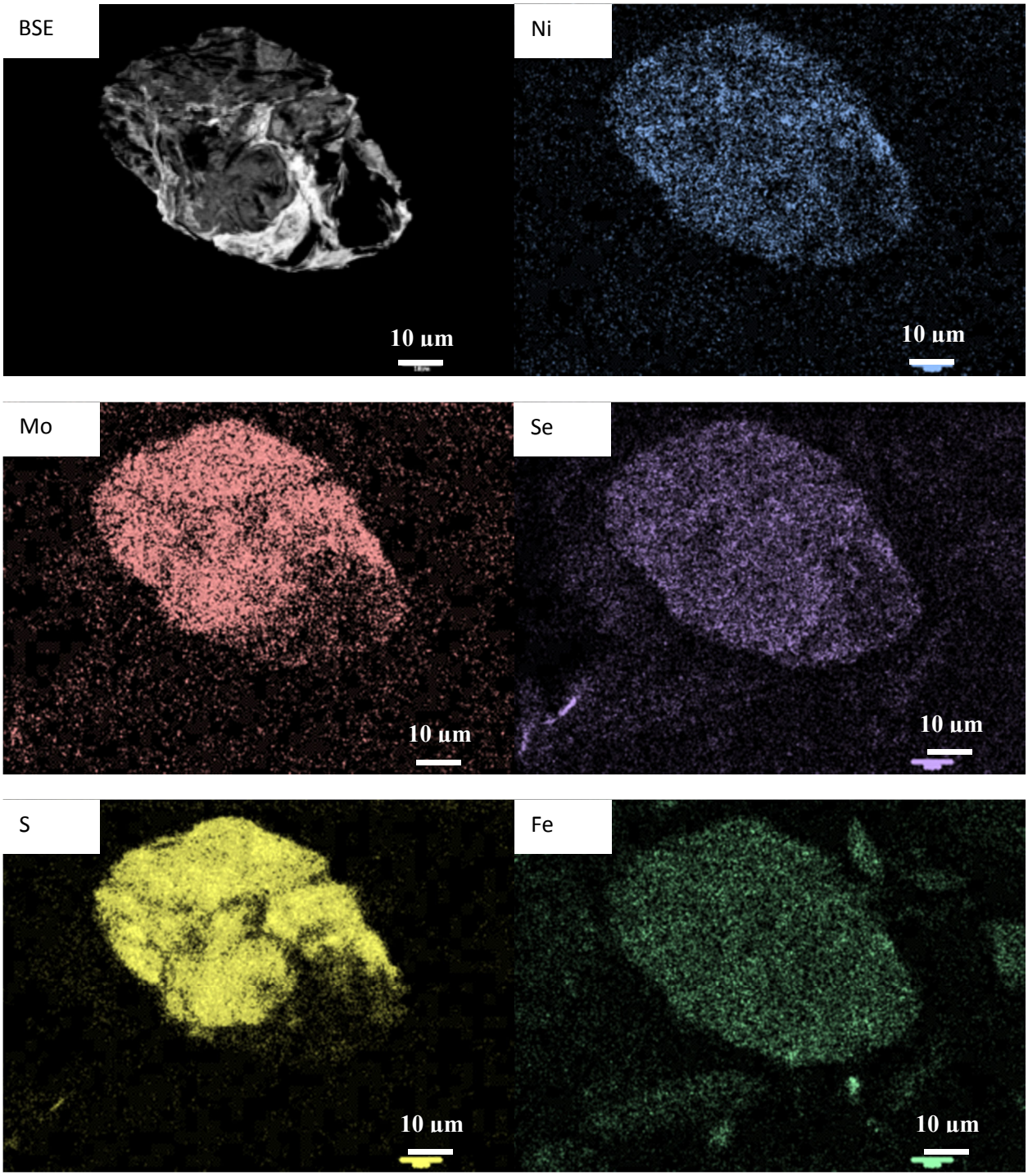

Figure 5.14 Association of Mo, Ni and Se in molybdenite and uraninite in MLM ore.

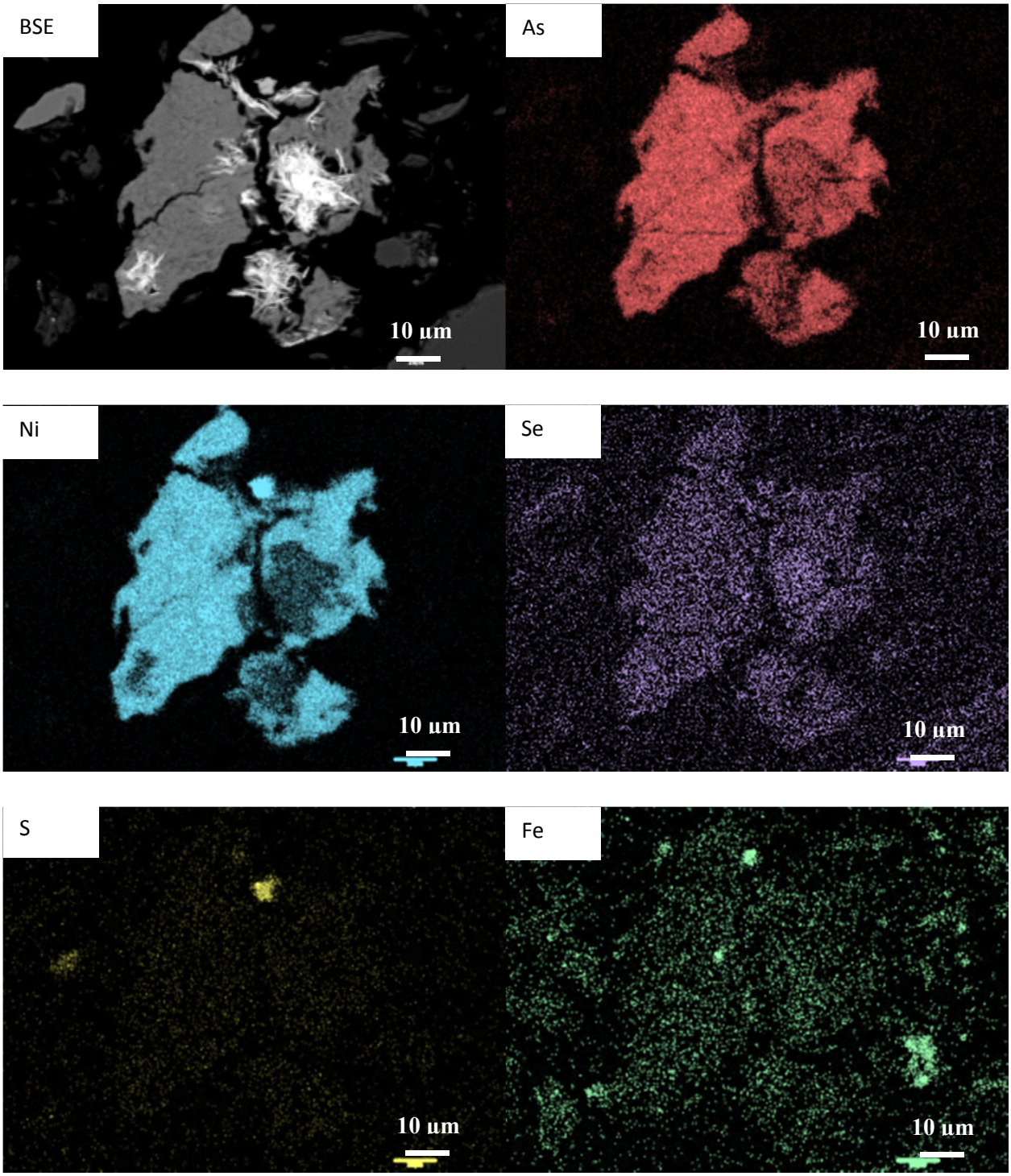

Figure 5.15 Association of As, Ni and Se in Ni-As phase-annabergite in GSW.

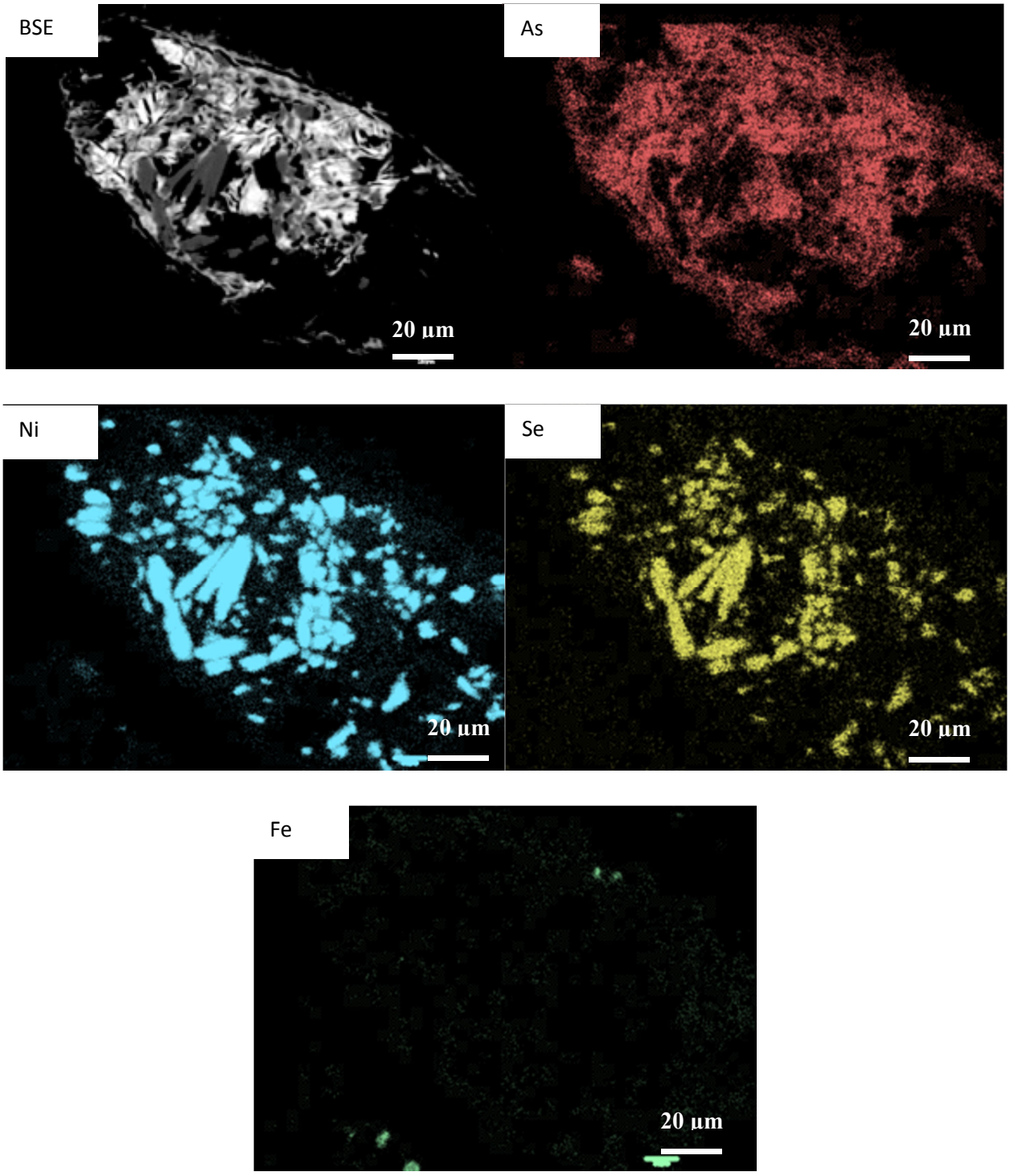

Figure 5.16 Association of As, Ni and Se in uraninite in GSW.

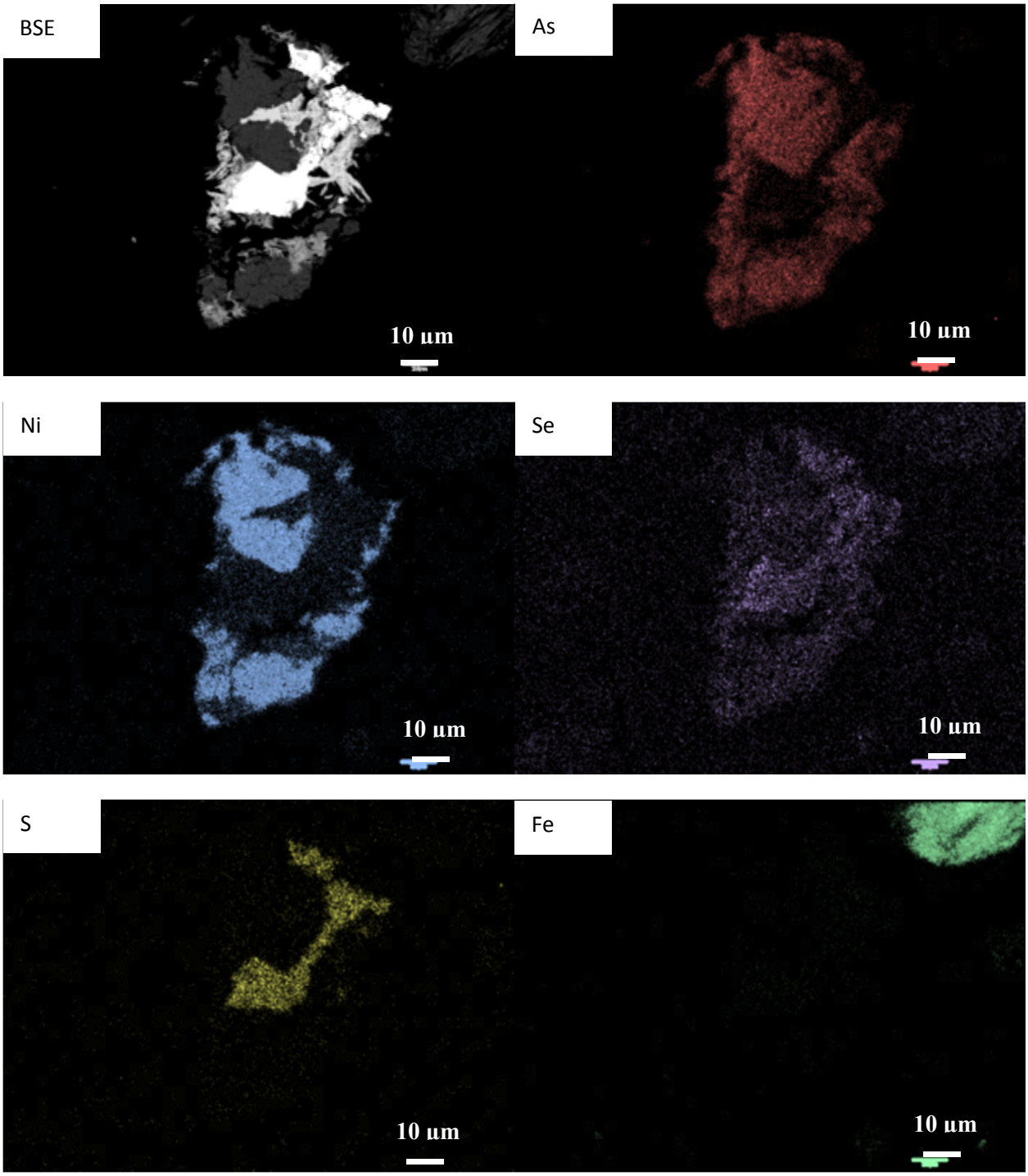

Figure 5.17 Association of As, Ni and Se in galena in GsW.

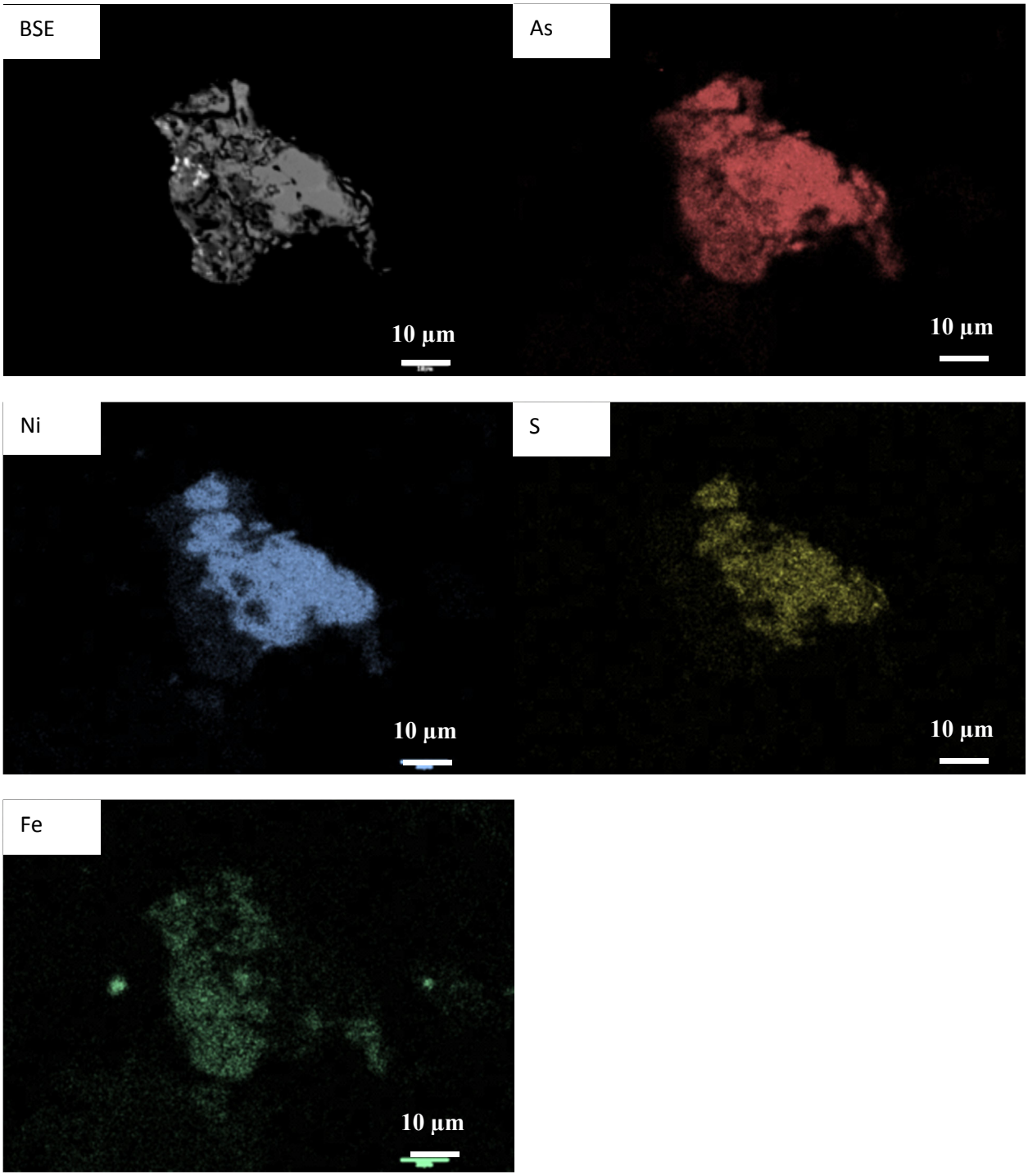

Figure 5.18 Association of As and Ni in scorodite in association with gersdorffite in GSW.

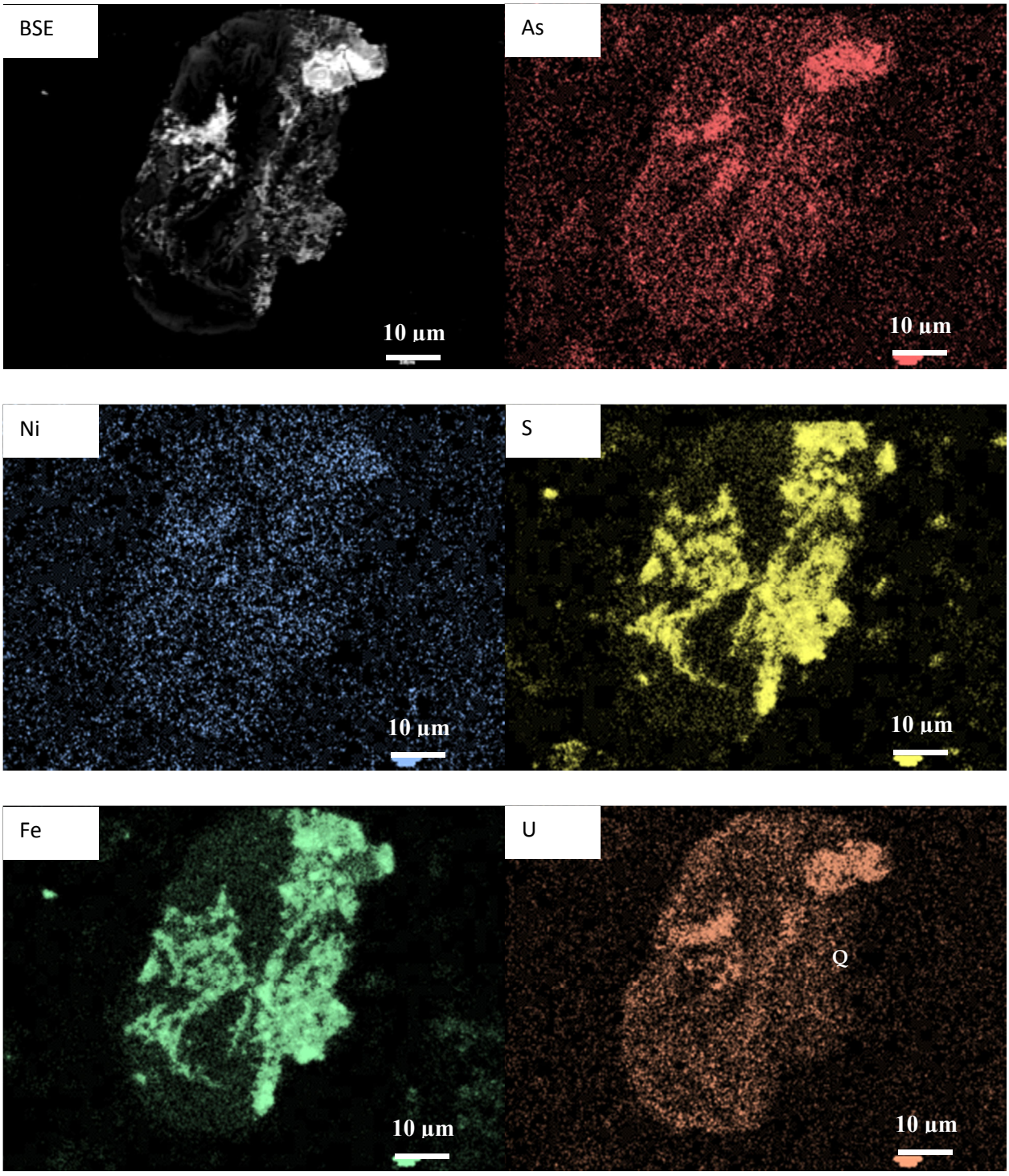

Figure 5.19 Association of As and Ni in the complex Fe-S-U-Ti-Si particle in LR1.

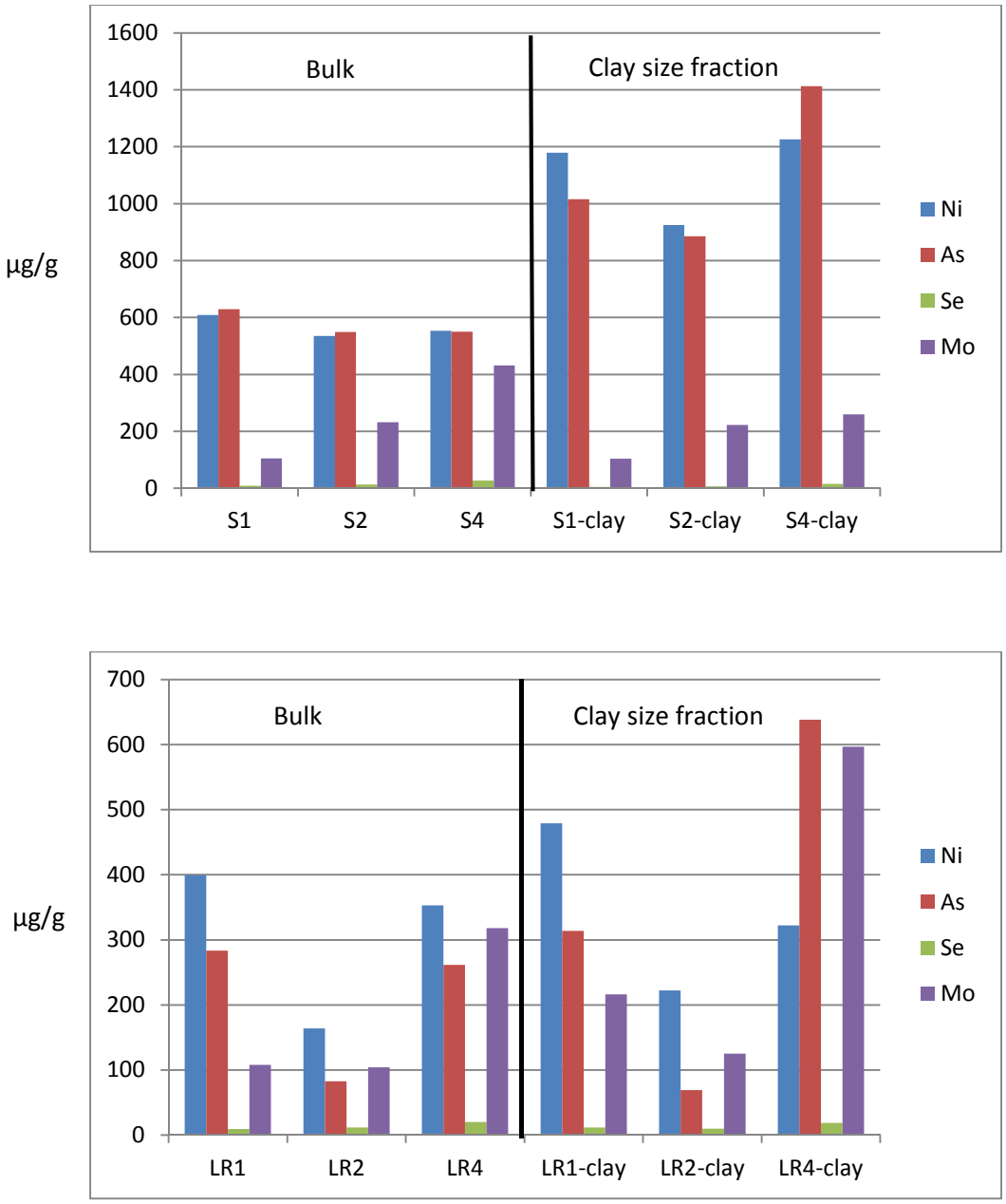

Figure 5.20 Distribution of EOCs in the clay size fractions of blends and leach residues.

5.2.5 Mineral Liberation Analysis

A major aim of this study was to demonstrate the usefulness of MLA technology to characterize U ore to better discriminate U- and EOC-bearing minerals. A dedicated mineral database based on characteristics X-ray spectra of minerals was developed at Memorial University of Newfoundland. This chapter will demonstrate the ability to detect (and quantify) some of the determined mineral characteristics.

Reconnaissance analysis was first performed using SEM to confirm the mineralogy previously determined by XRD. The results of the automated MLA analysis showed not only the presence of major minerals but minerals in trace amounts. Tables 5.6 and 5.7 summarize the revised estimated percentages of the minerals/phases present in the studied samples using MLA results. MLA analysis of the samples was first performed using particle mineral analysis to confirm the mineralogy previously determined by XRD. They compare well with XRD for major minerals but identify a much wider range of minor minerals that were below the detection limit for XRD, confirming that for trace mineralogy MLA can give much more information than XRD.

One of the significant results obtainable by MLA was the use of mineral maps to identify the associations of mineral phases with each other. This can be used not only to identify ore mineral associations but also to show gangue mineral associations. A significant result obtained from MLA analysis was the identification of secondary Ni-As phases in the Gartner special waste sample, i.e. annabergite and scorodite (Table 5.7). An example of the association of minerals is provided in Fig. 5.21.

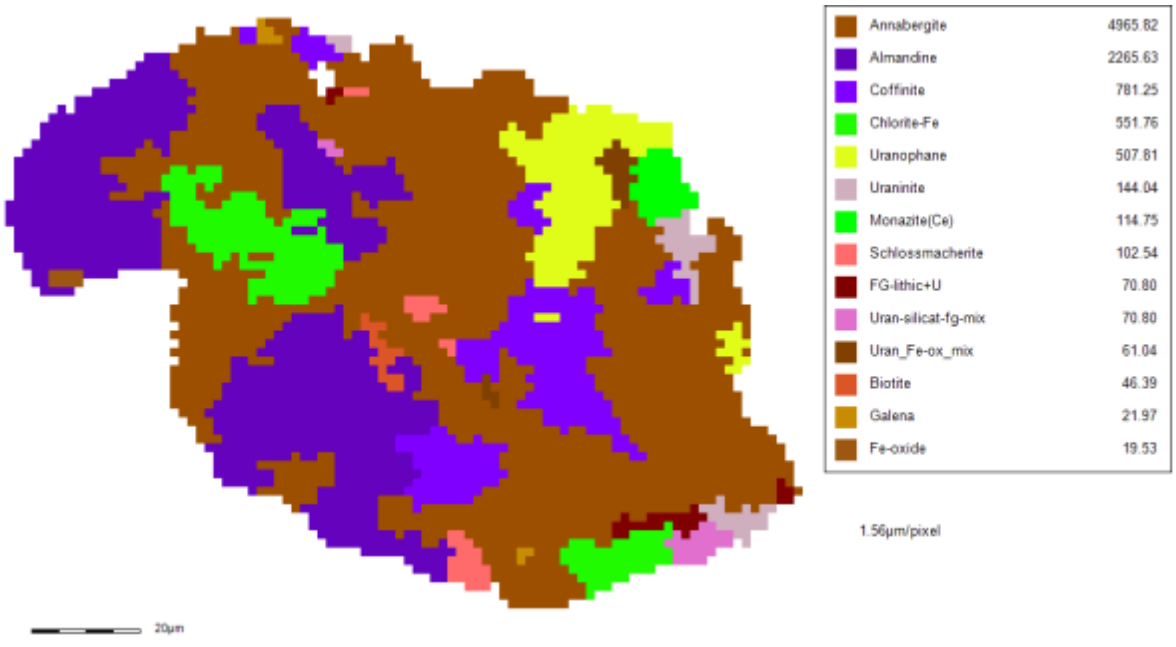

Figure 5.21 MLA particle map for GsW of annabergite-silicate associations.

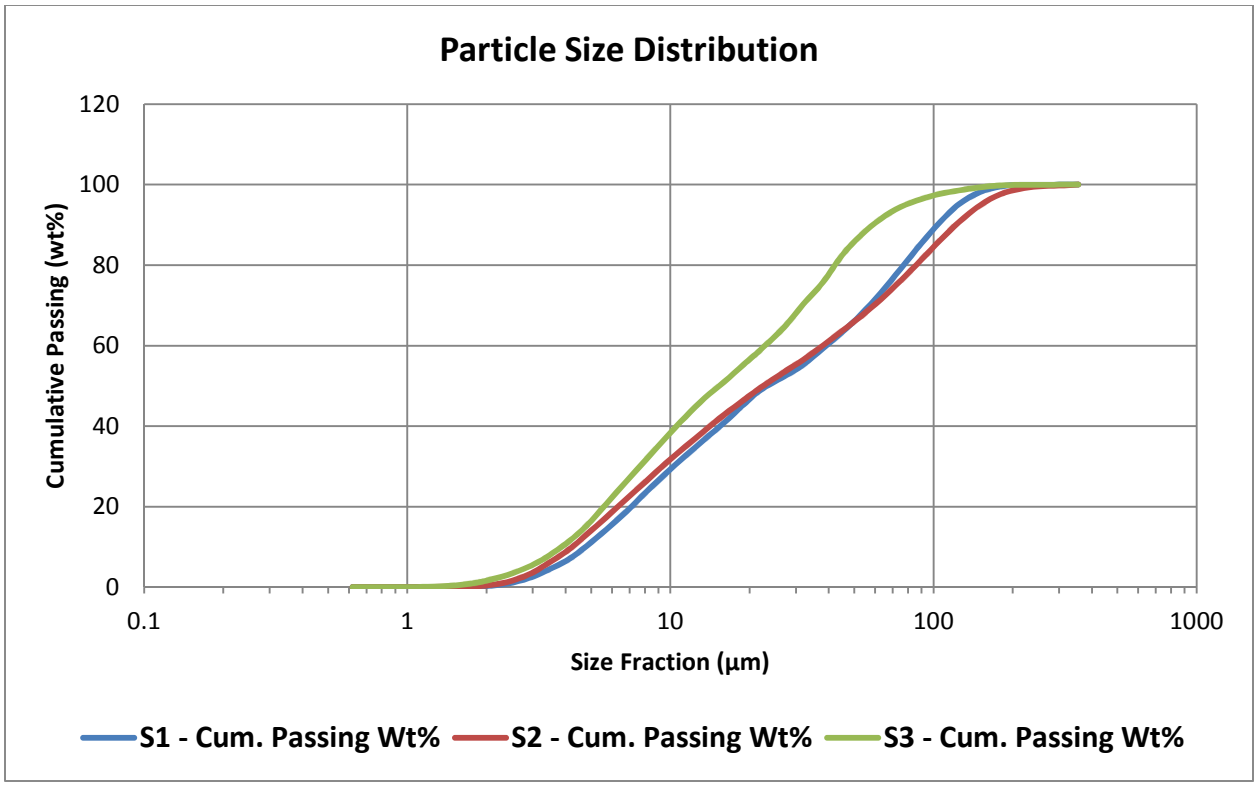

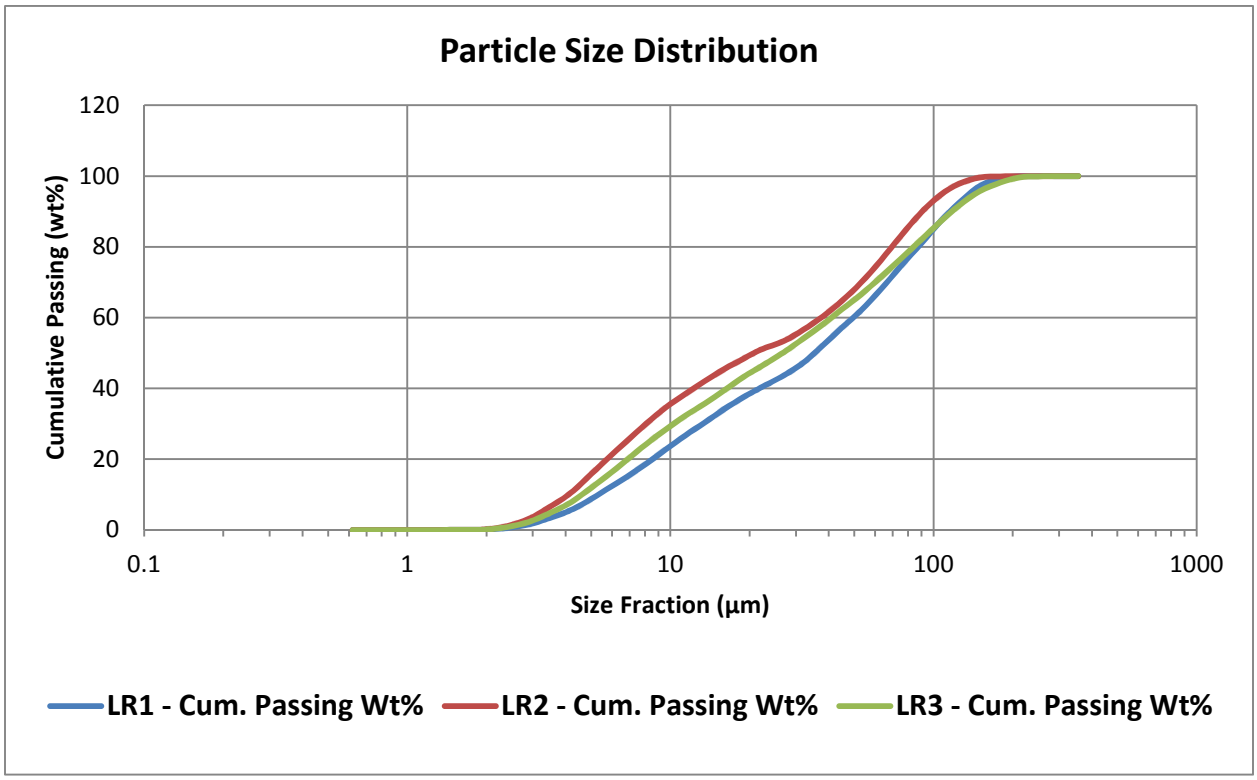

Figure 5.22 Particle size distributions in blends and leach residues.

5.2.5.1 Quantitative Modal Mineralogy

Modal abundance using MLA technology is very dependent upon several factors, which include sample mount integrity, SEM, and the MLA image analysis and X-ray classification database. Using the MLA classification algorithm (chi-squared probability) mineral phase names from the database library were assigned to discriminate segments of each particle. The processed MLA images on the blends and leach residues revealed the percentages of 19 different minerals and phase groups (listed in Table 5.6) previously identified by spot analysis and stored in the MLA database.

Quantitative modal mineralogy for the tested samples is shown in Tables 5.6 and 5.7. The processed MLA images on the blends and leach residues reveals the percentages of 19 different minerals and phase groups previously identified by spot analysis and stored in the MLA database.

Ores and special wastes

The two ores, McA and MLM, contain 39 wt% and 26 wt% quartz, respectively. But the most noticeable differences between their mineralogical compositions were the higher content of illite clay and mica type minerals, whereas McA ore contains a higher content of chlorite. Mica group and illite make up approximately 54 wt% of the materials. Sulphide (including arsenate) minerals make up 1.2 wt% and 0.5 wt% of McA and MLM respectively. Ore minerals were uraninite, uranophane and minor coffinite. The uraninite contents of the McA ore was about 6 times higher than that of the MLM. A considerable percentage of U is associated with fine-grained complex particles (Table 5.6; Fg-lithic+U). These particles will dissolve less favorably in acid leaching. Both ores showed most sulphides and U-bearing minerals in the <38c particle range (Appendix). However, McA showed most silicates in the coarser >38 μm particle range, and MLM contained them in the fines. The McA ore also showed a high content of carbonate, sulfate and inosilicates (amphibole and pyroxene). It was assumed that any fine carbonate particles would be readily dissolved in acid leaching.

Special wastes were rich in quartz. GSW and McW have the relatively higher Fe-oxide contents than the ores and DSW. McW showed the highest clay and mica contents among the waste samples. These samples were all poor in U-bearing minerals. However Gartner special

waste contains gersdorffite, millerite and arsenate minerals-annabergite and scorodite, which were the main source terms of As and Ni in the blends as the ores are monometallic. Wastes showed most sulphides, U-bearing minerals, and inosilicates in the fine particle range (Appendix).

Blends

Approximately 60 wt% of the materials in the S1 sample were quartz with 5.7 wt% uraninite, 1 wt% uranophane, 3.4 wt% chlorite, 1.8 wt% illite, 6.2 wt% mica, 3.8 wt% pyroxene, 0.7% carbonates and 0.6 wt% EOC-bearing sulphides, arsenates and Ni/Co-sulfates. Majority of quartz was occurring in the coarser particles. Pyrite, chalcopyrite, molybdenite, gersdorffite, galena, scorodite, and annabergite were present in minor amounts, but comparatively more abundant in the finer size fractions (<38 μm). Chlorite type clays exceeded illite and kaolinite in quantity, which relates to the main source material McA ore. Sulphide and U-bearing minerals were found in the finer particle size range (<38μm).

S2 sample was composed of approximately 55 wt% quartz, 6.2 wt% uraninite, 1.5 wt% uranophane, 4.3 wt% chlorite, 4.3 wt% illite, 9 wt % mica, 2.9 wt% pyroxene and 0.8 wt% EOC-bearing sulphides, arsenates and Ni/Co-sulfates. Majority of quartz was occurring in the coarser particles. Pyrite, chalcopyrite, molybdenite, gersdorffite, galena, scorodite, annabergite were present in minor amounts, but comparatively higher amount in finer size fraction (<38 μm). Illite type clays exceed and kaolinite in quantity, which relates to the change in blend materials and introducing MLM. Sulphide and U-bearing minerals were found in the finer particle size range (<38 μm).

Approximately 50 wt%, 2.1 wt%, 1.4 wt%, 1.7 wt %, 12.9 wt%, 17.3 wt%, 0.5 wt% and 0.4 wt% of the S3 were quartz, uraninite, uranophane, chlorite, illite, mica, pyroxene and EOC-bearing sulphides, arsenates and Ni/Co-sulfates. Pyrite, chalcopyrite, molybdenite, gersdorffite, galena, scorodite, and annabergite were present in minor amounts. However increase in molybdenite content is noticeable. Illite was the major clay in this blend, which relates to the major ore source as MLM. After quartz, mica and illite were the major minerals respectively. U-bearing minerals were found in the coarser particle size range (>38 μm). S3 showed most pyrite and chalcopyrite in coarse and fine particle range, respectively.

Leach residues

Major minerals present in LR1 were quartz, mica, feldspar, illite, pyroxene and fine-grained complex particles (Table 5.6; Silicates + Fg U mix). Few sulphide minerals like pyrite, chalcopyrite, molybdenite, gersdorffite and galena were also present in trace amounts. Sulfate minerals, barite and gypsum precipitate during the leaching process. Gypsum may be the result of the high carbonate content in S1.

LR2 composed primarily of quartz, mica, illite and feldspar. A few sulphide minerals like pyrite, chalcopyrite, molybdenite, galena and millerite were also present in trace amounts. Sulfate minerals such as barite precipitated during the leaching process.

Major minerals present in LR3 were quartz, mica, illite and feldspar. A few sulphide minerals like pyrite, chalcopyrite, molybdenite, millerite, galena and gersdorffite were also present in trace amounts. . Sulfate minerals such as barite precipitated during the leaching process.

5.2.5.2 Grain Size Distribution

Figure 5.22 shows the distribution of particles both in mill feeds and leach residues. Particle size plays an important role in the fate of the elements of concerns. The size fractions in the studied samples are outlined in Table 5.8. Sample S2 had the highest percentage of material in the coarsest fraction (> 75μm), whereas S3 has the lowest percentage of material in this size fraction. In acid leached product of S3, which was denoted as LR3, the coarsest fraction (>75 μm) increases to 4 times and the finer fraction (<11.4 μm) decreases. This observation indicates the selective leaching of finer particles and comparative increase of coarser particles that remained unleached or partially leached.

The plots in fig. 5.23 show the particle size distribution of pyrite, chalcopyrite, molybdenite and uraninite in blends. Pyrite grains show more or less similar size distribution. Both chalcopyrite and molybdenite particles were much coarser in S2. Uraninite particles were coarser in sample S3. Smaller particles have a larger surface area and are more leachable (Ruby et al. 1999). This observation explains the higher leaching proficiency of pyrite and chalcopyrite in S1.

Table 5.6 Mineral modal abundances in samples based on MLA work.

Minerals (wt%)	McA	MLM	GsW	DsW	McW	S1	S2	S3	LR1	LR2	LR3
Quartz	39.24	25.91	70.39	64.04	62.01	60.15	54.89	50.52	72.40	68.70	70.20
Illite	0.84	25.41	1.53	3.43	4.33	1.75	4.82	12.90	2.10	6.10	8.54
Chlorite	8.03	1.05	2.30	2.01	2.71	3.40	4.29	1.67	0.69	1.20	0.38
Mica	6.32	28.47	8.02	7.53	8.90	6.20	8.95	17.26	5.85	11.55	10.02
Feldspar	1.67	1.06	2.00	3.78	4.68	2.37	2.29	2.07	2.80	2.92	2.75
Fe-oxide	0.32	0.50	2.34	0.96	2.21	1.01	1.13	1.20	0.19	0.23	0.24
Ti-oxide	0.50	3.26	0.29	0.26	0.24	0.39	0.73	1.77	0.28	0.93	0.77
Kaolinite	1.07	1.07	1.58	0.92	0.72	0.52	1.05	0.75	0.65	0.70	0.81
Sulfide	1.20	0.45	0.40	0.40	0.50	0.60	0.80	0.44	0.30	0.60	0.50
Uraninite	13.40	1.97	0.10	0.07	0.32	5.65	6.20	2.10	0.01	0.00	0.05
Uranophane	2.71	0.25	0.01	0.04	0.13	1.00	1.54	1.39	0.05	0.00	0.00
Coffinite	0.07	0.12	0.08	0.00	0.01	0.05	0.08	0.52	0.00	0.00	0.05
Carbonate	1.16	0.02	0.09	0.37	0.79	0.72	0.59	0.17	0.00	0.00	0.00
Sulfate	0.06	0.02	0.11	0.05	0.89	0.08	0.06	0.03	0.22	0.12	0.11
Amplibole	3.00	0.01	0.15	0.46	2.12	1.76	1.37	0.10	0.05	0.05	0.06
Pyroxene	4.29	0.37	1.78	6.05	4.28	3.84	2.90	0.51	2.13	0.27	0.42
Almandine	2.66	0.22	0.66	0.43	0.61	1.31	1.61	0.47	0.14	0.19	0.19
Apatite	0.06	0.31	0.02	0.05	0.05	0.05	0.08	0.17	0.00	0.00	0.00
Silicates + Fg U mix	6.18	0.77	0.07	0.19	0.73	2.48	1.93	0.90	2.70	0.02	0.50
Fe-oxide + Fg U mix	0.25	0.17	0.10	0.02	0.05	0.19	0.20	0.31	0.19	0.00	0.06
Other + unknown	6.84	8.91	7.74	8.91	3.83	6.66	4.26	5.39	9.21	6.78	4.68
Total	100	100	100	100	100	100	100	101	100	100	100

* Fg U mix: Fine-grained U-bearing minerals

Table 5.7 Modal abundances of sulfides, sulfates and arsenates.

Minerals (wt%)	McA	MlM	GSW	DSW	McW	S1	S2	S3	LR1	LR2	LR3
Pyrite	0.71	0.28	0.06	0.35	0.37	0.30	0.40	0.24	0.21	0.37	0.31
Chalcopyrite	0.26	0.10	0.01	0.06	0.05	0.15	0.20	0.15	0.07	0.11	0.11
Colbaltite	<0.01	0.00	0.00	0.00	0.00	0.00	0.00	0.00	0.00	0.00	0.00
Molybdenite	0.01	0.04	0.00	0.00	0.00	0.01	0.02	0.03	<0.01	0.01	0.01
Gersdorffite	0.00	0.00	0.04	0.00	0.00	<0.01	<0.01	<0.01	<0.01	0.00	0.01
Scorodite	0.00	0.00	0.01	0.00	0.00	0.01	<0.01	0.00	0.00	0.00	0.00
Annabergite	0.00	0.00	0.21	0.01	0.00	0.02	0.02	0.02	0.00	0.00	0.00
Millerite	0.00	0.00	0.02	0.00	0.00	0.00	0.01	0.01	0.00	0.01	0.01
Sphalerite	0.00	0.00	0.00	0.00	0.02	0.00	0.00	0.00	0.00	0.00	0.00
Galena	0.17	0.04	0.01	0.00	0.02	0.09	0.10	0.02	0.06	0.08	0.02
Barite	0.06	0.02	0.11	0.05	0.89	0.08	0.06	0.03	0.16	0.12	0.11
Gypsum	0.00	0.00	0.00	0.00	0.00	0.00	0.00	0.00	0.06	0.00	0.00

Table 5.8 Particle size distribution.

Size fraction (μm)	Feed to pilot mill			Leach residues		
	S1	S2	S3	LR1	LR2	LR3
> 75	20.9	23.9	5.5	25.5	17.0	23.4
75 to 45	15.8	12.5	12.0	17.3	18.2	14.2
45 to 27	11.0	10.3	18.0	13.5	11.4	12.2
27 to 22	3.3	3.9	5.5	3.5	2.5	4.1
22 to 16	8.2	6.7	8.0	6.0	5.5	6.7
16 to 11.4	8.2	7.9	8.7	7.4	7.0	7.1
< 11.4	32.6	35.0	42.3	26.8	38.4	32.3
Total	100	100	100	100	100	100

5.2.5.3 Liberation And Leaching

Liberation is an important metallurgical parameter and automated mineralogy (MLA) was originally developed for the analysis of liberation. Liberation is the separation and enrichment of ore minerals from gangue minerals through size reduction. There are two types of liberation present: liberation by volume and liberation by free surface (FEI, 2011). Liberation by free surface was considered in this present study. Recovery is optimized when particles are fully separated as the exposed proportion of the material is most likely to dissolve in acid leaching.

Table 5.9 shows the liberation degree of some important minerals occurring in the studied samples. Liberation was compared for pyrite, chalcopyrite, molybdenite, annabergite, galena, uraninite and Uranophane. At target grind (<75 μm) 67%, 80%, and 66% liberation of U minerals were achieved in S1, S2 and S3 respectively (Table 5.9). The majority of the unliberated uraninite and uranophane were locked in silicates. S2 with the highest percentage of liberated U minerals showed nearly 100% ore recovery in acid leaching (Table 5.10).

The highest percentages of liberated minerals were achieved in the mill feed blend 2 (S2), and thus should have higher leaching proficiency. However, poor mineral liberation does not necessarily mean poor leaching proficiency, if the minerals are locked in or associated with the coarser particles. As seen in the grain size analysis (Fig. 5.23), S2 had coarser grain size distribution and lower recovery for pyrite, chalcopyrite, molybdenite, annabergite, and galena were attained compared to S1 and S3 (except uraninite). In S2 uraninite was liberated not only to the highest degree, but also has relatively finer grain size distribution (Fig. 5.23). It is clear

that both liberation degree and grain size distribution of the mineral collectively determine its recovery in acid leaching.

Table 5.9 Liberation degree of some important minerals.

Sample	Mineral	Monomer	Binary interlocking	Ternary interlocking	Total (%)
S1	Pyrite	49.9	38.6	11.5	100.0
	Chalcopyrite	66.2	26.0	7.8	100.0
	Molybdenite	13.6	45.9	40.5	100.0
	Annabergite	50.4	45.7	4.0	100.0
	Galena	76.8	22.3	1.0	100.0
	Uraninite	67.2	26.2	6.6	100.0
	Uranophane	67.2	35.2	14.4	100.0
S2	Pyrite	68.1	28.3	3.6	100.0
	Chalcopyrite	74.2	21.1	4.6	100.0
	Molybdenite	38.1	58.5	3.4	100.0
	Annabergite	71.6	20.0	8.5	100.0
	Galena	76.6	15.0	8.4	100.0
	Uraninite	80.0	17.4	2.6	100.0
	Uranophane	80.0	25.3	8.1	100.0
S3	Pyrite	35.3	27.5	37.2	100.0
	Chalcopyrite	43.5	37.4	19.1	100.0
	Molybdenite	24.2	39.0	36.8	100.0
	Annabergite	0.0	0.0	100.0	100.0
	Galena	30.7	40.9	28.4	100.0
	Uraninite	66.1	19.1	14.8	100.0
	Uranophane	66.1	32.1	42.1	100.0
LR1	Pyrite	80.0	14.4	5.6	100.0
	Chalcopyrite	47.7	43.8	8.5	100.0
	Molybdenite	91.8	0.0	8.2	100.0
	Annabergite	0.0	100.0	0.0	100.0
	Galena	56.5	24.4	19.1	100.0
	Uraninite	74.0	9.9	16.2	100.0
	Uranophane	74.0	12.1	76.6	100.0
LR2	Pyrite	79.6	16.6	3.8	100.0
	Chalcopyrite	78.1	21.2	0.7	100.0
	Molybdenite	58.1	41.9	0.0	100.0
	Annabergite	0.0	0.0	0.0	100.0
	Galena	72.6	21.1	6.3	100.0
	Uraninite	0.0	100	0.0	100.0
	Uranophane	71.7	28.3	0.0	100.0
LR3	Pyrite	81.9	17.7	0.5	100.0
	Chalcopyrite	68.9	30.1	1.1	100.0
	Molybdenite	98.7	1.1	0.2	100.0
	Annabergite	0.0	0.0	100	100.0
	Galena	65.8	29.8	4.4	100.0
	Uraninite	1.6	98.4	0.0	100.0
	Uranophane	100	0.0	0.0	100.0

Table 5.10 Unleached mineral percentages in leach residues.

Unleached (%) Primary Minerals			
Mineral	LR1	LR2	LR3
Pyrite	55	68	90
Chalcopyrite	36	40	51
Molybdenite	N/A	37	23
Gersdorffite	N/A	N/A	N/A
Scorodite	0	N/A	N/A
Annabergite	0	0	0
Millerite	N/A	73	70
Galena	52	58	70
Barite	Primary+Precipitation		
Gypsum	Precipitation		
Uraninite (U)	0	0	2
Uranophane	4	0	0
Coffinite	0	0	7
Quartz	94	91	97
Illite	93	92	46
Chlorite	16	20	16
Mica	74	94	41
Kaolinite	98	49	76
Silicate + fine-grained U mix	70	1	13
Fe-oxide + fine-grained U mix	98	0	12

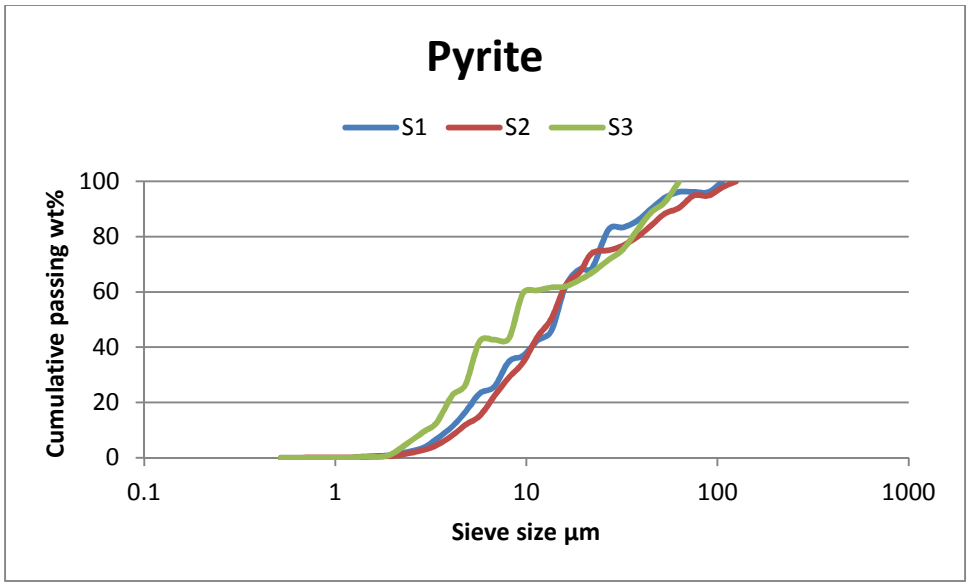
Pyrite
S1
S2
S3
Cumulative passing wt%
100
80
60
40
20
0
0.1
1
10
100
1000
Sieve size µm

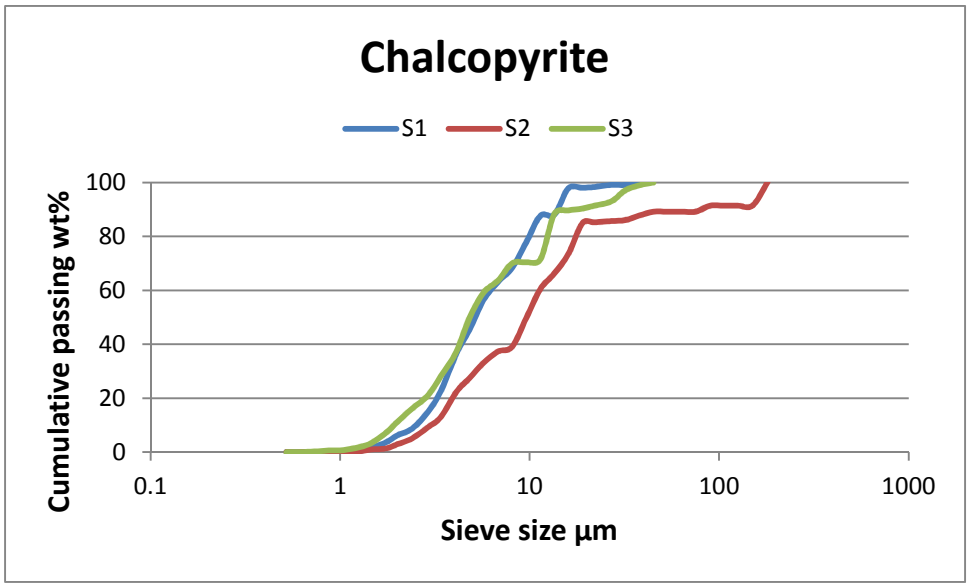
Chalcopyrite
S1
S2
S3
Cumulative passing wt%
100
80
60
40
20
0
0.1
1
10
100
1000
Sieve size µm

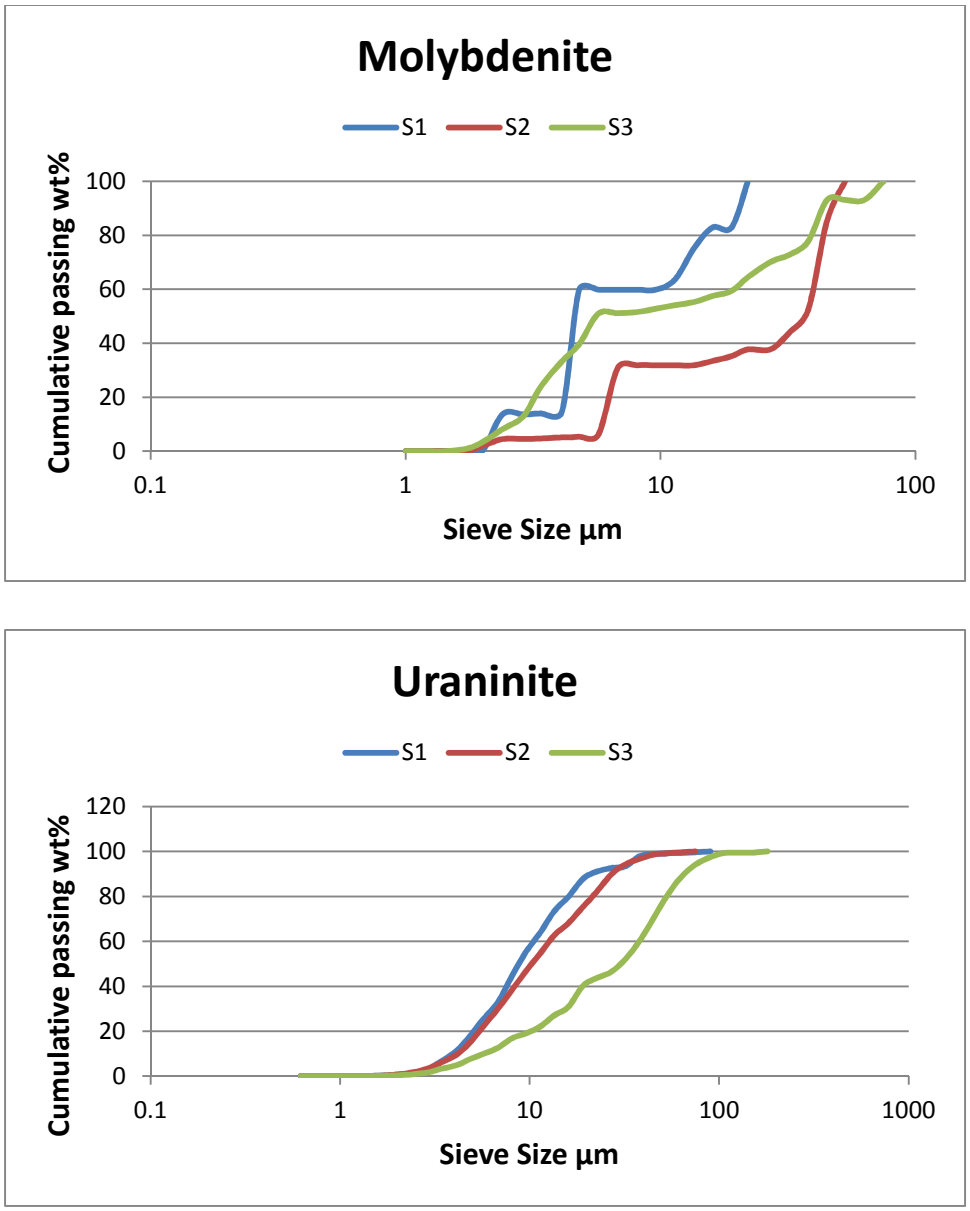

Figure 5.23 Grain size distributions of pyrite, chalcopyrite, molybdenite and uraninite in mill feeds.

Percentages of the unleached minerals in the leach residues are presented in table 5.10. Percentages of unleached minerals passed into leach residues vary considerably. The highest percentages of sulphide minerals, e.g. pyrite, chalcopyrite and galena remain unleached in LR3. Three types of uraninite have been identified- uraninite (liberated and interlocked), silicate with fine-grained uraninite association, and iron-oxide with fine-grained uraninite association (Fig.5.21; table 5.10). Even though uraninite (liberated and binary interlocked) shows 98-100%

leaching proficiency, fine-grained uraninite occurring within complex particles of silicate minerals remained unleached to a greater amount in LR1 and LR3. These results support and explain the presence of U in LR1 (1.6 wt %) and LR3 (0.6 wt%) analyzed by ICP-MS. Among the clays, chlorite showed a higher leaching proficiency than illite and kaolinite. Leaching proficiencies were different for different blends and mainly caused by of grain size distribution and mineral liberation.

5.3 Clay Minerals

The clay minerals were analyzed in the 2μm fractions (clay fraction) which were separated by centrifuging 2 grams of samples in 50 ml Calgon solution. The clay minerals and their properties were characterized using XRD, SEM and CEC methods. Changes in CEC was employed to support and supplement the changes of clay structures observed in the resulting leach residues as a result of acid leaching.

5.3.1 XRD Analysis

X-ray diffraction analyses showed that the clay mineralogy of the ores was dominated by chlorite, illite and kaolinite (Table 5.11). XRD data support the quantitative analyses of clay minerals by MLA and were found to be positively correlated (Fig. 5.24A). The McArthur River ore was dominated by chlorite (62 wt %), with considerable amounts of illite/mica (14 wt %) and kaolinite (8.2 wt %) in XRD spectra of the air dried and glycolated samples. Relatively higher intensity of the 002 chlorite (Ch) peak at ~14.3^0 2θ is characteristic of clinochlore. McGill et al. (1993) mentioned extensive chlorite alteration in the high-grade U mineralized zones in the basement at McArthur River. . The alteration end-members includes Fe-Mg chlorites (+/- sudoite), illite and kaolinite. Analysis of the clay fraction of this ore also indicated the presence of quartz and uraninite (Fig 5.25A).

The air-dried MLM clay fraction was dominated by illite, with considerable amounts of chlorite, kaolinite and micas (Table 5.11; Fig. 5.25A). Intense 003 chlorite (Ch) peak at ~21.5^0 2θ in MLM is characteristic of Al-rich chlorites (i.e. sudoite). The broad and asymmetrical 001 chlorite (Ch) peak at ~7^0 2θ could be resulted due to the presence of chlorite-vermiculite mixed-layer clay (Offler, 1994; Ruiz Cruz and Nieto, 2006). Both the 001 and 002 chlorite peaks were

shifted towards the high order d-spacing which happens in the presence of mixed-layer type of clays.

Table 5.11 Semi-quantitative clay minerals by Rietveld analysis.

Clay Minerals (wt%)	**McA**	**MlM**	**DsW**	**GsW**	**McW**	**S1**	**S2**	**S3**	**LR1**	**LR2**	**LR3**
Chlorite	61.9	26.9	28.8	38.7	24.3	46.9	37.5	26.4	25.5	27.9	26.5
Illite/mica	13.9	44.0	40.5	11.9	56.4	30.3	42.7	57.1	37.4	43.9	55.4
Kaolinite	8.2	17.7	6.5	20.0	19.3	17.9	14.2	16.0	21.7	27.7	14.5
Illite-smectite	ND	Trace	Trace	ND	ND	ND	ND	Trace	ND	ND	ND
Illite/mica-vermiculite ?	ND	ND	ND	ND	ND	ND	ND	Trace	Trace	ND	Trace

Table 5.12 Cation Exchange Capacity of Blends vs Leach Residues.

Name	Na (mg/L)	Mg (mg/L)	Al (mg/L)	K (mg/L)	CEC (cmol/kg)	Ba (mg/L)
S1	3.57	0.56	0.66	10.25	0.54	0.53
S2	3.86	1.40	0.34	9.37	0.56	1.66
S3	4.27	4.95	0.31	18.39	1.10	0.51
LR1	0.76	180.56	271.36	0.84	45.25	0.05
LR2	2.42	10.47	0.55	12.48	1.36	5.04
LR3	7.06	127.64	255.95	66.67	41.10	0.02

The air-dried DSW clay fraction was dominated by illite, with considerable amounts of chlorite, a minor amount of quartz and trace amounts of illite-smectite mixed-layer clays (Table 5.11; Fig. 5.25B). The asymmetrical 001 illite (I) peak with a broad shoulder between 9-10^0 2θ suggested the presence of illite-smectite mixed-layer clay.

Air-dried GSW clay fraction was dominated by chlorite, with considerable amounts of illite and minor amounts of quartz and orthoclase (Table 5.11; Fig. 5.25B). MLA analysis

indicated the clay minerals total to 5.4 wt %, which supports the report by Fortuna (1983). Ruhrmann (1987) also reported pervasive chloritization of the gneiss immediately below the unconformity at Gaertner. Fracture-controlled illitization and kaolinitization as well as quartz, and carbonate were found peripheral to the strongly chloritized zone (Ruhrmann, 1987).

McArthur River mineralized waste (McW) was composed of basement rocks surrounding the mineralized zones. Clay fraction of McW sample was found to be dominated by illite with substantial amounts of chlorite and kaolinite. In the basement, McA ore was characterized by an outer illite-rich alteration halo enclosing the structures that controlled the ore formation (McGill e al. 1993; Kotzer and Kyser 1995).

Clay fractions in the blends and leach residues were also analyzed with XRD. Quantitative analyses using the XRD and MLA were found to be positively correlated (Fig. 5.24A & B). S1 was chlorite dominated, but S2 and S3 were found to be dominated by illite. The broad illite peaks in S3 could be because of the existence of mixed-layer clay or due to coherent diffracting domains in the crystallites (poorly crystallized illite due to smaller grain size) (Gharrabi et al., 1998; Velde and Barré, 2009). Some of the peaks decomposed upon solvated with ethylene glycol. The 5.06 Å peak of the air dried S3 sample decomposed into 5.10, 5.06 and 5.02 Å peaks. The 3.36 Å peak decomposed into peaks at 3.39 and 3.34 Å. The 4.80 Å peak decomposed into peaks at 4.82 and 4.8 Å. Although not conclusive, 001 illite peak at 10.3 Å and a broad shoulder of the 14-14.3 Å peak at ~12 Å possibly suggested trace amounts of illite/mica-vermiculite type mixed-layer clay (Moore and Reynolds, 1997; Manceau et al., 2005). This peak did not change the position or intensity after the glycol saturation. The clay minerals were accompanied by quartz, and uraninite.

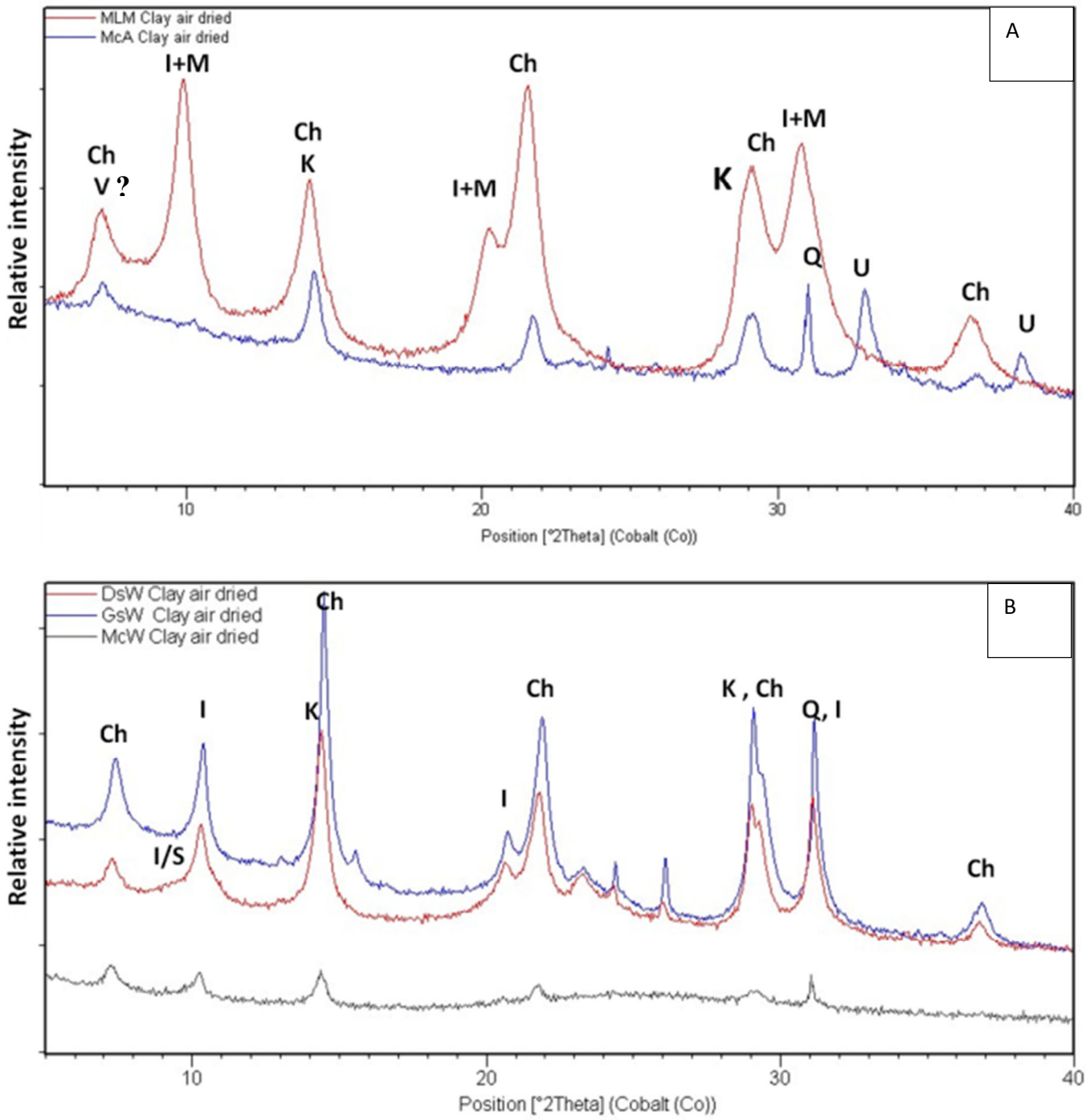

Figure 5.25 XRD diffractograms of the clay fractions of the ores (McA and MLM) and special wastes (DsW, GsW and McW) samples; where chlorite (Ch), kaolinite (K), illite (I), mica (M), brucite (B?), illite-smectite mixed layer (I/S), uraninite, quartz (Q).

The XRD spectra corresponding to acid-leached clays revealed some evidences of likely modifications in the clay structures (Fig. 5.26). The leach residues showed broad and asymmetric peaks (Fig. 5.26). The peaks broaden after acid leaching indicated an increased disorder. The14.25 Å peak in LR3 was well defined and intense compared to that of S3. The shoulder at ~12.2 Å might occurred due to the presence of mixed-layer trioctahedral illite/mica-vermiculite (Moore and Reynolds, 1997; Manceau et al., 2005). A superstructure peak at ~22.4 Å was identified in the low angle diffraction patterns of LR3 (Fig. 5.27). The illite peak at ~10 Å was also broad and showed a subtle high-angle shoulder. No notable deviations were observed in the XRD peaks of the LR2. Leach residues also contained quartz in the clay fraction. The hkl peaks of chlorite and the 011 peak of quartz at 3.35 Å have significantly lower intensities in the LR2 than LR1 and LR3. Overall the hkl peaks of chlorite reduced intensity significantly compared to kaolinite in the residues. It appears that chlorite was more susceptible to dissolution during acid leaching than illite and kaolinite (Brandt et al., 2003; Lowson et al., 2005).

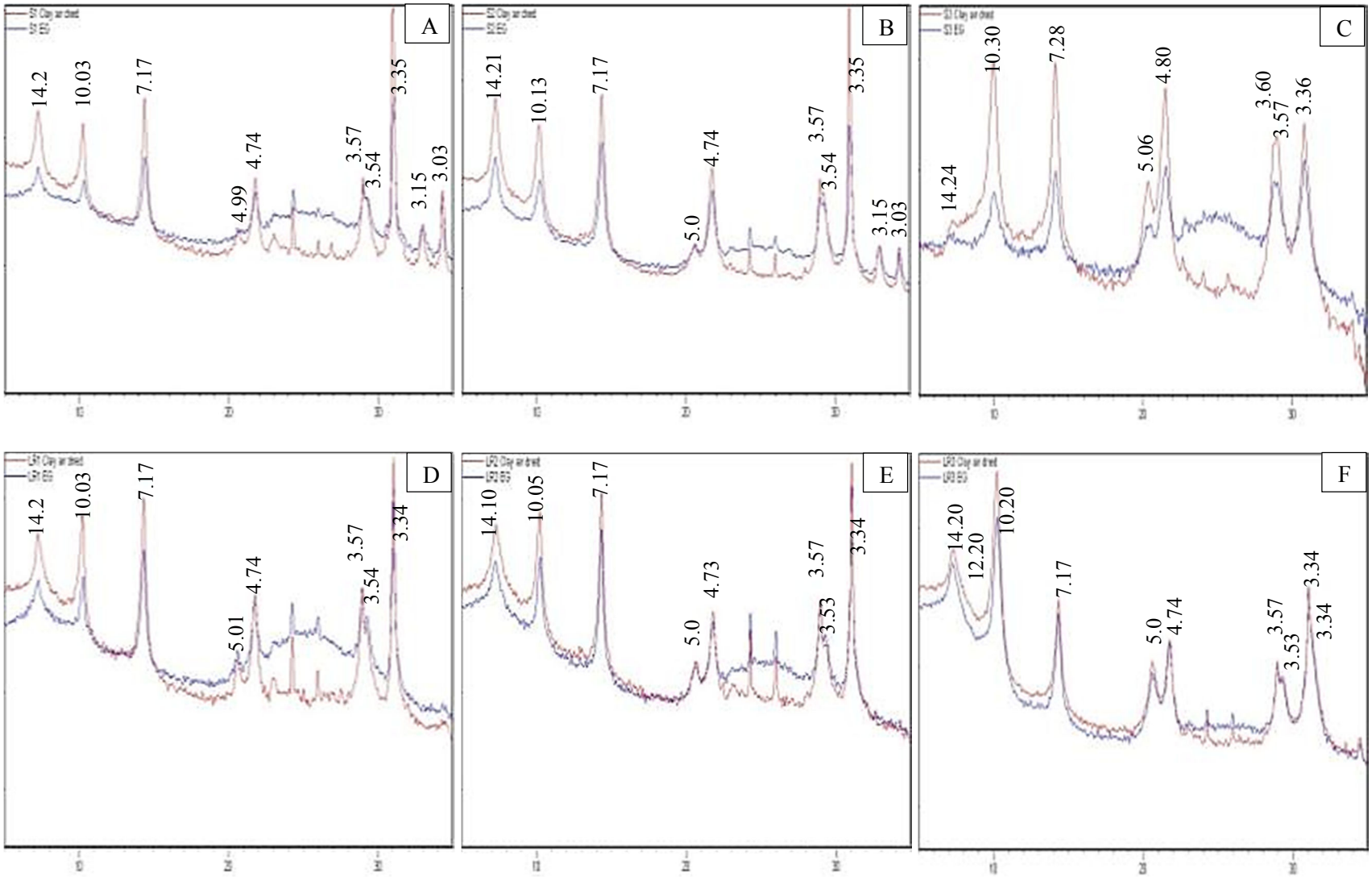

Figure 5.26 X-ray diffraction patterns of the clay fractions in blends (S1, S2 and S3) and leach residues (LR1, LR2 and LR3). Spacing in Angstrom units.

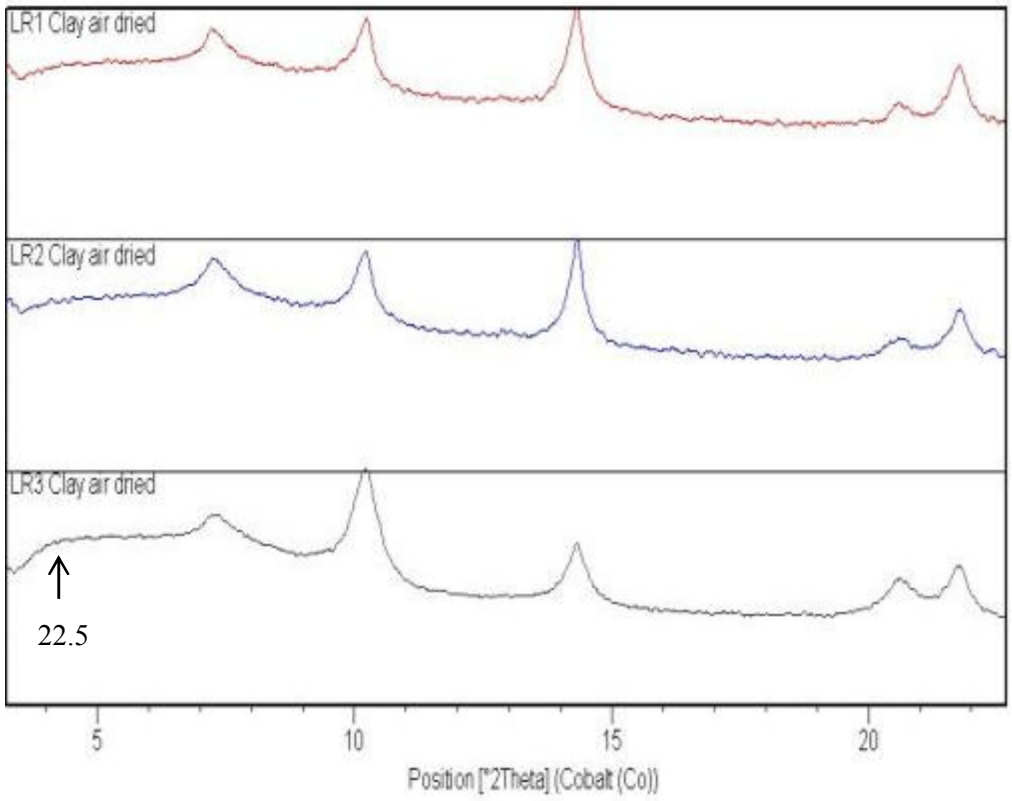

Figure 5.27 Comparison between the X-ray diffraction patterns of the clay minerals in the leach residues. Spacing in Angstrom units.

5.3.2 Cation Exchange Capacity (CEC)

CEC values from the $BaCl_2$ compulsive exchange method (Gillman and Sumpter, 1986) were measured for the solids before and after the acid leaching. The results are shown in Table 5.12. Cation values of Na, Mg, Al, and K were put in the equation 1. Ca values were excluded as gypsum was found in the leach residues. Greater values of Ca in the leach residues might be the result of ionic substitution Ba in gypsum. The CEC values were clearly many folds higher in the leach residues compared the values in the blends. S3 has the maximum CEC value of 1.1 cmol/kg among the blends. LR1 and LR3 had CEC values of 45.3 and 41.1 cmol/kg respectively. The Ba concentrations in the extracts from $BaCl_2$ exchange positively correlated the concentrations of the cations (Al, K, Mg and Na) (Table 5.12). Higher CEC occurred as Ba replaces the exchangeable cations in the clay minerals with higher CEC.

Along with the permanent layer charges, the negative variable charges at the unsatisfied broken bond edges and exposed OH^- terminated planes of the clay minerals were responsible for the CEC. During acid leaching, the surfaces of the clay minerals were severely attacked by the H_2SO_4. As a result, numerous exposed OH^- terminated planes were created and adsorbed base cations and metals. High illite contents and the presence of possible mixed layer clay minerals could cause the higher CEC values in the leach residues.

The crystallinity and size of the clay minerals can affected the release of the cations. Leach residues had both low crystallinity and low grain sizes of the clay minerals and release higher amount of Al, Fe, Mg and K. The protons replace the exchangeable cations at first during acid leaching and then they react with the layers (Cicel and Komadel, 1994). Some of the acid activated clay structures change to their Al, Fe, Mg and K form as the protons get replaced by cations released from silicates during acid leaching.

CEC change was most likely caused by two parameters: particle size reduction of the clay minerals, and the transformation of their structure. The higher CEC values might suggested that the phyllosilicates were altered to some level during the acid leaching of the blends. The transformation of the mica type structure into illite/mica-vermiculite could play some role to change the CEC values. Kuwahara and Aoki (1995) showed that vermiculite and mixed layer mica-vermiculite were formed in the acid alteration process of phlogopite. The SEM analysis of the clay fractions showed indication of alteration of mica type minerals (Fig. 5.28). These images also confirmed that the attack of acid occurred from the particle edges. Illite/mica minerals can altered to other 2:1 minerals through the extraction of interlayer potassium by hydrated cations such as Ca and Mg. Also a comparatively large amount of isomorphous replacement of their main cations, the exchange of Si^{4+} for tetrahedral Al^{3+}, results a large number of exchange sites and a high CEC in vermiculite. In vermiculite, the exchange of Al^{3+} for Si^{4+} in tetrahedra creates 1 negative site for each substitution. On the other hand, destruction of the octahedral and tetrahedral sheets of 2:1 layer clay minerals during acid leaching can reduce the CEC in LR2 (Fig. 5.9).

The XRD and CEC data can be explained by means of the mechanisms of acid activation of mica which is exemplified in Fig. 5.29. Acid alteration causes hydrogen metasomatism and subsequent base cation leaching. At low pH, hydrolysis occurs and cations are more mobile.

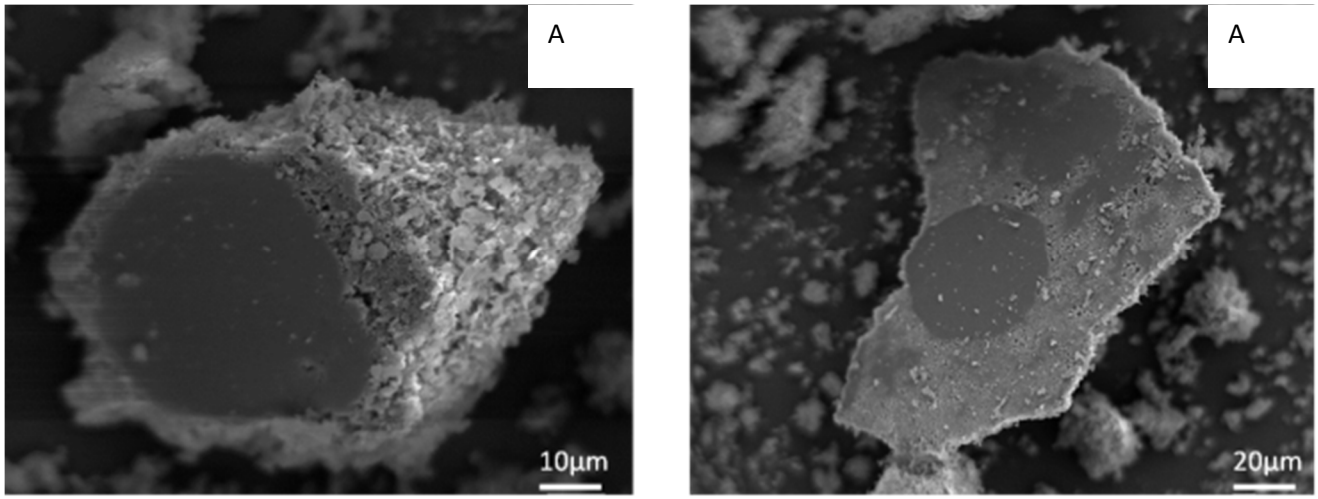

Figure 5.28 Secondary electron images of clay fractions; A) LR1 and B) LR2.

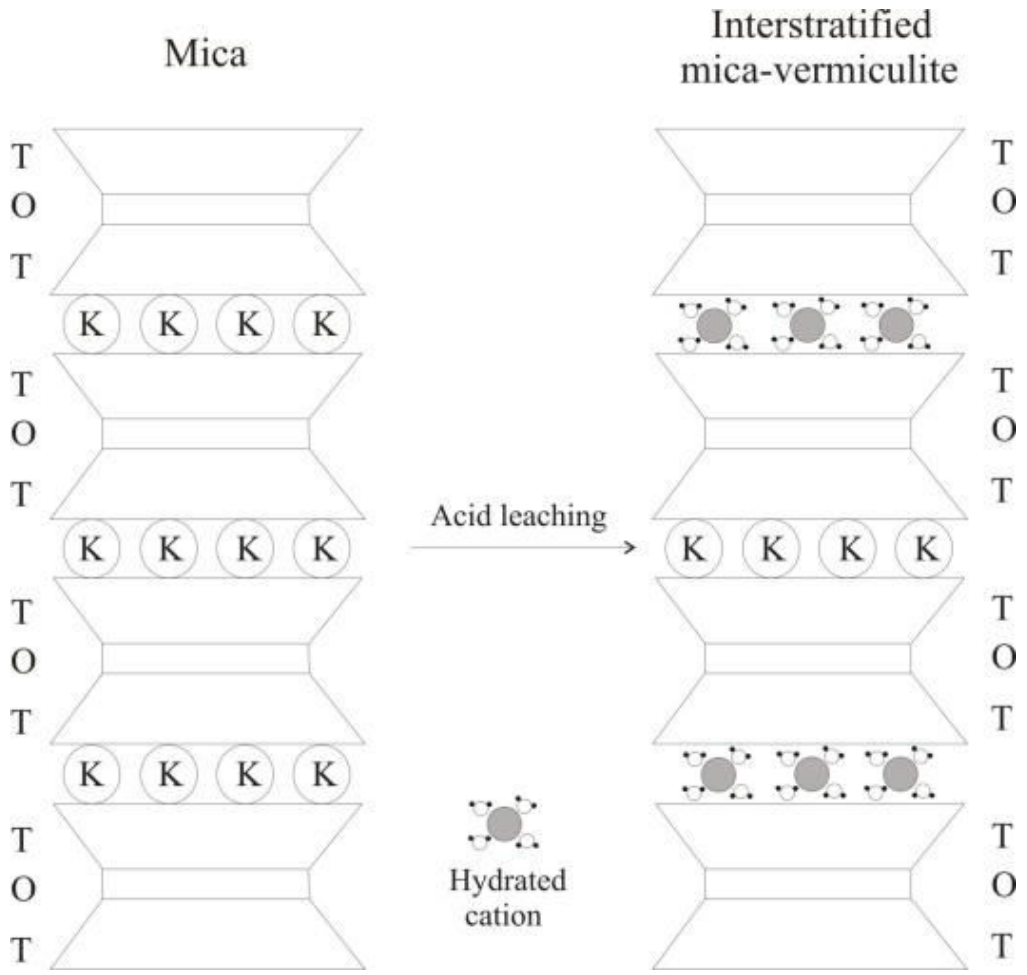

Figure 5.29 Acid alteration of mica structure and formation of mixed-layer clay.

T: Si tetrahedron; O: Al octahedron

During acid leaching, potassium (K^+) held by the 2:1 T-O-T structures can be replaced by cations such as hydrogen (H^+) or hydrated strong base cations (e.g. Ca and Na, as released by the dissolution of primary silicates and carbonates). If any mixed-layer clays were formed, they would be non-expanding illite/mica-vermiculite clays. Moreover, vermiculite has higher affinity of metal ions and total capacity for metal ions (Abollino et al., 2008). The higher Ni and As contents in the clay fractions of both the blends and leach residues support this observation.

CHAPTER 6

SUMMARY AND CONCLUSION

The U tailings have the potential to contaminate local groundwater and surface waters. As major component of the tailings, leach residues mostly contain unleached primary minerals and/or some secondary minerals. To predict the long-term controls on EOCs in tailings porewaters, the minerals hosting As, Mo, Ni, and Se in U ores and waste rocks and leach residues from the Key Lake mining operation, Saskatchewan were determined. The clay minerals were also analyzed to explain their alteration during acid leaching because they have an important role in controlling pore water geochemistry and sedimentation/consolidation behavior of the tailings.

Elemental analysis indicated that the optimum level of U and EOCs removal was in the blend S2 that was created from McArthur and Millennium ores. About 61 %, 88% and 67% of the S1, S2 and S3, respectively were dissolved during acid leaching. The U, Fe and Pb were the most abundant analytes with minor amounts of As, Mo, Ni, and Se. The total assay in leach residues decreased significantly after the milling of the blends. Gaertner special waste contained the highest concentrations of As and Ni, whereas the Millennium ore contained Mo and Se.

The ores consisted of quartz, chlorite, illite, mica minerals (muscovite/biotite), pyroxene, feldspar and uraninite. Uraninite was the primary ore mineral of U with some secondary coffinite and uranophane minerals. Uraninite particles varied in shapes on the basis of their liberated state. The unliberated particles were mostly associated with silicates and sulphides. Uraninite in McA ore frequently occurred in chlorite, clinopyroxenes, pyrite and chalcopyrite, whereas uraninite was found in association with mica, illite, quartz and molybdenite in MLM ore.

The reservoirs for As, Mo, Ni, and Se (in ores and blends) were dominated by sulphides including cobaltite, gersdorffite, molybdenite, pyrite, galena and chalcopyrite, secondary Ni-arsenates (annabergite), Fe-arsenate (scorodite) and Ni-Co/Ni-sulfates. The primary As-bearing minerals were cobaltite, gersdorffite, Ni-arsenate, molybdenite and Ni-sulfate whereas Ni was present mainly within Ni-sulfate, cobaltite, gersdorffite, Ni-arsenate, Ni-Co-sulfate, cobaltite, molybdenite, galena, chalcopyrite and pyrite. The average concentration of Ni was higher than the other three EOCs in the source materials. The maximum quantities of As and Ni were found

in arsenate and Ni-sulfate phases. Se was widespread pyrite, chalcopyrite, Ni-sulfate and molybdenite whereas Mo was not detected in any sulphides except the molybdenite.

Sources of EOCs in McA ore was primarily cobaltite with trace amount of EOCs presented in pyrite and chalcopyrite. MLM ore contained EOCs within gersdorffite, molybdenite with hints of EOCs in pyrite and chalcopyrite. The special wastes were source of EOCs as both primary and secondary minerals. Pyrite and chalcopyrite contained traces of EOCs in the DSW. Secondary Ni-arsenates (annabergite and scorodite) and Ni-Co/Ni-sulfates in GSW were major As, Mo, Ni, and Se bearing minerals, and were most likely the product of oxidation of arsenide minerals in special waste rocks. Oxidation removed S, Ni and As from the sulphide and sulf-arsenide minerals and produced sulfates and arsenates (e.g. annabergite-an oxidation product of nickeline). Analyses also showed that sulphides and arsenates occurred in trace amounts in the ores and special waste rocks (0.5 to 1.0 wt %).

The distribution of EOCs in the blends and leach residues was found to be controlled by the particle sizes of the reservoir minerals. Clay size fraction (<2μm) contained relatively higher quantities of Ni and As compared to Se and Mo. Se and Mo were more evenly distributed in the bulk and clay size fractions of both the blends and leach residues. These data suggest that the EOCs are associated not only with the sulphides, arsenates and the Ni-Co/Ni-sulfates, but also with the clay minerals. High adsorption of the clay minerals allow the clays to retain cations and oxyanions of metals and metalloids within the T-O-T interlayer structure and on the mineral surface.

Liberation of environmentally important minerals from multiphase ores is necessary in ore milling and processing. The data showed that minerals of environmental concern (e.g. pyrite, chalcopyrite, gersdorffite and uraninite) remained unliberated within silicates even after the size reduction process. These minerals were also found unleached in the leach residues. About 55 to 90% pyrite, 36 to 51% chalcopyrite, 23 to 37% molybdenite, and 52 to 70% galena remained unleached in the resulting leach residues after milling of the ore blends. The percentages of unleached minerals varied between mill feeds and were dependent on the grain-size distribution and the degree of mineral liberation.

CEC analysis indicated an increase of the CEC values in the leach residues, which might be the result of evolution of 2:1 layers into high-charge layers during the milling or particle size reduction of the clay minerals. However, these data were not conclusive to confirm any clay alteration during acid leaching. Detailed CEC and surface area measurement along with transmission electron microscopy analysis of the clay fractions are needed to stablish this hypothesis.

CHAPTER 7

SUGGESTIONS FOR FUTURE RESEARCH

Concentrations of EOCs in the U ores from the Athabasca Basin vary both spatially and vertically. As a result, variable concentrations of EOCs occur in the vertical section of the tailings (Shaw et al., 2011). This study characterized samples from McArthur River Zone 2 that has much lower As, Mo, Ni and Se concentrations relative to concentrations in the Key Lake ore bodies. Other ore zones (A, B and 4) at McArthur River are scheduled for mining in the near future. Their EOC concentrations and mineralogy might differ from the zone studied here. Further analyses are required to determine the distribution of EOCs in alternate ore zones at McArthur River as well as Millennium.

Leaching experiments are recommended on ores, blends and leach residues to investigate the environmental activity of heavy metals. Partitioning of metals within minerals present in the residue will better assist in the long-term tailings stabilization.

The initial stage in predicting and preventing acid rock drainage is to characterize the acid generating and neutralizing minerals present in the waste rocks and the tailings. Acid producing potential static tests could be undertaken on the waste rocks and the tailings to categorize them into acid producing and stable non-acid producing materials.

Studies of the clay minerals using TEM and IR are recommended to establish the influence of clay minerals on U extraction at the Key Lake mill. The mineralogical and geochemical impacts of H_2SO_4 on the clay minerals should be analyzed as a function of pH and exposure time through a series of batch experiments. Association of EOCs and U with the clay minerals are also needed to examine for improving the understanding of the porewater chemistry in the tailings.

REFERENCES

Abdallah, S.M., El-Hussaini, O.M., Mahdy, R.M., 2009. Towards a more safe environment: Disposability of uranium by some clay sediments in Egypt. Aust. J. Basic Applied Sci. 3, 1476-1488.

Abdelouas, A., 2006. Uranium Mill Tailings: Geochemistry, Mineralogy, and Environmental Impact. Elements 2, 335–341.

Abollino, O., Giacomino, A., Malandrino, M., Mentasti, E., 2008. Interaction of metal ions with montmorillonite and vermiculite. Appl. Clay Sci. 38, 227–236.

Alexandre, P., Kyser, K., Polito, P., Thomas, D., 2005. Alteration Mineralogy and Stable Isotope Geochemistry of Paleoproterozoic Basement-Hosted Unconformity-Type Uranium Deposits in the Athabasca Basin, Canada. Econ. Geol.

Ammann, L., Bergaya, F., Lagaly, G., 2005. Determination of the cation exchange capacity of clays with copper complexes revisited. Clay Miner. 40, 441.

Austin, L.G., Luckie, P.T., 1988. The problems of quantifying mineral liberation: a review. Part. Part. Syst. Char. 5, 3,122-129.

Bailey, S.W., 1975. Chlorites. In: Gieseking JE (ed) Soil components, vol II. Springer-Verlag, New York
(Chapter 7).Bailey, S.W., 1980a. Summary and recommendations of AIPEA nomenclature committee: Clay and Clay Minerals. 28, 73-78.

Bailey, S.W., 1980b. Structures of layet silicates: in Brindley, G.W., and Brown, G., editors, Crystal Structures of Clay Minerals and Their X-Ray Identification, Monograph No. 5. Mineralogical Society, London, 1-123.

Beauchemin, D., 2008. Inductively coupled plasma mass spectrometry. Anal. Chem. 80, 4455–86.

Bergaya, F., Lagaly, G., 2013. General Introduction: Clays, Clay Minerals, and Clay Science. Develop. Clay Sci. 5, 1–19.

Bergaya, F., Theng, B.K.G., Lagaly, G., 2006. Handbook of Clay Science. Developments in Clay Science, Elsevier Science, Amsterdam, 1, 1246.

Beshears, C. J., 2010. The Geology and Geochemistry of the Millennium Uranium Deposit, Athabasca Basin, Saskatchewan, Canada. University of Manitoba, MSc Thesis.

Bethke, C.M., Reynolds, R.C., 1986. Recursive method for determining frequency factors in interstratified clay diffraction calculations. Clays Clay Miner. 34, 224–226.Beaufort, D., Patrier, P., Laverret, E., 2005. Clay alteration associated with proterozoic unconformity-type uranium

deposits in the east Alligator Rivers uranium field, Northern Territory, Canada. *Economic Geology.100*, 515–536.

BGC Engineering Inc., 2010. Oil Sands Tailings Technology Review. Oil Sands Research and Information Network, University of Alberta, School of Energy and the Environment, Edmonton, Alberta. OSRIN Report No. TR-1, 136.

Bharadwaj, B., Moldovan, B., Yesnik, L., Grant, S., Piche, J., 2010. Cameco Corporation- the Key Lake uranium mill: current status and vision for the future. In Proceedings of the 3rd International Conference on Uranium ,Uranium 2010; Lam, E. K., Rowson, J. W., Ozberk, E., Eds.; Saskatoon, SK, Canada, 1, 327.

Bonifazi, G., Massacci, P., 1995. Ore liberation modelling by minerals topological evaluation. Miner. Eng. 8, 6, 649-658.

Boulet, M.P, Larocque, A. C. L., 1998. A comparative mineralogical and geochemical study of sulphide mine tailings at two sites in New Mexico, USA. Environ. Geol. 33, 2-3, 130-142.

Bowell, R.J., Grogan, J., Hutton-Ashkenny, M., Brough, C., Penman, K., Sapsford, D.J., 2011. Geometallurgy of uranium deposits. Miner. Eng. 24, 12, 1305-1313.

Bragg, W.L., 1913. The diffraction of short electromagnetic waves by a crystal. Proc. Cambridge Phil. Soc.17, 43-57.

Brandt, F., Bosbach, D., Krawczyk-Bärsch, E., Arnold, T., & Bernhard, G., 2003. Chlorite dissolution in the acid ph-range: a combined microscopic and macroscopic approach. Geochimica et Cosmochimica Acta. 67(8), 1451 - 1461.

Brigatti, M.F., Galan, E., Theng, B.K.G., 2013. Structure and Mineralogy of Clay Minerals. Develop. Clay Sci. 5, 20–81.

Cabri, L.J., 1981. Relationship of mineralogy for the recovery of PGE from ores. In: Cabri, L.J., ed., Platinum-Group Elements: Mineralogy, Geology, Recovery. Can. Inst. Min. Met. Petrol. 23, 233-250.

Cameco Corporation, 2008. McAthur River Operation, Northern Saskatchewan, Canada. NI 43-101 Technical Report.

Cameco, 2010. Key Lake Extension Project Description. Cameco Corporation. Safety, Health, Environment & Quality.

Cameco, 2010. Key Lake Extension Project: Project Description 2010.

Canadian Council of Ministers of the Environment, CCME, 1999. Canadian Environmental Quality Guidelines. Environment Canada, Ottawa.

Chapman, H.D., 1965. Cation-exchange capacity. In: C. A. Black, ed. Methods of soil analysis-Chemical and microbiological properties. Agronomy. 9, 891-901.

Charland, A., Kormos, L.J., Whittaker, P.J., Arrué-Canales, C.A., Fragomeni, D., Lotter, N.O., Mackey, P, Anes, J., 2006. A case study for the integrated use of automated mineralogy in plant optimisation: the Montcalm concentrator. Proc. Auto. Mineral. MEI Conference.

Claassen, R., 1993. Mineralogical controls on the bacterial oxidation of refractory Barberton gold ores. FEMS Microbiol. Rev. 11, 197–205.

Cloutier, J., Kyser, K., Olivo, G.R., Alexandre, P., Halaburda, J., 2009. The Millennium uranium deposit, Athabasca Basin, Saskatchewan, Canada: An atypical basement-hosted unconformity-related uranium deposit. Econ. Geol.104, 815–840.

Dai, Z., Bos, J.-A., Lee, A., Wells, P., 2008. Mass balance and mineralogical analysis of flotation plant survey samples to improve plant metallurgy. Miner. Eng., ‘‘Flotation 2007’’, special ed., 21, 826-831.

Davis, M.J.B., 2013. Automated mineral analysis of mine waste. Master of Science Thesis, Department of Geological Sciences and Geological Engineering, Queen’s University Kingston, Ontario, Canada.

de Boer, J. H., Lippens, B. C., Linsen, B. G., Broekhollf, J. C. P., Van der Heuvel, A., Osinga, T. J., 1966. The t-curve of multimolecular N2 adsorption. J. Coll. Interface Sci. 21, 405-414.

Derome, D., Cathelineau, M., Cuney, M., Fabre, C., Lhomme, T., Banks, D.A., 2005. Mixing of sodic and calcic brines and uranium deposition at McArthur River, Saskatchewan, Canada: A Raman and laser-induced breakdown spectroscopic study of fluid inclusions. Econ. Geol. 100, 8, 1529-1545.

Donahue R., Hendry M. J., 2003. Geochemistry of arsenic in uranium mine mill tailings, Saskatchewan, Canada. Appl. Geochem.18, 1733–1750.

Donahue R., Hendry M. J., Landine P., 2000. Distribution of arsenic and nickel in uranium mill tailings, Rabbit Lake, Saskatchewan, Canada.Appl. Geochem.15, 1097–1119.

Donahue, R., 2000. Geochemistry of arsenic in uranium mill tailings, Saskatchewan, Canada. PhD thesis, University of Sskatchewan, 195.

Donahue, R., Hendry, M.J., 2003. Geochemistry of arsenic in uranium mine mill tailings, Saskatchewan, Canada. Appl. Geochem. 18, 1733–1750.

Douglas, G., Shackleton, M., Woods, P., 2014. Hydrotalcite formation facilitates effective contaminant and radionuclide removal from acidic uranium mine barren lixiviant. Appl. Geochemistry 42, 27–37.

Drits, V.A., 2003. Structural and chemical heterogeneity of layer silicates and clay minerals. Clay Miner. 38, 403–432.

Drits, V.A., Dainyak, L.G., Muller, F., Besson, G., Manceau, A., 1997. Isomorphous cation distribution in celadonites, glauconites and Fe-illites determined by infrared, Mossbauer and EXAFS spectroscopies. Clay Miner. 32, 153–179.

Ecometrix, 2005. Key Lake Project: Environmental Risk Assessment 2005.

Eslinger, E., Pevear, D., 1988. Clay Minerals for Petroleum Geologists and Engineers. SEPM Short Course Notes no. 22, 405.

Essilfie-Dughan, J., Hendry, M. J., Warner, J., Kotzer, T., 2012. Microscale mineralogical characterization of As, Fe, and Ni in uranium mine tailings. Geochim. Cosmochim. Acta. 96, 336–352.

Essilfie-Dughan, J., Hendry, M.J., Warner, J., Kotzer, T., 2013. Arsenic and iron speciation in uranium mine tailings using X-ray absorption spectroscopy. Appl. Geochemistry 28, 11–18.

Essilfie-Dughan, J., Pickering, I. J., Hendry, M. J., George, G. N., Kotzer, T., 2011. Molybdenum speciation in uranium mine tailings using x-ray absorption spectroscopy. Environ. Sci. Technol. 45,455–460.

Fandrich, R., Gu, Y., Burrows, D., Moeller, K., 2007. Modern SEM-based mineral liberation analysis. Int. J. Miner. Process. 84, 310–32.0

Farquharson, C.G., Craven, J.A., 2009. Three-dimensional inversion of magnetotelluric data for mineral exploration: An example from the McArthur River uranium deposit, Saskatchewan, Canada. J. Appl. Geophy. 68, 4, 450-458.

Fayek, M., Kyser, T.K., 1997. Characterization of multiple fluid-flow events and rare-earth-element mobility associated with formation of unconformity-type uranium deposits in the Athabasca Basin, Saskatchewan. Can. Mineral. 35, 627–658.

FEI, 2011. MLA System User Training Course, Powerpoint Presentation. Queen's University.

Fleischer, M. (1955). Minor elements in some sulphide minerals. *Economic geology; fiftieth anniversary volume 1905-1955*, Editor: Alan M. Bateman. 970-1024.

Floody, M.C., Theng, B.K.G., Reyes, P., Mora, M.L., 2009. Natural nanoclays: applications and future trends – a Chilean perspective, Clay Miner. 44,161–176.

Forssberg E., Nilsson L., 1987. Treatment of uranium extraction residues, Erzmetall. 40, 398.

Fortuna, P., 1983. Key Lake Project - Quarternary Investigation: Unpubl. Consult. Rep. Key Lake Min. Corp. by Eldor Resour. Limited.

Fragomeni, D., Boyd, L.J., Charland, A., Kormos, L.J., Lotter, N.O., Potts, G., 2005. The Use of End-Members for Grind-Recovery Modelling, Tonnage Prediction and Flowsheet Development at Raglan. Can. Miner. Processor., 75–98.

Gabelman, J.W., 1988. Classification of uranium deposits. Ore Geol. Rev.

Gandhi, S.S., 2007. Significant Unconformity Associated Uranium Deposits of the Athabasca Basin, Saskatchewan and Alberta, and Selected Related Deposits of Canada and the World. Geological Survey of Canada, Open File 5005, Saskatchewan Industry and Resources, Open File 2007- 11, CD-ROM.

Gaudin, A., Petit, S., Rose, J., Martin, F., Decarreau, A., Noack, Y., Borschneck, D., 2004. The accurate crystal chemistry of ferric smectites from the lateritic nickel ore of Murrin Murrin (Western Australia). II. Spectroscopic (IR and EXAFS) approaches. Clay Miner. 39, 453–467.

Gharrabi, M., Velde, B., & Sagon, J. P. (1998). The transformation of illite to muscovite in pelitic rocks; constraints from X-ray diffraction. Clays and Clay Minerals. 46(1), 79 - 88.

Gillman, G.P., 1979. A proposed method for the measurement of exchange properties of highly weathered soils. Aust. J. Soil. Res. 17, 129-139.

Gillman, G.P., Sumpter, E.A., 1986. Modification to the compulsive exchange method for measuring exchange characteristics of soils. Aust. J. Soil Res. 24, 61-66.

Gillman, G.P., Sumpter. E.A., 1986. Modification to the compulsive exchange method for measuring exchange characteristics of soils. Aust. J. Soil Res. 24, 61-66.

Goldhaber, S.B., 2003. Trace element risk assessment: essentiality vs. toxicity. Regul. Toxicol. Pharmacol. 38, 232–242.

Gomez, M. a, Hendry, M.J., Koshinsky, J., Essilfie-Dughan, J., Paikaray, S., Chen, J., 2013. Mineralogical controls on aluminum and magnesium in uranium mill tailings: Key Lake, Saskatchewan, Canada. Environ. Sci. Technol. 47, 7883–91.

Goodall, W.R., Scales, P.J., 2007. An overview of the advantages and disadvantages of the determination of gold mineralogy by automated mineralogy. Miner. Eng. 20, 506-517.

Gu, Y., 2003. Automated scanning electron microscope based mineral liberation analysis: an introduction to JKMRC/FEI mineral liberation analyser. J. Miner. Mater. Char. Eng. 2, 1, 33-41.

Gu, Y., Napier-Munn, T., 1997. JK/Philips mineral liberation analyzer– an introduction. Miner. Process. Conf., 2.

Gu, Y., Sugden, T., 1995. A highly integ rated SEM - EDS- IP system automated quantitative mineral analysis, Proceedings of the third biennial symposium on SEM imaging and analysis: applications and techniques, University of Melbourne, Aust. Soci. Elect. Micro.

Hall, G.E.M., 1992. Inductively coupled plasma mass spectrometry in geoanalysis. J. Geochemical Explor. 44, 201–249.

Hall, J.S., 1977. Composite mineral particles –analysis by automated scanning electron microscopy, PhD thesis, JKMRC, The University of Queensland, Brisbane.

Health Canada, 2012. Guidelines for Canadian Drinking Water Quality—Summary Table. Water, Air and Climate Change Bureau, Healthy Environments and Consumer Safety Branch, Health Canada, Ottawa, Ontario.

Heinrich, G., Kyser, K., Chipley, D., Lam, E., 2010. The determination of selenium and molybdenum distribution in uranium ore and mill solids. In Proceedings of the 3rd International Conference on Uranium,Uranium 2010; Lam, E. K., Rowson, J. W., Ozberk, E., Eds.; Saskatoon, SK, Canada, August 15-18, 1, 609.

Heinrich, K. J. F., 1964. Adv. X-ray Anal. 7, 325-39.

Hendershot, W.H., Duquette, M., 1986. A simple barium chloride method for determining cation exchange capacity and exchangeable cations. Soil Sci. Soc. Am. J. 50, 605-608.

Hendricks, S.B., Teller, E., 1942. X-ray interference in partially ordered layer lattices. J. Chem. Phys. 10, 147–167.

Henley, K.J., 1983. Ore-dressing Mineralogy: A Review of Techniques, Applications and Recent Developments. Geolog. Soc. S. Afri. 7, 175–200.

Hepper, E.N., Buschiazzo, D.E., Hevia, G.G., Urioste, A., Antón, L., 2006. Clay mineralogy, cation exchange capacity and specific surface area of loess soils with different volcanic ash contents. Geoderma 135, 216–223.

Hiatt E.E., Kyser T.K., 2007. Sequence stratigraphy, hydrostratigraphy, and mineralizing fluid flow in the Proterozoic Manitou Falls Formation, eastern Athabasca Basin, Saskatchewan. Geol. Surv. Canada. 588, 489–506.

Hiller, E., Petrák, M., Tóth, R., Lalinská-Voleková, B., Jurkovič, L., Kučerová, G., Radková, A., Sottník, P., Vozár, J., 2013. Geochemical and mineralogical characterization of a neutral, low-sulphide/high-carbonate tailings impoundment, Markušovce, eastern Slovakia. Environ. Sci. Pollut. Res. Int. 20, 7627–42.

Hoeve, J., Quirt, D., Rawsthorn, K., 1985b. Uranium mineralization and host rock alteration in relation to clay mineral diagenesis and evolution of the Athabasca Basin, northern Saskatchewan. Geologique Int. Resumes 27, 9, 1, 354.

Hoeve, J., Quirt, D.H., 1984. Mineralization and host rock alteration in relation to clay mineral diagenesis and evolution of the middle-proterozoic, Athabasca Basin, northern Saskatchewan, Canada. Saskatchewan Research Council, SRC Technical Report 187, 187.

Hoeve, J., Rawsthorn, K., and Quirt, D. 1985. Clay minerals as a clue to uranium mineralization in the Athabasca Basin. Can. Inst. Min. Metall. 32, 258.

Hohndorf, A., Strnad, J. G., Carl, C., 1989. Age determination of basement units in the Key Lake uranium deposit area, Saskatchewan, Canada. International Atomic Energy Agency, Vienna, TECDOC-500, 381 -409.

Hooshiar, A., Uhlík, P., Kaminsky, H.W., Shinbine, A., Omotoso, O.l., Liu, Q., Ivey, D. G., Etsell, T.H., 2010. High resolution transmission electron microscopy study of clay mineral particles from streams of simulated water based bitumen extraction of Athabasca oil sands. Appl. Clay Sci. 48, 3, 466 -474.

Hooshiar, M. A. F., 2011. Characterization of clay minerals in the athabasca oil sands in water extraction and nonaqueous solvent extraction processes. PhD Thesis, Department of Chemical and Materials Engineering, University of Alberta, 7.

Huang, Y.-P., Liu, Z.-S., Zheng, C., Gao, R.-Y., 2009. Recent developments of molecularly imprinted polymer in CEC. Electrophoresis 30, 155–162.

ı´cˇel, B., Komadel, P., 1994. Structural formulae of layer silicates. Amonette, J.E., Zelazny, L.W., eds., Quantitative Methods in Soil Mineralogy. Soil Science Society of America Miscellaneous Publication, Madison, WI, 114-136.

IAEA, International Atomic Energy Agency, 2004. The long-term stabilization of uranium mill tailings- IAEA TEC-DOC-1403, Vienna.

Jamieson B., Frost S., 1997. The McArthur river project: high grade uranium mining. The Uranium Institute, 22nd Annual Symposium, London.

Jansen, W., Slaughter, M., 1982. Elemental Mapping of minerals by electron micro-probe. Am. Mineral. 67, 521-533.

Jefferson, C.W., 2007. Unconformity-associated uranium deposits of the Athabasca basin, saskatchewan and alberta. Geol. Assoc. Canada, Miner. Depos. Div. Spec. Publ. 273–305.

Jenner, G.A., Longerich, H.P., Jackson, S.E., Fryer, B.J., 1990. ICP-MS-a powerful tool for high-precision trace-element analysis in earth sciences: Evidence from analysis of selected U.S.G.S. reference samples. Chem. Geol. 83, 133-148.

Jiang, L., Zhou, H., Peng, X., 2007. Bio-oxidation of pyrite, chalcopyrite and pyrrhotite by Acidithiobacillus ferrooxidans. Chinese Sci. Bull. 52, 2702–2714.

Johnston, C.T., Tombácz, E., 2002. Surface chemistry of soil minerals. In: Dixon, J.B., Schulze, D.G., eds., Soil Mineralogy withEnvironmental Applications. Soil Science Society of America,Madison, Wisconsin, USA, 37–67.

Jones, M. P., 1987. Applied mineralogy: a quantitative approach. London. Norwell, MA, Graham & Trotman.

Jones, M.P., 1987. Applied mineralogy: a quantitative approach. Graham & Trotman, London, Norwell, MA.

Kawano, M., Tomita, K., 1991. Mineralogy and genesis of clays in postmagmatic alteration zones, Makurazaki volacanic area, Kagoshima prefecture, Japan. Clays Clay Miner. 39, 597-608.

Kenichi Sakata et al., Inductively coupled plasma mass spectrometer and method, US patent 6265717 B1.

Kersten, M., Förstner, U., 1986. Chemical fractionation of heavy metals in anoxic estuarine and coastal sediments. Water Sci. Technol. 18, 121-130.

King, R P, 1993. Basic image analysis for mineralogy. ICAM'93 Demonstration Workshop Manual, 119 -139.

Klemic, H., 1962. Uranium occurrence in sedimentary rocks of Pennsylvania.

Komadel, P., Madejová, J., 2013. Handbook of Clay Science, Developments in Clay Science, Developments in Clay Science. Elsevier.

Koshinsky, J., Essilfie-Dughan, J., Moldovan, B.J., Hendry, M.J., 2012. Secondary Mineral Phases in a Uranium Mill Pilot Study: Assessing the Mill Model. Proceedings of the international conference: Goldschmidt 2012, Poster Session.

Kotzer, T.G., Kyser, T.K., 1995. Petrogenesis of the Proterozoic Athabasca basin, northern Saskatchewan, Canada, and its relation to diagenesis, hydrothermal uranium mineralization and paleohydrology. Chem. Geol. 120, 45-89.

Kuwahara, Y., Aoki, Y., 1995. Dissolution process of phlogopite in acid solutions. Clays Clay Miner. 43, 39–50.

Landa, E.R., 2004. Uranium mill tailings: nuclear waste and natural laboratory for geochemical and radioecological investigations. J. Environ. Radioact. 77, 1–27.

Landa, E.R., Phillips, E.J.P., Lovley, D.R., 1991. Release of226Ra from uranium mill tailings by microbial Fe(III) reduction. Appl. Geochemistry.

Langlois, P., Holmes, J., 2001. Process Development at Raglan Concentrator. Can. Miner. Processor. 427-451.

Leißner, T., Mütze, T., Bachmann, K., Rode, S., Gutzmer, J., Peuker, U.A., 2013. Evaluation of mineral processing by assessment of liberation and upgrading. Miner. Eng. 53, 171–173.

Lener, J., Bibr, B., 1984. Effects of molybdenum on the organism: a review. J. Hyg. Epidemiol. Microbiol. Immunol. 29, 405–419.

Lesher, C.M., 1999. Komatiic Peridotite-hosted Ni–Cu,PGE Deposits of the Raglan Area, Cape Smith Belt, New Québec. Laurentian University Mineral Exploration Research Centre, 205.

Levins D.M., Davy D.R., 1983. Management of wastes from uranium mining and milling. Conf. Proc., Radioactive Waste Manasement, 141.

Lide, D.R., ed., 1994. "Molybdenum". CRC Handbook of Chemistry and Physics. 4. Chemical Rubber Publishing Company, 1

Lieu, A., 2004. Characterization of Metals Distribution and Their Leaching Behavior in a Uranium Mine Waste Rock Pile, Key Lake, Saskatchewan, Canada. M.Sc. Thesis, University of Saskatchewan.

Liu, D.J., Hendry, M.J., 2011. Controls on 226Ra during raffinate neutralization at the Key Lake uranium mill, Saskatchewan, Canada. Appl. Geochemistry.

Liu, Z.-S., Zheng, C., Yan, C., Gao, R.-Y., 2007. Molecularly imprinted polymers as a tool for separation in CEC. Electrophoresis 28, 127–136.

Lorenzen, J.S.J., van Deventer, L., 1994. The interrelationship between mineral liberation and leaching behaviour. Int. J. Miner. Process. 41, 1-15.

Lotter, N.O., 1995. A Quality Control Model for the Development of High-Confidence Flotation Test Data. M.Sc. Chem. Eng. Thesis, University of Cape Town.

Lotter, N.O., 2005. Statistical Benchmark Surveying of Production Concentrators. Ph.D. Met. Eng. Thesis, McGill University, Montréal.

Lotter, N.O., Kowal, D.L., Tuzun, M.A., Whittaker, P.J., Kormos, L.J., 2003. Sampling and flotation testing of Sudbury Basin drill core for Process Mineralogy modelling. Miner. Eng. 16, 857–864.

Lotter, N.O., Laplante, A.R., 2007. The campaign survey model – a case study at the Raglan Mine, Québec. Miner. Eng. 20, 480–486.

Lotter, N.O., Whittaker, P.J., Kormos, L.J., Stickling, J.S., Wilkie, G.J., 2002. The development of process mineralogy at Falconbridge limited, and application to the Raglan mill. CIM Bull. 95, 1066, 85-92.

Lottering, M.J., Lorenzen, L., Phala, N.S., Smit, J.T., Schalkwyk, G.A.C. 2008. Mineralogy and uranium leaching response of low grade South African ores. Miner. Eng. 21, 1, 16-22.

Lowson, R. T., Comarmond, M.-C. J., Rajaratnam, G., & Brown, P. L., 2005. The kinetics of the dissolution of chlorite as a function of pH and at 25°C. Geochimica et Cosmochimica Acta. 69(7), 1687 - 1699.

MacEwan, D.M.D., 1958. Fourier transforms methods for studying X-ray scattering from lamellar systems. II. The calculation of X-ray diffraction effects from various type of interstratification. Kolloidzeitschrift 156, 61–67.

Macht, F., Eusterhues, K., Pronk, G.J., Totsche, K.U., 2011. Specific surface area of clay minerals: Comparison between atomic force microscopy measurements and bulk-gas, N2 and -liquid, EGME adsorption methods. Appl. Clay Sci. 53, 1, 20–26.

Magalha˜es, M. C. F., 2002. Arsenic. An environmental problem limited by solubility. Pure Appl. Chem.74, 1843–1850.

Maksimovic, G.W., Brindley, Z., 1974. The nature and nomenclature of hydrous nickel-containing silicates [WWW Document]. Clay Miner. URL http://www.minersoc.org/pages/Archive-CM/Volume_10/10-4-271.pdf (accessed 7.16.14).

Manceau, A., Tommaseo, C., Rihs, S., Geoffroy, N., Chateigner, D., Schlegel, M.,Tisserand, D., Marcus, M. A., Tamura, N.,Chen, Z.-S., 2005. Natural speciation of Mn, Ni, and Zn at the micrometer scale in a clayey paddy soil using X-ray fluorescence, absorption, and diffraction. Geochimica et Cosmochimica Acta. 69(16), 4007 - 4034.

McGill, B.D., Marlatt, J.L., Matthews, R.B., Sopuck, V.J., Homeniuk, L.A., Hubregtse, J.J., 1993. The P2 North uranium deposit Saskatchewan, Canada. Expl. Min. Geol. 2, 321-331.

McKay, N., Wilson, S., Lacouture, B., 2007. Ore characterisation of the Aqqaluk deposit at Red Dog. Can. Miner. Processor. 39, 55–74.

McLaren, R.G., Cameron K.C, 2000. Inorganic soil colloids. Soil Science: Sustainable Production and Environmental Protection. Oxford University Press, New Zealand. 2, 159–167.

Moldovan, B.I., Hendry, M.J., 2005. Characterizing and quantilying controls on arsenic solubility over a pH range of 1-11 in a uranium mill-scale experiment. Environ. Sci. Technol. 39, 4913–4920.

Moldovan, B.J., Jiang, D.T., Hendry, M.J., 2003. Mineralogical characterization of arsenic in uranium mine tailings precipitated from iron-rich hydrometallurgical solutions. Environ. Sci. Technol. 37, 873–879.

Moldovan, B.J., Jim Hendry, M., Harrington, G.A., 2008. The arsenic source term for an in-pit uranium mine tailings facility and its long-term impact on the regional groundwater. Appl. Geochemistry.

Moore, D.M., Reynolds, R.C., Jr., 1997. X-ray diffraction and the identification and analysis of clay minerals. Ox-ford University Press, Oxford, 214.

Morrison S. J., Cahn L. S., 1991. Mineralogical residence of alpha-emitting contamination and implications for mobilization from uranium mill tailings. J. Contam. Hydrol. 8, 1-21.

Nilsson, L., Forssberg, E., 1988. Solubility of radionuclide species from uranium mill tailings, Miner. Eng. 1, 4, 295-310.

Offler, B., 1994. Characterisation of the low grade metamorphism in the Nambucca Block (NSW, Australia). Revista Geologica de Chile. 21, 285 - 293.

Olesik, J. W., 2014. Inductively Coupled Plasma Mass Spectrometers. H. D. Holland, Ed. Treatise on Geochemistry, Elsevier. 2, 309-336.

PANalytical, 2009. Personal conversations with Allan Ball-PANalytical Sales Representative.

Percival, J. B. M., 1990. Clay mineralogy, geochemistry and partitioning of uranium within the alteration halo of the cigar lake uranium deposit, Saskatchewan, Canada. PhD Thesis, Department of Earth Science, Carleton University.

Pérez-Barnuevo, L., Pirard, E., Castroviejo, R., 2013. Automated characterisation of intergrowth textures in mineral particles. A case study. Miner. Eng. 52, 136–142.

Pesquera, C., Gonzalez, F., Benito, I., Blanco, C., Mendioroz, S., Pajares, J., 1992. Passivation of a Montmorillonite by the Silica created in Acid Activation. J. Mater. Chem. 2, 907–911.

Petruk, W., 1976. The application of quantitative mineralogical analysis of ores to ore dressing. CIM Bull. 767, 146–153.

Petruk, W., 1986. The MP- SEM- IPS image analysis system. CANMET Report 87- 1E, CANMET, Dept. Energy, Mines, And Resources, Canada.

Petruk, W., 1988. Automatic image analysis for mineral beneficiation, J. Metals, 40:29 –31.

Petruk, W., 1988. The capabilities of the micro-probe Kontron image analysis systems: application of mineral beneficiation. Scan. Microsc. 2, 1247–1255.

Petruk, W., 2000. Applied mineralogy in the mining industry. Elsevier Science BV.

Petruk, W., Hughson, M.R., 1977. Image analysis evaluation of the effect of grinding media on selective flotation of two zinc–lead–copper ores. CIM Bull. 787, 128–135.

Petruk, W., Schnarr, J.R., 1981. An evaluation of the recovery of free and unliberated mineral grains, metals and trace elements in the concentrator of Brunswick Mining and Smelting Corporation Limited. CIM Bull. 833, 132-159.

Peyerl, W., 1983. The Metallurgical Implications of the Mode of Occurrence of Platinum-group Metals in the Merensky Reef and UG-2 Chromitite of the Bushveld Complex. Geol. Soc. S. Afri. 7, 295-300.

Plancon, A., 1981. Diffraction by layer structures containing different kinds of layers and stacking-faults. J. Appl. Crystallogr. 14, 300–304.

Poppe, L.J., Paskevich, V.F., Hathaway, J.C., Blackwood, D.S., 2001. A laboratory manual for x-ray powder diffraction. U. S. Geological Survey Open-File Report 01-041.

Poppe, L.J., Paskevich, V.F., Hathaway, J.C., Blackwood, D.S., 2002. A laboratory manual for x-ray powder diffraction. USGS open file report, 1-41.

Price W. A., 2009. Prediction Manual for Drainage Chemistry from Sulphidic Geologic Materials. MEND Report 1.20.1

Quirt, D.., Kotzer, T., Kyser, T.K., 1991. Tourmaline, phosphate minerals, zircon, and pitchblende in the Athabasca Group: Maw Zone and McArthur River areas, Saskatchewan; in Summary of Investigations 1991, Saskatchewan Geological Survey, Sask. Energy Mines, Misc. Rep. 91-4.

Rainbird, R.H., Stern, R.A., Rayner, N., Jefferson, C.W., 2007. Age, provenance, and regional correlation of the Athabasca Group, Saskatchewan and Alberta, constrained by igneous and detrital zircon geochronology, in Jefferson, C.W. and Delaney, G., eds., EXTECH IV: Geology and Uranium Exploration Technology of the Proterozoic Athabasca Basin, Saskatchewan and Alberta: Bulletin 588: Geological Survey of Canada ,also Special Publication 18: Saskatchewan Geological Society, Special Publication 4: Geological Association of Canada, Mineral Deposits Division, 193-210.

Ramaekers, P., 1979. Stratigraphy of the Athabasca Basin; in Summary of Investigations 1979, Saskatchewan Geological Survey, Sask, Miner, Resour, Misc. Rep. 79-10, 154-160.

Ramaekers, P., 1981. Hudsonian and Helikian basins of the Athabasca region, northern Saskatchewan; in Campbell, R.H.A, ed., Proterozoic Basins of Canada. Geol. Surv. Can., Pap. 81-10, 219-233.

Ramaekers, P., 1990. Geology of the Athabasca Group, Helikian in Northern Saskatchewan; Sask. Energgy Mines. Rep. 195, 49.

Restarick, C.J., 1976. Pulp sampling techniques for steady state assessment of mineral concentrators. In: Proceedings, Sampling Symposium, Australasian Institute of Mining and Metallurgy, 161–168.

Reynolds Jr., R.C., 1985. NEWMOD, A Computer Program for the Calculation of Basal X-Ray Diffraction Intensities of Mixed-Layered Clays. R.C. Reynolds, Hanover, NH.

Reynolds, R.C., 1967. Interstratified clay systems: calculation of the total one-dimensional diffraction function. Am. Mineral. 52, 661–672.

Reynolds, R.C., 1980. Interstratified clay minerals. In: Brindley, G.W., Brown, G., Eds., Crystal Structures of Clay Minerals and Their X-ray Identification. Mineralogical Society, London, 249–303.

Ring R.J., Levins D.M., 1982. Radionuclides in Process and Wastes Streams at an Operating Uranium Mill, Management of Wastes from Uranium Mining and Milling, Proc. Symp., Albuquerque, IAEA, 247.

Riveros, P.A., Dutrizac, J.E., Spencer, P., 2001. Arsenic disposal practices in the metallurgical industry. Can. Metall. Quart., 40, 395–420.

Robinsky E.I., 1981. Uranium Tailing Disposal by the Thickened Tailing Discharge System. Conf. Proc., Uranium Mill Tailings Management.

Ross, G.M., Milkereit, E., Eaton, D., White, D., Kanasewich, E.R., Burianyk, M.J.A., 1995. Paleoproterozoic collissional oreogen beneath the Western Canada sedimentary basin imaged by Lithoprobe crustal seismic-reflection data. Geol. 23, 195-199.

Roy, C., Halarburda, J., Thomas, D., Hirsekorn, D., 2005. Millennium deposit—basement-hosted derivative of the unconformity uranium model: Uranium production and raw materials for the nuclear fuel cycle—supply and demand, economics, the environment and energy security: International Atomic Energy Agency Proceedings Series, 111-121.

Rubiera, F., Arenillas, A., Fuente, E., Miles, N., Pis, J.., 1999. Effect of the grinding behaviour of coal blends on coal utilisation for combustion. Powder Technol. 105, 351–356.

Ruby, M.V., Schoff, R., Brattin, W., Goldade, M., Post, G., Harnois, M., Mosby, D.E., Casteel, S.W., Berti, W., Carpenter, M., Edwards, D., Cragin, D., Chappell, W., 1999. Advances in

evaluating the oral bioavailability of inorganics in soil for use in human health assessment. Enviro. Sci. Technol. Vol. 33, pp. 3697-3705.

Rudnick, R.L., Gao, S., 2003. The Composition of the Continental Crust, pp. 1-64. In The Crust ,ed. R.L. Rudnick Vol. 3, Treatise on Geochemistry, eds. H.D. Holland and K.K. Turekian, Elsevier-Pergamon, Oxford.

Ruhrmann, G., 1987. The gaertner uranium orebody at key lake (northern saskatchewan, canada) after three years of mining: an update of the geology. Econ. Miner. Sask., Spec. Publ. 8, 120-137.

Ruiz Cruz, M. D., & Nieto, J. M., 2006. Chemical and structural evolution of "metamorphic vermiculite" in metaclastic rocks of the betic cordillera, malaga, spain: a synthesis. The Canadian Mineralogist. 44(1), 249 - 265.

Ruzicka, V., 1993. Vein uranium deposits. Ore Geol. Rev. 8, 247-276.

S.W., Berti, W., Carpenter, M., Edwards, D., Cragin, D., Chappell, W., 1999. Advances in evaluating the oral bioavailability of inorganics in soil for use in human health assessment. Enviro. Sci. Technol. 33, 3697-3705.

Sainz-Diaz, C. I., Hernández-Laguna, A., Dove, M. T., 2001. Theoretical modeling of cis-vacant and trans-vacant configurations in the octahedral sheet of illites and smectites. Physics and Chemistry of Minerals. 28, 5, 322-31.

Sawnhey, B.J., 1977. Interstratification in layer silicates, in Dixon, J.B., Weed, S.B., Kittrick, J.A., Milford, M.H., and White, J.L. ,eds., Minerals in soil environments, Soil Sci. Soc. Am., Madison, Wis., 405-434.

Schulze, D.G., 2002. Anintroductiontosoilmineralogy.In:Dixon, J.B., Schulze, D.G., Eds., Soil Mineralogy with Environmental Applications. Soil Science Society of America, Madison, Wisconsin, USA, 1–35.

Scissons K., 1997. Saskatchewan Uranium Mine Tailings-Quantity to end of 19%. Saskatchewan Environment and Resource Management. Memo. Fie -37 - 20 - 0 - 0.

Shaw S. A., Hendry M. J., Essilfie-Dughan J., Kotzer T., Wallschla¨ger D., 2011. Distribution, characterization, and geochemical controls of elements of concern in uranium mine tailings, Key Lake, Saskatchewan. Canada. Appl. Geochem. 26, 2044-2056.

Sibbald, T.I.I., Quirt, D., 1987. Uranium deposits of the Athabasca basin: Saskatchewan Research Council Publication R-855-1-G-87, 79.

Smith, R. S., Wood, G. R. and Powell, B., 2010, Detection of alteration at the Millennium uranium deposit in the Athabasca Basin: a comparison of data from two airborne electromagnetic systems with ground resistivity data. Geophys. Prospect. 58, 1147–1158.

Somot S., Pagel M. and Thiry J., 1997. Speciation of radium in uranium mill tailings from Ecarpie`re, Vende ´e, France.C. R.l'Acade ´mie. Sci., Paris325, 111–118.

Sparks, D.L., 2003. Environmental Soil Chemistry, Acad. Press, 352.

Stefanova, V., Kmetov, V., Canals, A., 2003. Application of internal standardization in ICP-QMS through discrete sample introduction methodologies. J. Anal. At. Spect. 18, 1171.

Strnad, J. G., Hohndorf, A., Carl, C., 1992. Athabasca Basin Uranium Province, Canada: metallogenetic outline and geo-chronological framework. In Precambrian metallogeny related to plate tectonics. Edited by G. Gaal and K. J. Schulz. Precambrian Research.

Suryanarayana, C., Norton, M.G., 1998. X-ray Diffraction: A Practical Approach. Microsc. Microanal. 4, 513–515.

Sutherland, D., Gottlieb, P., Jackson, R., Wilkie, G., Stewart, P., 1988. Measurement in section of particles of known composition. Miner. Eng. 1, 4, 317-326.

Sutherland, D.N., Gottlieb, P., 1991. Application of automated quantitative mineralogy in mineral processing. Miner Eng. 4, 7-11, 753-762.

Sylvester, P.J., 2012. Use of the Mineral Liberation Analyzer, MLA for mineralogical studies of sediments and sedimentary rocks. Mineral. Assoc. Can. Short Course 42, 1-16.

Taylor, S.R., 1964. The abundance of chemical elements in the continental crust-a new table: Geochim. Cosmochim. Acta. 28, 1273-1285.

Tempelman-Kluit, D.J., 1970. The relationship between sulphide grain size and metamorphic grade of host rocks in some strata-bound pyritic ores. Can. J. Earth Sci. 7, 1339–1345.

Tessier,A.,Campbell, P.G.C.,Bisson,M., 1979. Sequential extractionfor the speciation of particulate trace metals. Anal. Chem. 51, 844-851

Thomas, D., 2002. Observations on structural and alteration features—Millennium zone, Cree extension project: Insights into a basement-hosted uranium model: Unpublished report, Saskatchewan, Cameco Corporation, 42.

Thomas, D.J., Matthews, R.B., Sopuck, V., 2000. Athabasca Basin, Canada unconformity - type uranium deposits: Exploration model, current mine developments and exploration directions, in Geology and Ore Deposits 2000: The Great Basin and Beyond: Geological Society of Nevada Symposium, Reno, Nevada, May 15-18 2000, Proceedings, 1, 103-126.

Tran, H.T., Ansdell, K., Bethune, K., Watters, B., Ashton, K., 2003. Nd isotope and geochemical constraints on the depositional setting of Paleoproterozoic metasedimentary rocks along the margin of the Archean Hearne craton, Saskatchewan, Canada. Precambrian Res. 123, 1–28.

Triffett, B., Veloo, C., Adair, B.J.I., Bradshaw, D.J., 2008. An investigation into the recovery of molybdenite in the Kennecott Utah copper bulk flotation circuit. Miner. Eng. ‘‘Flotation 2007’’, special ed., 21, 832-840.

Tsunashima, A., Brindley, G. W., Bastovanov, M., 1981. Adsorption of uranium from solutions by montmorillonite; compositions and properties of uranyl montmorillonites. Clays Clay Miner. 29, 1, 10-16.

US Environmental Protection Agency, US EPA, 1998. Arsenic in Drinking Water: Arsenic Research Plan. Office of Water.

USEPA, 2009. National primary drinking water regulations, EP 816-F-09-004.

Van Olphen, H., 1963. An Introduction to Clay Colloid Chemistry. Interscience, New York.

Van Tonder, E., Deglon, D.A., Napier-Munn, T.J., 2010. The effect of ore blends on the mineral processing of platinum ores. Miner. Eng. 23, 621–626.

Velde, B., Meunier, A., 2008. The Origin of Clay Minerals in Soils and Weathered Rocks. Springer Berlin Heidelberg, 406.

Velde, P., & Barré, P. (2009). Soils, Plants and Clay Minerals: Mineral and Biologic Interactions. Springer Science & Business Media, 359.

Von Pechmann E., 1985. Mineralogy of the Key Lake U-Ni orebodies, Saskatchewan, Canada: Evidence for their forma-tion by hypogene hydrothermal processes. In Geology of Uranium Deposits,eds. T. Sibbald and W. Petruk. Can. Institu. Min. Metallur. 32, 27-37.

Voudouris, P. C., Melfos, V., Spry, P. G., Kartal, T., Schleicher, H., Moritz, R., Ortelli, M., 2013. The pagoni rachi/kirki cu-mo re au deposit, northern greece: mineralogical and fluid inclusion constraints on the evolution of a telescoped porphyry-epithermal system. The Canadian Mineralogist. 51(2), 253 - 284.

Waseda, Y., Matsubara, E., Shinoda, K., 2011. X-Ray Diffraction Crystallography. Springer Berlin Heidelberg, Berlin, Heidelberg.

WHO, 2011. Guidelines for Drinking-water Quality. World Health Organization, 4th ed.1, 514.

Wilson, M.J., 1987. X-ray powder diffraction methods, in Wilson, M.J., ed. A handbook of determinative methods in clay mineralogy, Chapman and Hall, New York, NY, 26-98.

Wittry, D.B., 1958. Resolution of electron probe microanalyzers. J. Appl. Phys. 29, 1543-1548.

Xstrata Nickel, 2008. Ore Reserves and Mineral Resources. Xstrata Nickel Publication.

Xu, J., Wang, W., Mu, B., Wang, A., 2012. Effects of inorganic sulfates on the microstructure and properties of ion-exchange treated palygorskite clay. Colloids and Surfaces A: Physicochemical and Engineering Aspects. 405, 59-64.

Zhang, G., Wasyliuk, K., Pan, Y., 2001. The characterization and quantitative analysis of clay minerals in the Athabasca basin, Saskatchewan: Application of shortwave infrared reflectance spectroscopy: Can. Miner. 39, 1347-1363.

Appendix A
Elemental assay of the studied samples

Elements (µg/g)	MCA	MLM	GSW	DSW	MCW	S1	S2	S3	LR1	LR2	LR3
Li	303.71	651.74	61.30	82.68	100.87	142.48	234.93	182.73	116.16	165.86	140.55
Na	1253.71	809.53	974.22	1584.36	1841.06	1316.14	1274.04	1261.70	1090.80	1336.34	1183.91
Mg	24091.77	15197.90	8487.44	13289.78	14145.66	15658.37	12190.90	9572.24	10604.36	8642.89	9275.01
Al	61182.12	112486.40	34642.20	47459.41	51190.17	47293.85	45465.46	54008.63	45065.03	50008.51	48078.68
P	479.99	588.72	314.93	390.54	317.80	388.94	382.39	293.67	283.47	153.32	174.82
K	4867.47	40224.49	5544.25	13578.24	14596.36	9335.90	12524.51	19176.36	9603.37	13393.13	17460.28
Ca	30171.59	3349.57	2137.81	7514.14	19378.05	21203.06	15407.29	6652.59	30986.07	1511.20	6446.21
Sc	82.10	45.12	11.32	7.52	9.09	30.15	15.10	26.93	15.43	9.42	13.76
Ti	3276.81	18442.35	1860.07	2191.01	2133.56	2370.92	4138.77	3632.54	2691.58	4983.39	3493.56
V	1105.11	1418.30	122.00	174.91	206.15	393.43	722.16	574.36	250.62	314.67	434.03
Cr	101.02	159.87	38.62	49.53	51.89	67.13	82.16	78.36	162.61	102.94	206.79
Mn	327.94	83.64	78.15	132.77	164.03	209.72	190.14	127.73	112.52	37.36	67.17
Fe	29549.07	17979.34	11443.38	19137.04	25789.14	23753.64	19789.44	19189.62	14422.44	7116.12	12877.41
Co	210.80	69.13	87.48	46.04	55.52	130.37	123.68	63.68	86.25	67.14	33.80
Ni	92.24	143.72	1687.00	200.15	81.83	609.27	535.38	553.02	399.10	164.00	353.22
Cu	524.88	300.16	60.78	117.57	215.71	297.50	327.88	230.22	212.99	193.67	146.66
Zn	46.13	30.65	64.69	32.20	37.30	81.31	40.21	46.42	44.78	19.80	25.31
Ga	19.83	48.40	10.12	13.77	12.41	13.46	16.32	18.49	11.96	16.98	17.65
Ge	3.35	3.05	1.31	1.40	1.43	2.12	2.36	2.22	2.57	2.68	2.27
As	119.88	96.96	1826.70	221.24	45.05	628.61	549.46	549.71	283.50	82.43	261.52
Se	12.99	26.44	8.99	1.37	3.08	8.92	12.75	27.10	9.45	11.76	20.22
Rb	14.94	58.60	14.85	37.52	39.12	24.18	18.23	37.73	25.07	27.23	35.47
Sr	141.79	90.57	175.25	189.05	138.51	165.59	135.68	146.92	230.51	140.65	143.71
Y	412.70	77.09	25.94	23.72	34.14	151.72	169.79	93.68	74.18	20.48	32.91
Zr	204.99	181.30	179.21	166.32	149.74	167.96	172.06	164.99	180.91	195.26	135.87
Nb	15.11	18.87	6.84	8.98	8.90	10.48	12.20	9.23	12.35	13.84	8.98
Mo	377.89	849.72	17.86	42.95	89.01	104.72	231.48	432.03	107.78	104.31	317.82

Ag	3.02	3.21	0.87	0.39	0.54	1.13	1.74	1.84	1.36	1.89	1.77
Cd	0.06	ud	0.28	0.18	0.11	0.11	0.09	0.01	0.13	0.07	ud
Sn	6.99	8.39	2.27	3.49	3.72	3.80	3.16	5.15	3.92	4.88	2.35
Sb	11.60	14.38	13.41	2.32	1.40	9.47	10.27	16.84	13.31	10.50	14.07
Cs	0.57	1.11	0.33	1.20	1.34	0.78	0.64	0.88	0.94	0.89	0.91
Ba	291.93	148.35	171.50	162.25	2136.92	388.23	274.50	497.60	558.47	374.80	517.08
La	21.09	3.83	28.38	33.49	26.74	28.93	19.63	21.07	38.93	26.75	22.21
Ce	49.00	10.24	56.15	66.11	52.55	58.98	43.30	44.83	80.47	56.45	45.37
Pr	7.18	1.56	6.27	7.43	6.19	7.23	5.53	5.28	9.75	6.92	5.22
Nd	34.03	7.19	22.02	25.68	22.83	28.57	23.26	20.52	36.20	24.88	18.25
Sm	21.47	3.42	4.92	5.10	4.59	10.70	10.55	6.36	9.00	4.06	3.96
Eu	7.58	1.48	1.08	0.98	1.08	3.56	3.60	2.10	2.33	0.66	1.05
Gd	68.10	13.78	6.40	5.69	6.39	28.69	31.25	17.53	15.97	3.49	7.14
Tb	15.14	3.47	1.18	0.97	1.16	6.22	6.93	4.21	3.29	0.62	1.56
Dy	126.83	33.00	8.23	6.28	7.89	50.77	57.91	38.11	25.56	4.13	12.87
Ho	17.61	4.41	1.28	1.01	1.26	7.07	7.93	5.13	3.56	0.70	1.76
Er	37.52	9.21	2.98	2.48	3.22	15.05	17.09	11.26	7.50	1.86	3.77
Tm	4.48	1.14	0.37	0.30	0.44	1.89	2.07	1.32	0.92	0.23	0.46
Yb	25.66	6.22	2.38	1.90	2.62	10.28	11.93	7.31	5.13	1.53	2.59
Lu	2.70	0.64	0.29	0.26	0.34	1.13	1.24	0.74	0.59	0.21	0.26
Hf	4.43	4.96	4.69	4.82	4.23	4.32	4.20	4.41	5.20	5.88	3.73
U	132600.10	21263.75	1864.94	1585.25	2577.64	44862.78	57556.51	24356.36	14611.35	100.57	6028.58
Pb	13619.66	2041.00	218.19	170.16	226.06	4959.81	6437.20	2577.24	7030.49	6216.94	1889.27
Th	25.23	8.67	11.64	14.63	12.74	19.01	13.43	13.23	20.30	16.35	11.31

Appendix B
Calculated elemental assay using MLA

Elements (µg/g)	McA	MLM	GSW	DSW	McW	S1	S2	S3	LR1	LR2	LR3
Al	37100	83800	30800	28900	33400	24700	38700	65200	25200	33100	33000
As	100	0	800	100	0	100	200	100	200	100	100
Ba	400	700	700	300	5300	500	400	500	1000	1000	900
C	1500	0	200	600	1200	900	800	700	0	0	0
Ca	29500	3100	5000	15000	19100	19500	16600	7200	15100	1900	5100
Ce	100	100	200	100	200	200	300	100	600	0	100
Co	0	0	0	0	0	0	100	0	0	0	0
Cu	900	300	0	200	200	500	700	600	300	400	400
F	700	2900	800	1000	1000	600	1000	3100	900	1400	1800
Fe	57200	22200	33000	35000	46300	37700	40200	37000	28200	16400	22100
H	3100	6300	2200	2000	2300	1900	3100	5400	1500	2100	2400
K	8100	42500	8900	13700	15000	8100	13000	41500	11500	17800	22400
La	100	100	400	200	300	200	200	0	400	100	200
Mg	26500	33300	17600	19900	21800	17100	23000	36700	17500	21700	25300
Mn	0	0	0	100	300	100	100	0	0	100	0
Mo	0	200	0	0	0	0	100	500	0	0	0
Na	1400	600	1300	1500	1600	1300	1000	500	3500	4100	1900
Nd	0	0	0	0	0	0	100	0	200	0	0
Ni	0	0	900	0	0	100	100	0	0	100	200
O	426900	491600	508900	503200	493400	478500	455200	426200	499300	506600	504400
P	200	700	400	300	300	300	400	200	400	100	200
Pb	18900	3300	500	300	800	7200	12800	20400	5100	6000	1400
S	5100	2000	700	2200	3500	2000	3700	2100	2100	3500	2400
Si	253300	267300	380900	371600	347000	345800	295900	207800	370400	377200	363800
Th	0	0	0	0	0	0	0	0	100	0	0
Ti	3200	19500	3100	2200	1700	2100	4900	11300	2300	6100	6000
U	125400	19300	2700	1300	4600	50700	87200	132800	13700	0	5500
W	0	0	0	100	400	0	0	0	0	100	0
Zn	0	0	0	0	100	0	0	0	0	0	0
Zr	100	200	100	300	100	100	100	100	500	100	300